

Editor-in-Chief B.E.Paton

Editorial board:

Yu.S.Borisov	V.F.Grabin
A.Ya.Ishchenko	V.F.Khorunov
B.V.Khitrovskaya	I.V.Krivtsun
S.I.Kuchuk	Yatsenko
Yu.N.Lankin	V.K.Lebedev
V.N.Lipodaev	L.M.Lobanov
V.I.Makhnenko	A.A.Mazur
O.K.Nazarenko	I.K.Pokhodnya
I.A.Ryabtsev	K.A.Yushchenko
N.M.Voropai	A.T.Zelnichenko

International editorial council:

N.P.Alyoshin	(Russia)
U.Diltey	(Germany)
Guan Qiao	(China)
D. von Hofe	(Germany)
V.I.Lysak	(Russia)
N.I.Nikiforov	(Russia)
B.E.Paton	(Ukraine)
Ya.Pilarczyk	(Poland)
P.Seyffarth	(Germany)
G.A.Turichin	(Russia)
Zhang Yanmin	(China)
A.S.Zubchenko	(Russia)

Promotion group:

V.N.Lipodaev, V.I.Lokteva
A.T.Zelnichenko (exec. director)

Translators:

I.N.Kutianova, V.F. Orets,
T.K.Vasilenko, N.V.Yalanskaya

Editor

N.A.Dmitrieva
Electron galley:
I.S.Batasheva, T.Yu.Snegiryova

Address:

E.O. Paton Electric Welding Institute,
International Association «Welding»,
11, Bozhenko str., 03680, Kyiv, Ukraine
Tel.: (38044) 287 67 57
Fax: (38044) 528 04 86
E-mail: journal@paton.kiev.ua
http://www.nas.gov.ua/pwj

State Registration Certificate
KV 4790 of 09.01.2001

Subscriptions:

\$324, 12 issues per year,
postage and packaging included.
Back issues available.

All rights reserved.

This publication and each of the articles
contained herein are protected by copyright.
Permission to reproduce material contained in
this journal must be obtained in writing from
the Publisher.

Copies of individual articles may be obtained
from the Publisher.

CONTENTS

SCIENTIFIC AND TECHNICAL

*Smiyan O.D., Kuchuk-Yatsenko S.I., Kharchenko G.K.,
Zyakhor I.V., Butkova E.I. and Nikolnikov A.V.* Distribution of
interstitial impurities within the joining zone in friction welding 2

*Kulik V.M., Vasiliev V.G., Grigorenko G.M., Savitsky M.M. and
Doroshenko L.K.* Phase and structural transformations in
welding and arc treatment of 30KhGSA steel joints 6

*Labur T.M., Grinyuk A.A., Taranova T.G., Kostin V.A. and
Poklyatsky A.G.* Features of micromechanism of fracture in
joints of aluminium-lithium alloys produced by plasma welding 11

Makhnenko O.V. and Muzhichenko A.F. Mathematical
modelling of thermal straightening of cylindrical shells and
shafts with distortions along their longitudinal axis 17

Ignatenko A.V. Mathematical model of transportation of
hydrogen by edge dislocation 23

INDUSTRIAL

Shlepakov V.N., Ignatyuk V.N., Kotelchuk A.S. and Gitin Yu.M.
Mechanized repair welding of metallurgical complex units
using flux-cored wire 28

*Yushchenko K.A., Chekotilo L.V., Nastenka G.F., Danilov
Yu.B., Kachanov V.A., Kabashny A.I., Ivanuna S.N., Dorn V.R.,
Ilienka V.V., Ambrozyak N.V., Kisly B.P. and Khodan T.M.*
Extension of life of large-size concentrated sulphuric acid
storage tanks 34

Eryomin E.N. Modification of weld metal in electroslag welding
of KhN77TYuR refractory alloy 38

Poklyatsky A.G., Ishchenko A.Ya. and Yavorskaya M.R.
Strength of joints on sheet aluminium alloys produced by
friction stir welding 42

Gavrish V.S., Rudenko P.M. and Podola N.V. System of
automatic control and monitoring of resistance spot welding 45

NDT OF WELDED JOINTS

Gushcha O.I., Brodovoj V.A. and Smilenko V.N. Determination
of main directions and values of residual stresses in highly
textured materials by acoustic method 49

BRIEF INFORMATION

News 51

NEWS

The 60th IIW Annual Assembly 52

Cooperation of the E.O. Paton Electric Welding Institute with
Indian Centers on Welding Industry Personnel Training 54

Developed at PWI 22, 27, 37



DISTRIBUTION OF INTERSTITIAL IMPURITIES WITHIN THE JOINING ZONE IN FRICTION WELDING

O.D. SMIYAN, S.I. KUCHUK-YATSENKO, G.K. KHARCHENKO, I.V. ZYAKHOR, E.I. BUTKOVA and A.V. NIKOLNIKOV
E.O. Paton Electric Welding Institute, NASU, Kiev, Ukraine

Distribution of interstitial impurities (oxygen and hydrogen) in joints on steel 10G2FB produced by friction welding was studied using the local mass-spectral analysis procedure and equipment fitted with a laser probe. The nature of distribution of interstitial impurities in the joining zone produced by different friction welding methods (conventional and inertia) was experimentally determined.

Keywords: friction welding, conventional friction welding, inertia friction welding, joining zone, interstitial impurities, local content, plastic and elastic deformation zones

Local mass-spectral analysis procedure and equipment using an electron beam [1] and laser [2] probes were employed in studies [1, 2] to estimate the local content and distribution of gas-forming interstitial impurities (hydrogen, oxygen, nitrogen and carbon) in joints produced by pressure welding. It was determined that explosion welding of plates of steel St3 caused increase in the content of hydrogen, oxygen and carbon in the joining zone [1]. As shown in study [2], increase in the content of the above impurities within the joining zone was also fixed in stud joints on alloy AMg6, produced by percussion capacitor-discharge welding. In that case, the sorption of gases from a gap between the billets welded by metal was considered to be the main mechanism of absorption of impurities by a solid body.

It is of interest to study distribution of interstitial impurities in the joints produced by other methods of pressure welding, e.g. friction welding (FW), which is characterised by formation of a joint in the solid phase. Oxide films present on edges of the billets are destroyed and expelled from a joint during heating and plastic deformation of the billets. Formation of the joint occurs in application of pressure after the billets stop rotating. We failed to find any publications concerning determination of the local content and distribution of interstitial impurities in a zone of the FW joint. However, with other methods of pressure welding the local clusters of interstitial impurities are reported [1, 2] to have a negative effect on mechanical properties of welded joints.

The purpose of this study was to investigate the distribution of oxygen and hydrogen in joints produced by FW. Investigations were conducted on welded samples of steel 10G2FB using the EKHO-4M unit. The average content of interstitial impurities in the base metal was 1.5 ppm ($1.3 \cdot 10^{-4}$ wt.%) [H] and 0.003 wt.% [O]. The values of ion currents of H^+ and O^+ were measured during the investigations after extracting them from a solid body by pulsed local melting of metal at the preset point of a sample using a

focused laser beam. The intensity of these signals corresponded to the local content of interstitial impurities in metal. The values of the ion currents were fixed using the MX7301 mass spectrometer. Duration of an irradiation pulse was 5 ms, power of the pulse was 7.5 J, and maximal temperature at the irradiation points was 8000 K.

Rods 18 mm in diameter, made from steel 10G2FB, were welded. The samples were turned from pipe segments with a wall thickness of 18.5 mm. The rods were welded using the upgraded welding machine ST-120 designed by the E.O. Paton Electric Welding Institute for friction welding with controlled deceleration [3], in which it is possible to vary thermal-deformation conditions of formation of joints. Welded joints were produced by two FW methods differing in thermal and deformation welding cycles, i.e. conventional (CFW) and inertia friction welding (IFW). Cyclograms of variation of such process parameters as rotation frequency n and pressure P with time τ are shown in Figure 1. Distribution of temperature within the joining zone in CFW and IFW is shown in Figure 2. The CFW mode is usually called soft, and the IFW mode --- rigid.

In CFW (Figure 1, a), the pressure in heating was $P_h = 50$ MPa, and rotation frequency n of one of the billets remained constant ($n = 20$ s $^{-1}$). Forging pressure $P_f = 100$ MPa was applied after a rapid forced deceleration of rotation. Duration of the welding cycle was $\tau = 6$ s, upsetting (shortening of billets in welding) was 5 mm, maximal temperature in a joint was about 1593 K, and duration of metal dwelling at a temperature of 1373--1593 K was about 4--5 s. The deformation effect on metal within the joining zone at a stage of formation of the joint was characterised by the presence of mostly a radial component. Width of the heat-affected zone (HAZ) in CFW was almost identical over the entire cross section of the billets. For the joints investigated it was approximately 11--12 mm, and width of the plastic deformation zone was about 8 mm.

In IFW (Figure 1, c), the initial rotation frequency at $P_h = 50$ MPa was 40 s $^{-1}$. The rotation frequency decreased to zero during the deceleration process due

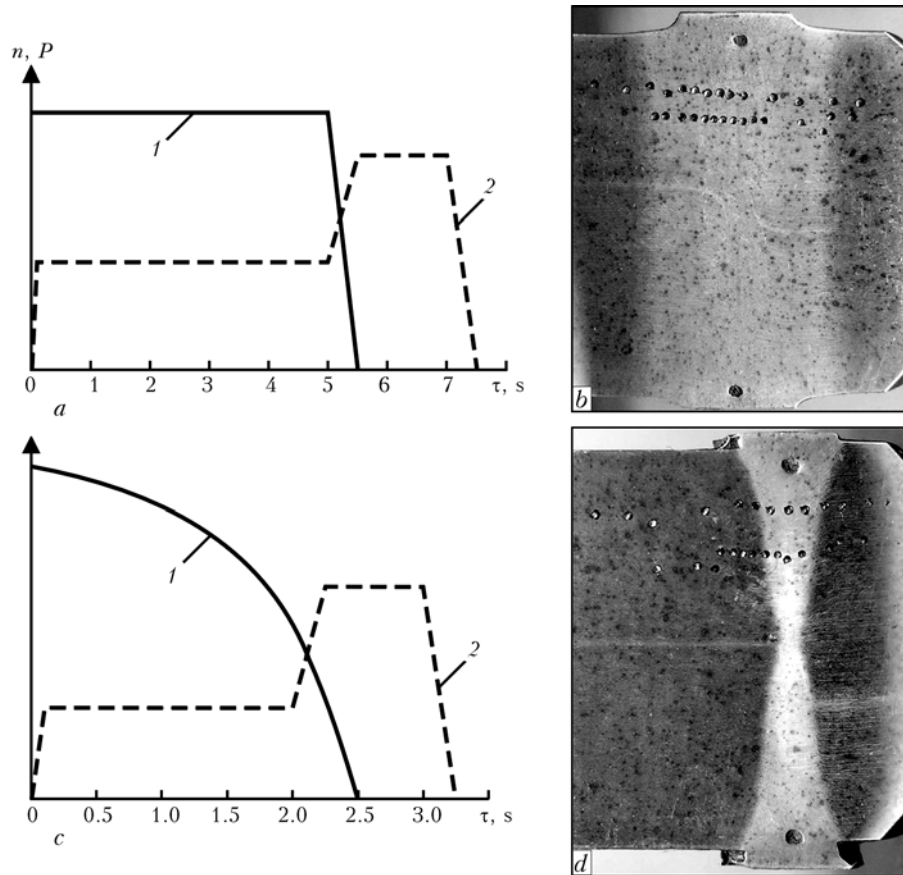


Figure 1. Cyclograms of variation of rotation frequency n (1) and pressure P (2), and macrosections of joints produced by conventional (a, b) and inertia (c, d) friction welding

to friction forces in a joint, and $P_f = 100$ MPa was applied upon reaching the $n = 12.5$ s⁻¹ frequency. Duration of the welding cycle was 2.5 s, and upsetting was 5 mm. Duration of metal dwelling at a temperature above 1373 K was about 2 s. The effect on metal of the joint at a stage of its formation was characterised by the presence of radial and tangential components of deformation. In IFW, the plastic deformation zone had the characteristic X-like shape, its width at the central part of the cross section was 1.5–2.0 mm, and that in the peripheral part was 5 mm. Measurements of the content of interstitial impurities were made in a region of the cross section, where the plastic deformation zone was 3.5–4.0 mm wide.

Figure 3 shows the distribution of hydrogen and oxygen in metal of the joining zones produced by different FW methods. Typical microstructure of a joint is shown in Figure 4.

Compared with the base metal, zones of the FW joints (Figure 3, a) are characterised by an almost 2 times decrease in the hydrogen content in a region about 4 mm wide. The hydrogen content decreases 5 times along the joining line (zone 1 in Figure 4), compared with the base metal (zone 6). Total width of the zone of variation in the hydrogen content corresponds to width of the plastic deformation zone and amounts to about 8 mm. Decrease in the hydrogen content approximately 2 times takes place in a zone about 8 mm wide (Figure 3, b). The oxygen content decreases approximately 6 times along the joining line.

Peaks of increase in the oxygen content, which are 2 times as high as those in the base metal, are observed at a distance of 4 mm, symmetrically about the joining line. Location of these peaks corresponds roughly to boundaries of the plastic deformation zone. In CFW, interstitial impurities are distributed almost symmetrically about the joining line.

In zones of the IFW joints (see Figure 3), the most pronounced decrease in the hydrogen content takes place in a region about 2 mm wide, symmetrically about the joining line. Decrease in the oxygen content approximately 1.5 times occurs in a region about 2 mm wide. Like in CFW, here there are peaks of the oxygen content, which are 2 times as high as the oxygen content of the base metal. They are located at a distance

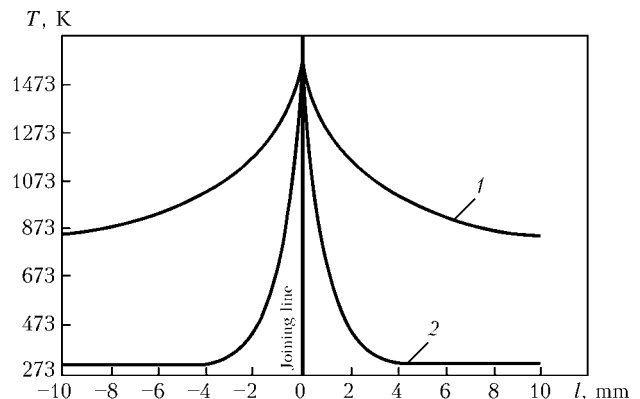


Figure 2. Distribution of temperature within the joining zone in CFW (1) and IFW (2) [4]: 1 — distance from the joining line

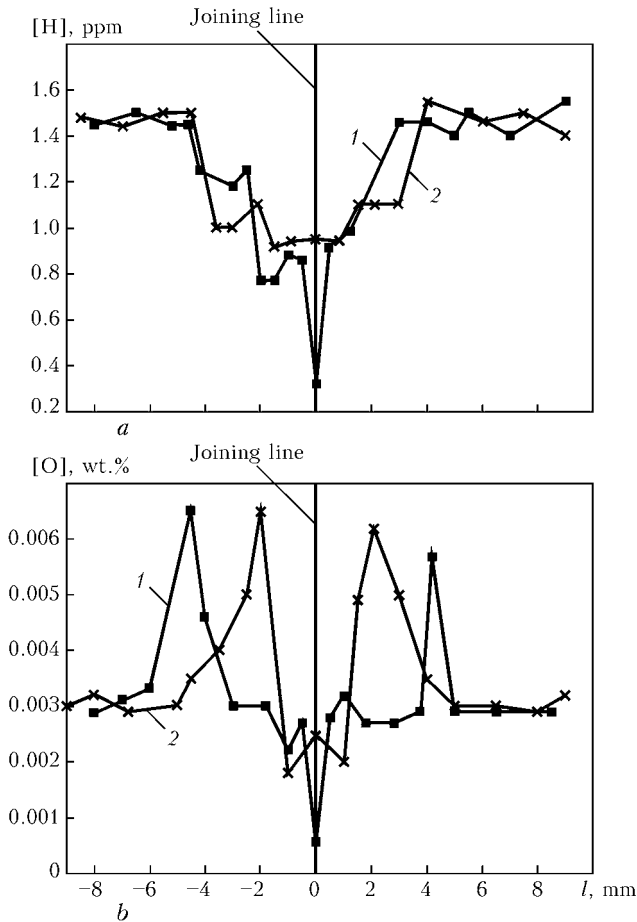


Figure 3. Distribution of hydrogen (a) and oxygen (b) in zones of the joints on steel 10G2FB produced by CFW (1) and IFW (2)

of about 2 mm from the joining line, which corresponds to boundaries of the plastic deformation zone. Total width of a region of variation in the hydrogen and oxygen contents is about 8 mm, which is in excess of width of the plastic deformation zone.

In all modes of FW under investigation, the values of average rotation frequency n and pressure P were identical, but duration of their impact on metal, as well as the law, following which n and P varied with time, especially at the final stage of welding, were different.

With both FW methods, decrease in the hydrogen and oxygen contents occurred within the joining zone. Minimal content of interstitial impurities was fixed along the joining line, which was a high-temperature region (zone 1 in Figure 4). This is a region where

interaction of the mating surfaces is concentrated in friction, and it can be conditionally regarded as a «third body» [5]. Metal here is affected by a temperature of about 1373–1593 K and substantial plastic deformation, and features the presence of a big amount of dislocations. Fine-grained structure (grain size 10–11) is formed in zone 1 as a result of full primary recrystallisation. Metal of this zone undergoes full phase transformation (ferrite and pearlite transform into austenite), and transforms into a fine-grained ferrite-pearlite mixture during cooling. Decrease in the hydrogen content along the joining line seems to be caused by migration of hydrogen from the joining zone (compression zone) together with flash formed during the welding process, as well as its loss in the inter-grain regions in recrystallisation of metal [6], during turning of grains and formation of new equiaxed grains.

Decrease in the oxygen content along the joining line is not identical to its increase in the contact volumes of metal, which were not subjected to plastic deformation. This distribution of oxygen can be explained by the effect of several factors. The first is the contact friction, as well as the associated heating of metal and its deformation in a radial direction, which provide dispersion and displacement of oxide phases and adsorbed films from the contact zone to flash. The second factor is the process of fracture of oxides in metal by dislocations of the deforming metal. So, according to [7–9], plastic deformation of metal within the contact zone causes an atom-by-atom fracture of oxide phases by dislocations, transfer of oxygen to the solid solution, and its partial migration from the compression zone. As a result, the contact volumes of metal are enriched with oxygen. The third factor is the character of distribution of temperature within the joining zone, which determines position of maximum of an oxygen peak with respect to the HAZ boundary. The combined effect by the above factors determines locations of the concentrated peaks of oxygen and their intensity.

Formation of both deformed grains, elongated in radial and tangential directions, and recrystallised grains takes place in zones 2 and 3 (see Figure 4), directly adjoining the recrystallised zone, where the temperature and degree of deformation are lower. A

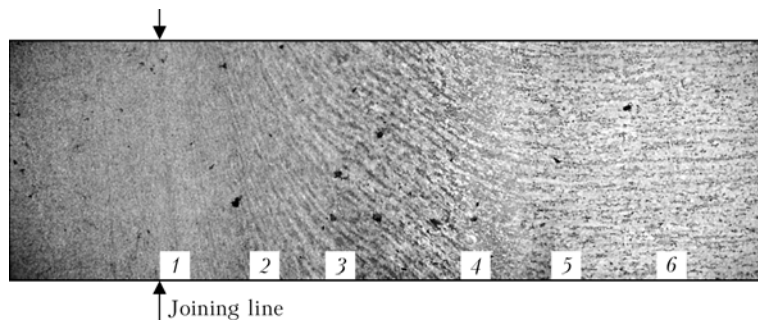


Figure 4. Microstructure of IFW joint on steel 10F2FB: 1–6 — see explanations in the text ($\times 100$)



decreased content of interstitial impurities is also fixed in this zone with both FW methods. With distance from the joining line, no recrystallised grains are detected in regions deformed by friction, but the character of orientation of grains changes (zone 4). This zone gradually transforms to a zone of elastic deformation (zone 5), which is part of HAZ outside the plastic deformation zone, and then to the base metal zone (zone 6). The boundary of variation in the hydrogen content in CFW propagates through zones 3–4, i.e. approximately through the plastic deformation zone. In IFW, the region with a decreased hydrogen content includes also zone 5.

Width of the zone of variation in the hydrogen content in the soft mode of CFW corresponds approximately to that of the plastic deformation zone. Difference in the hydrogen content in the rigid mode of IFW propagates to a larger depth of metal from the contact surface, compared with width of the plastic deformation zone. This effect is attributable to the fact that in IFW the rate of plastic deformation of metal within the contact zone is in excess of that in CFW. Reportedly [10], increase in the deformation rate causes growth of the rate of mass transfer of interstitial atoms.

Ascending diffusion, at which a directed drift of atoms takes place, is caused by the local gradients of stresses in crystals, when, according to the Gorsky effect, the interstitial atoms are concentrated mostly in a tension zone [11]. As found in studies [6, 7], metal of a steel pipe loses hydrogen in compression, and sorbs it in tension. The extent of a loss and absorption of hydrogen is affected by the deformation and its rate. Under a pulsed deformation, an avalanche of dislocations is formed in metal. This avalanche traps hydrogen and transports it. Depth of displacement of the atoms of hydrogen and oxygen is determined not only by the deformation rate, but also by the size of an atom. Transportation of interstitial atoms in the deformation zone is stabilised at a distance that is inversely proportional to sizes of the atoms [6, 10].

The biggest decrease in the oxygen content is fixed along the joining line (zone 1 in Figure 4), and it is most significant in CFW. The maximal temperature of metal within the contact zone in heating and subsequent deformation in forging after interruption of rotation (CFW mode) leads to a substantial (6 times) decrease in the oxygen content along the joining line. Location of the oxygen content peaks (twice as high as the oxygen content of the base metal) coincides with a boundary of the plastic and elastic deformation zones (zones 4 and 5 in Figure 4). Apparently, the oxygen atoms during plastic deformation are transported by nuclei of the dislocations accumulated at the boundary of the plastic and elastic deformation zones [12].

Analysis of the data obtained suggests that local plastic deformation reaches the highest development within the joining zone 1.5–2.0 mm wide (in CFW) and up to 4 mm wide (in IFW). This results is ex-

pected, because in CFW, owing to a rapid interruption of rotation, the temperature of the surface layers at the moment of application of increased forging force P_f is maximal, compared with other FW methods, and metal in the joining plane is more plastic and can be more readily deformed in a radial direction.

When increased force P_f is applied to rotating billets in IFW, i.e. at the presence of the radial and tangential components of deformation, the plastic and elastic deformation zones widen due to the metal layers having a lower temperature, which is evidenced by the level of content of interstitial impurities in this region. The character of variations in the contents of hydrogen and oxygen with distance from the contact surfaces towards the base metal proves the presence of a substantial effect of tangential deformations in the given welding mode.

CONCLUSIONS

1. In the FW joints on steel 10G2FB, the content of hydrogen and oxygen within the joining zone is decreased, compared with their content in the base metal.
2. Transfer of hydrogen and oxygen from the joining zone to the contact volumes of metal is stabilised at the boundary of the plastic and elastic deformation zones.
3. Variation in a ratio of radial and tangential components of deformation in FW can be used to control not only the temperature of metal in the joining zone, character and intensity of deformation, but also the local content and distribution of interstitial impurities in a welded joint.

1. Smiyan, O.D., Zheni-Majskaya, L.O., Lysak, V.I. et al. (1985) Nitrogen, oxygen and carbon distribution in the joining zone of explosion welded metals. *Avtomatich. Svarka*, **2**, 29–33.
2. Butkova, E.I., Smiyan, O.D., Kaleko, D.M. et al. (1988) Hydrogen and oxygen distribution in weld metal during capacitor discharge percussion stud welding of AMg6 alloy. *Ibid.*, **2**, 17–22.
3. Zyakhor, I.V. (2001) Modern equipment for friction welding. *The Paton Welding J.*, **7**, 48–52.
4. Lebedev, V.K., Chernenko, I.A., Vill, V.I. et al. (1987) *Friction welding*: Refer. Book. Leningrad: Mashinostroenie.
5. Kuchuk-Yatsenko, S.I., Zyakhor, I.V. (2002) Mechanism of bimetal joints formation in friction welding. *The Paton Welding J.*, **7**, 2–9.
6. Smiyan, O.D. (2004) *Redistribution of interstitial and alloying elements in thermal and deformation treatment, and its effect on initiation and propagation of cracks in metal*: Syn. of Thesis for Dr. of Techn. Sci. Degree. Kiev: PWI.
7. Smiyan, O.D., Zheni-Majskaya, L.O., Gavrilyuk, L.S. (1986) Influence of explosion treatment of metal on hydrogen content and redistribution. In: *Explosion welding and properties of welded joints*. Volgograd: VPI.
8. Smiyan, O.D. (2002) Atomic mechanism of interaction between environment material and deformed metal. *Fizyka ta Khimiya Tv. Tila*, **4**, 662–674.
9. Smiyan, O.D., Kruzhkov, A.G. (1972) About some peculiarities of movement of gas diffusion flows in metals. *Doklady AN SSSR*, **202**(6), 1311–1313.
10. Gertsriken, D.S., Mazanko, V.F., Tyshkevich, V.M. et al. (1999) *Mass transfer in metals at low temperatures under conditions of external interactions*. Kiev: IMF.
11. (1996) *Solid state physics*: Encyclopedia. Ed. by V.G. Bariakhtar. Vol. 1. Kiev: Naukova Dumka.
12. Smiyan, O.D. (2004) Mechanism of formation of equilibrium grain nuclei during recrystallization of structural steels. *Metalofizyka ta Novitni Tekhnologii*, **4**, 571–578.



PHASE AND STRUCTURAL TRANSFORMATIONS IN WELDING AND ARC TREATMENT OF 30KhGSA STEEL JOINTS

V.M. KULIK, V.G. VASILIEV, G.M. GRIGORENKO, M.M. SAVITSKY and L.K. DOROSHENKO

E.O. Paton Electric Welding Institute, NASU, Kiev, Ukraine

Considered are structural changes in weld metal of 30KhGS type on high-strength steel joints occurring in welding and arc treatment. Under these conditions austenite transformation of hardened metal of the joint occurs at temperatures close to A_1 and A_3 of steel in as-delivered state. Subsequent cooling provides recovery of the hardening structure. Short-time heating in the intercritical temperature range causes formation of a substantial amount of temper ferrite and reduction of the amount of martensite formed during subsequent cooling at the expense of increase of the ferrite and bainite components. This leads to the highest decrease in hardness and increase in impact toughness of the metal. This improvement of properties and increase in crack resistance of the welded joints takes place after short-time heating to tempering temperatures.

Keywords: arc welding, high-strength steel, heat-affected zone, arc treatment, heating, cooling, dilatometry, differential thermal analysis, hardness, impact toughness, delayed cracking

TIG welding is used in fabrication of light-weight welded structures from sheet high-strength steels, which provides sound formation of the joint, acceptable chemical and structural homogeneity of the joint metal, thus simplifying performance of subsequent heat treatment to achieve high values of strength and service properties of the weldment.

In welding of high-strength steels there is the risk of cold crack formation in the hardened weld metal or in the HAZ overheated region, which initiate immediately after or a certain time after welding. In order to avoid cracking related to martensite content in the structure [1], heating is performed before, during and after welding with subsequent immediate furnace tempering. This leads to deterioration of the labour conditions, complication of the technological process and increase of the weldment cost, requires application of additional equipment and is not always feasible in engineering terms. Change of the structure and improvement of cold cracking resistance of the HAZ metal in high-strength sheet steel is achieved by short-term thermal impacts in multipass welding and arc treatment [2]. It is obvious that such changes can also be anticipated in the weld metal.

The purpose of this paper is investigation of the phase and structural transformations in the welded joints (primarily, in welds), which can have delayed cracking susceptibility. Sheet steel 30KhGSA 3.2 mm thick used in fabrication of different products including car cylinders [3], was subjected to single- and two-pass A-TIG and TIG butt welding. Through-thickness penetration of the butt was performed in the first pass and in the second pass with electrode weaving incomplete penetration of 1.5–2 times greater width than that of the earlier formed joint was performed (with or without melting of Sv-18KhMA filler

wire). Tungsten-rhenium thermocouple VR20/5 of 0.35 mm diameter mounted on the reverse side, was used to establish that heating of the metal of the joint not melting when the second welding pass is made, occurs at temperatures not lower than 1100–1250 °C, i.e. definitely higher along its entire height. In the first and second welding passes, which are the hardening passes for 30KhGSA steel, the metal is cooled at the rates of 9–16 °C/s [4, 5]. In this case the surface concavity is reduced and eliminated, reinforcement and two-layer structure of the weld is produced, and joint formation is improved.

Phase and structural transformations during the heating-cooling cycle were studied by the method of high-speed dilatometry [2]. Samples of 3 × 8 × 75 mm size cut out across the welded joint with weld location in the central part, were heated by passing current up to different temperatures and cooled at argon blowing, thus simulating the thermal cycles of welding and arc treatment. Change of the sample temperature and width (weld length) was recorded using a two-coordinate potentiometer H307/1, heating duration by the stopwatch, cooling time by a special time marker. Since depending on the arc treatment mode without metal melting its heating occurs at the rate $w_s = 80$ –240, and cooling $w_{6/5} = 6$ –24 °C/s [6], their average value was assigned at thermal cycle simulation: $w_s = 160$ –180 and $w_{6/5} = 10$ –13 °C/s. The base metal was studied in a similar fashion for comparison. For determination of temperature intervals of solidification the differential thermal analysis was also performed [7] at heating and cooling at the rate of 80 °C/min.

Welded joint resistance to cold cracking was evaluated by delayed cracking tests with load lowering during development of microplastic deformation [8]. The structure and impact toughness of the welded joint metal was studied.

The method of differential thermal analysis was used to establish that the nature of solidification of



molten steel 30KhGSA, filler wire Sv-18KhMA and the weld, produced by melting or without it, is two-stage, which is indicated by the presence of two salient points on the cooling curve (Figure 1). The second salient point (at a lower temperature) is indicative of peritectic transformation, which according to Fe-C constitutional diagram is characteristic for steels with 0.16–0.51 % C. Peritectic transformation at solidification is noted in steel 35KhGS, as well as in Fe-Si-C alloys with 0.63–0.74 % C and 1.5–4.0 % Si [9].

Under the conditions of continuous cooling solidification of weld metal of 30KhGS type is of peritectic nature and starts with formation of ferritic dendrites. Nucleation of austenite with 0.16 % C content, partially or completely isolating ferrite from the liquid, occurs on their boundary at the temperature of peritectic transformation at interaction of low-carbon (0.1 %) δ -ferrite and carbon liquid phase. Poor contact of ferrite with carbon liquid (or its absence) hinders austenitisation, and untransformed regions can remain in the axes of ferritic dendrite branches. $\alpha \rightarrow \gamma$ transformation in them can occur at subsequent high-temperature cooling with formation of low-carbon austenite. Solidification is completed by formation of high-carbon austenite from the remaining liquid with increased content of carbon and other chemical elements. Therefore, a single-phase austenitic structure or austenitic structure with ferrite in the dendrite axes can be produced in the solidified weld metal, and austenite in individual microvolumes has different stability at cooling.

Dendritic structure of the primary microstructure in sheet steel weld metal is shown in Figure 2. Dimensions, structure and direction of the dendrites are determined by the welding mode and weld pool parameters. In the cross-section of the single-layer and first layer of a two-layer weld with the penetration form factor $\phi = b/h = 1.0$ –1.5 they are predominantly columnar, oriented from the base metal towards the center, almost equiaxed at the fusion zone and often disoriented in the center. In the second layer metal with the form factor of 4–6 the dendrites are finer, have another form (with a smaller number and size of the nuclei of second order axes), more oriented towards the face surface.

Redistribution of chemical elements on the solidification front as a result of their different solubility in the liquid and solid phases leads to a gradual enrichment of the liquid and then of the solidifying metal in them. Therefore, carbon and alloying element content in the weld metal compared to the base metal rises by 1–1.1 times at the depth of about 0.3 mm and by 1.1–1.2 times at the distance of 0.02–0.03 mm from the surface, where solidification ends. The content of carbon and silicon with an increased liquation coefficient of 0.87 and 0.34, for δ -iron, rises, and content of chromium and manganese with liquation coefficients of 0.05 and 0.16 decreases, respectively [10]. Macrochemical inhomogeneity of the type of a zonal one in the second layer of the weld forms as a result

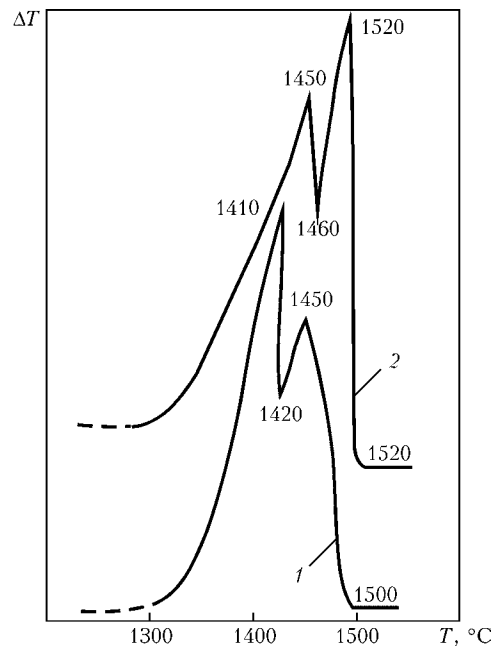


Figure 1. Differential thermal curve of cooling of the molten weld metal (30KhGSA steel) without (1) and with (2) filler metal

of metal solidification, oriented, predominantly, towards the surface.

Subsequent cooling at the hardening rate of $w_{6/5} = 9$ –14 °C/s under the conditions of welding causes transformation of austenite of the solidified metal into a martensite-bainite mixture both in single- and two-layer welds (Figure 3), similar to that running in the HAZ metal [2]. Presence of the initial microchemical and microstructural inhomogeneity can cause microinhomogeneity of the secondary structure in the weld metal in the form of weekly-etching sections (most probably, containing residual austenite).

Metal of the single-layer weld has the microhardness $HV_{0.05/30}$ 260–405, HAZ — $HV_{0.05/30}$ 405–440. Increase of $w_{6/5}$ within the above limits when making the second welding pass at a lower heat input without melting of the filler wire causes an increase of microhardness of the second layer metal, cooled from the liquid state to $HV_{0.05/30}$ 321–345 and HAZ metal in the first weld layer to $HV_{0.05/30}$ 460–480. A lowering of weld metal microhardness in the first layer to $HV_{0.05/30}$ 221–356 due to its short-time heating without melting and of HAZ metal at the second layer to $HV_{0.05/30}$ 221–268 as a result of pulsed thermal impact of a transversely oscillating arc is observed. In welding using filler wire with a smaller



Figure 2. Primary microstructure of two-layer weld metal ($\times 50$)

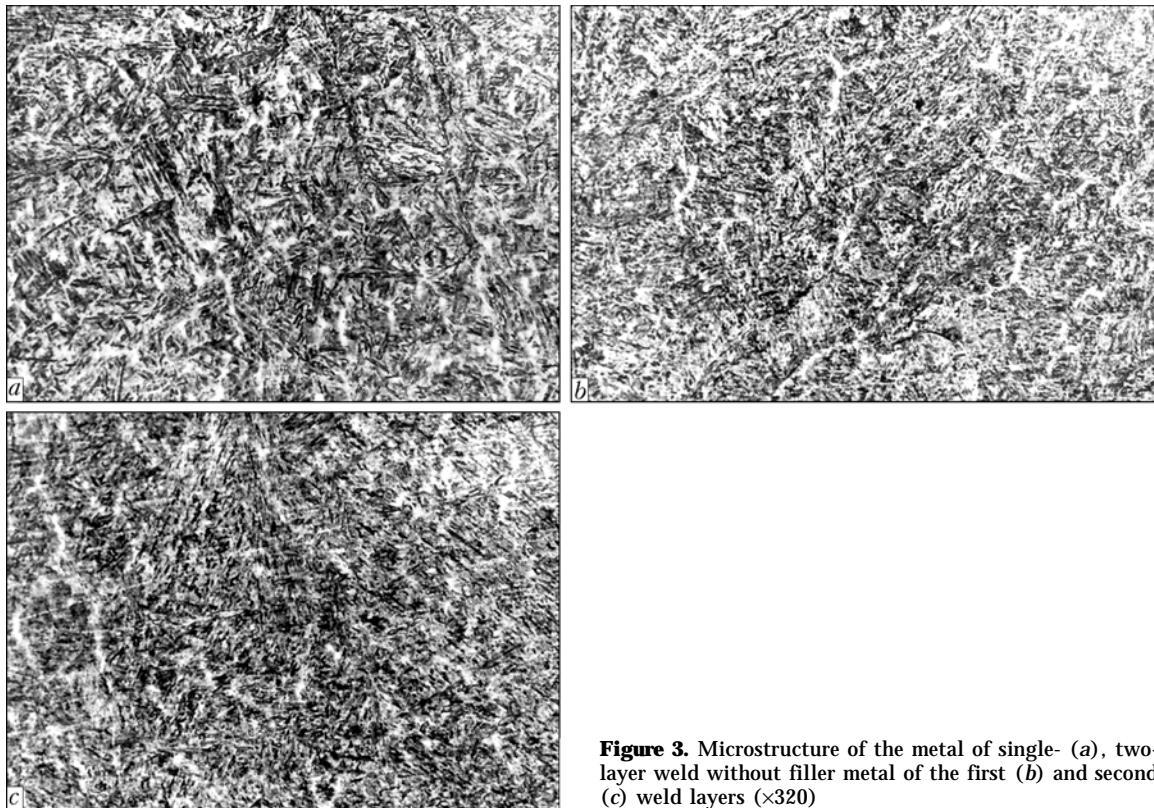


Figure 3. Microstructure of the metal of single- (a), two-layer weld without filler metal of the first (b) and second (c) weld layers ($\times 320$)

content of carbon than in the base metal, the hardness of the second weld layer decreases 1.05–1.10 times.

Mechanism of formation of the HAZ metal structure was established by dilatometric studies described in [2]. Heating of heat-softened (as-delivered) 30KhGSA steel occurs without development of temper transformations. When temperatures of 720–760 °C are reached, the dilatometric curve shows salient points, which can be caused by carbide coagulation and steel transition from the ferro- into the paramagnetic state. Rapid heating causes 50–100 °C increase of austenite transformation temperatures $A_{c1} = 835$ and $A_{c3} = 930$ °C (reference values $A_1 = 740$ –785 °C

and $A_3 = 830$ –875 °C [4]). Cooling after short-time (for 1–2 s) overheating up to temperatures of 1330–1350 °C (as in welding) is accompanied by austenite transformation (at temperatures of 655–225 °C) with formation of 49 % of martensite, 48 % of bainite and 3 % of ferrite in the structure.

Transformations occurring in the metal of the weld and HAZ close in their composition are similar (Figure 4, Tables 1 and [2]). However, unlike the simulated HAZ, in which the overheating and hardening structures were created at first heating, the weld metal is that hardened object, on which simulation of arc treatment is performed. Presence of hardening structure predetermines running of the following transformations at the heating stages at tempering: second (residual austenite decomposition) and third (carbide) at elevated temperatures of 180–550 and 460–660 °C. The transformations are more clearly revealed at differential dilatometric analysis of weld metal (Figure 5). Critical points A_{c1} and A_{c3} decrease to values of 750–765 and 860–890 °C close to A_1 and A_3 of heat-softened steel. During cooling at triple cycles of high-temperature heating–cooling of the earlier hardened metal, bainite (520–330 °C), martensite (350–185 °C) and, possibly, ferrite (700–500 °C) transformations are observed (Table 1). Bainite transformation in the weld metal occurs monotonically or with a change of the rate at temperatures of 410–380 °C. Lowering of the temperature of short-time heating from 1150 to 970–920 °C causes an earlier decomposition of the weld metal austenite (increase of F_s). In the absence of ferrite transformation, an earlier transformation of austenite in the bainite region occurs (increase of B_s and B_e) and delay of its com-

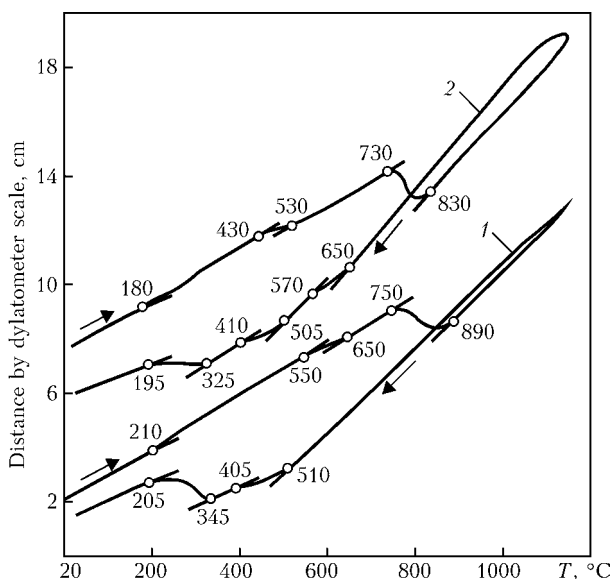


Figure 4. Dilatograms of 30KhGSA steel and metal of welds without (1) and with (2) filler metal



Table 1. Transformations at cooling after short-time heating of 30KhGSA steel welded joint

Studied region	Heating #	$\dot{\sigma}_s, \text{ } ^\circ\text{N}$	Transformation temperature, $^\circ\text{C}$						Final structural components, %			
			F_s	F_e	B_s	B_e	\dot{I}_s	\dot{I}_e	\dot{I}	F_t	B	F
HAZ	1*	1340	610	550	495	350	350	225	49	--	48	3
	2	1150	600	580	500	350	350	225	55	--	39	5
	3	1150	620	600	510	355	355	220	55	--	39	6
	4	1150	605	585	510	350	350	225	55	--	37	8
Weld, w/f	1	1150	670-590	510	510	345	345	205	38	--	55	7
	2	1150	670-590	500	500	340	340	210	39	--	48	13
	3	1150	635-590	505	505	345	345	220	39	--	50	11
Weld, f	1	1150	615-570	515	515	330	330	240	33	--	60	7
	2	1150	610-580	520	520	325	325	240	33	--	63	4
	3	1150	620-595	505	505	330	330	235	37	--	61	2
Weld, w/f	1	970	--	--	515	350	350	200	85	--	15	--
Weld, f	1	920	700	610	520	410	350	185	54	--	21	25
	2	920	680	590	525	400	335	180	46	--	23	31
	3	920	690	600	505	410	345	190	44	--	28	28
Weld, w/f	1	840	630	520	520	410	325	N/D				
Weld, f	1	820	690	610	520	385	225	N/D	25.5	34	22	18.5
	2	820	690	605	530	380	200	Same	23	34	23	20
Weld, w/f	1	800	715	670	N/D							
Weld, f	1	790	715	630	515	340	340	250	5	80	15	---
	2	1370	---	---	515	340	340	240	37	---	63	---
	3	820	675	640	520	400	400	230	22	34	22	22

Note. M --- martensite; B --- bainite; F --- ferrite of transformation; F_t --- temper ferrite, indices: s --- start, e --- end, w/f --- without filler, f --- with filler; asterisk at the number --- simulation of formation of the overheated region of the HAZ metal.

pletion in the martensite region (M_e lowering). This results in increased content of martensite and martensite with ferrite in the weld metal structure as a result of lowering of the bainite component fraction. Multiple nature of short-time heating above A_{c3} of the hardened weld metal promotes a slight increase of the fraction of martensite component (by 1-4 %) of the structure at a high (260-290 $^\circ\text{C}$) overheating and its lowering by 10 % at a low (40-60 $^\circ\text{C}$) overheating. Considering the technological features of welding without melting and with melting of the filler wire, the pre-formed structure of weld metal contains 33-85 % of martensite, 15-63 % of bainite and 0-31 % of ferrite, and the HAZ metal --- 55 % of martensite, 37-39 % of bainite and 5-8 % of ferrite.

Lowering of austenite transformation temperatures ($A_{c1} = 730 \text{ }^\circ\text{C} < A_1$ and $A_{c3} = 830 \text{ }^\circ\text{C} \leq A_3$) was observed in the weld metal pre-quenched in water for martensite after furnace heating. Such an operation heating promotes an earlier start ($F_s = 650 \text{ }^\circ\text{C}$) and delayed completion ($M_e = 185 \text{ }^\circ\text{C}$) of austenite transformation at cooling after fast short-term heating and reduction of the amount of martensite to 24 % in the structure due to increase of the amount of ferrite (24 %). High furnace tempering of the weld metal forming the structure of tempering sorbite, contrarily, promotes A_{c1} increase

to $800 \text{ }^\circ\text{C} > A_1$ and of A_{c3} up to $875 \text{ }^\circ\text{C} \geq A_3$, increase of the share of martensite (50 %) and ferrite (30 %) structural components as a result of lowering of the amount of bainite component (20 %). Therefore, in multipass welding and arc treatment a greater lowering of austenite transformation temperatures can be anticipated in the more hardened joint metal and increase of these temperatures in welding of less hardened steels under the conditions of delayed cooling. With increase of the number of short-time heating impacts up to the temperature of 1150 $^\circ\text{C}$ an increase of

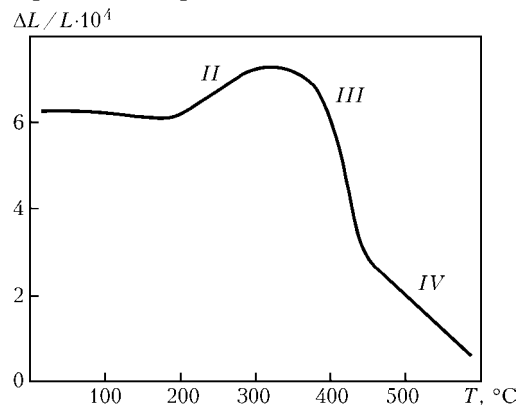


Figure 5. Differential dilatometric curve at weld metal heating: II-IV --- transformations at tempering

**Table 2.** Influence of short-time heating temperature T_h on HRC hardness and crack resistance τ_{fr} of butt joint on 30KhGSA steel

$\dot{O}_h, ^\circ\text{N}$	Weld HRC	Weld $a_n, \text{J/cm}^2$	τ_{fr}, min (fracture site)
Without heating	49	--	1.5–3.5 (weld)
1140–1250	38 41	--	1.5–9.0 (weld)
920–970	47	73	0.5–5.0 (weld)
800–840	27	122	--
630	35	111	--
480–550	--	--	55, no fr. (weld --- FZ with undercuts)
420–450	40	105	49 (weld --- FZ with undercuts)

Note. The following abbreviations are used: FZ --- fusion zone; no fr. --- no fracture.

martensite fraction up to 38 % at the expense of ferrite (7 %) in the structure of weld metal pre-quenched in water and increase up to 39 % of the fraction of bainite component at lowering of the fraction of martensite (39 %) and ferrite (12 %) components in the structure of pre-tempered weld metal are observed.

At lowering of heating temperature to 840–820 °C (in the intercritical temperature range) the austenite transformation in the weld metal is incomplete, and the structure, in addition to the newly formed austenite, preserves a significant amount of temper ferrite F_t . Decomposition of a reduced amount of austenite does not cause any essential change of the transformation temperatures. However, it leads to lowering of the amount of the formed martensite and increase of the total amount of the more ductile ferrite and bainite components of the structure. Heating to temperatures below A_{c1} is accompanied only by transformations at tempering, which may proceed completely and not be revealed already during the second heating.

Short-time heating of the weld metal lowers its hardness (Table 2), similar to HAZ metal [2], and increases the butt joint resistance to cold cracking. The greatest lowering of hardness and increase of impact toughness, respectively, are achieved at heating up to high tempering temperatures (630 °C) and in the intercritical temperature range (800–840 °C), which result in formation of a minimum amount of martensite and maximum amount of ferrite. Short-time arc heating up to tempering temperature (480–550 °C) leads to a considerable increase of crack resistance, right up to delayed cracking prevention at testing ($\sigma = 380$ –390 MPa). The highest hardness, lowest values of weld impact toughness and joint crack resistance are noted after small overheating above A_{c3} , when the maximum amount of martensite forms in the metal structure. Delayed cracking of the tested joint occurs predominantly along the weld, which is attributable to increased density of crystalline structure imperfections of the cast metal compared to rolled steel and its chemical inhomogeneity caused by

liquation of carbon, sulphur, phosphorus and other elements [11]. Such a feature is manifested stronger in single-layer welds with crystallites oriented towards each other. On the whole, the influence of short-time heating temperature on the change of the structure and properties of the weld and HAZ metal is similar. It is compensated by subsequent furnace treatment, including a relatively long-time soaking above A_{c3} , in particular, before hardening.

In conclusion, it should be noted that a peritectic transformation is observed at solidification of weld metal of steel 30KhGSA, which predetermines the increase of microchemical and microstructural inhomogeneity. Prevalence of the vertical component of solidification after penetration with the form factor of 4–6 causes an increase of the content of carbon, silicon, chromium and manganese in the weld metal at the surface.

Similarity of transformations of weld metal and overheated metal of the HAZ section close in their composition, predetermined obtaining a basically uniform M-B structure of the entire joint, on the whole, which is refined as a result of partial melting and short-time heating above A_{c3} in welding and arc treatment.

The hardened condition of the joint metal leads to lowering and fast heating to increase of the austenite transformation temperatures. Under the conditions of welding and arc treatment of the hardened metal of the joint and furnace heating of thermally softened steel these temperatures are close. After repeated short-time heating above A_{c3} the hardening structure is preserved in the weld and HAZ metal and the proportion of its components changes.

Phase transformations, structure and properties of the weld metal are controlled by the temperature and duration of short-time heating. At heating up to intercritical temperatures and tempering temperatures an essential lowering of the hardness, increase of impact toughness and cold cracking resistance is achieved. Furnace supercritical heating eliminates the difference in the welded joint properties.

1. Makarov, E.L. (1981) *Cold cracks in welding of alloy steels*. Moscow: Mashinostroenie.
2. Kulik, V.M., Vasiliev, V.G. (2006) Variations in structure and properties of HAZ metal in welded joints on 30KhGSA steel at arc treatment. *The Paton Welding J.*, **7**, 16–21.
3. Paton, B.E., Savitsky, M.M., Kuzmenko, G.V. (1994) Prospects of application of high-strength medium-alloy steels in welded high-pressure cylinders for motor transport. *Avtomatich. Svarka*, **3**, 4–9.
4. Popov, A.A., Popova, L.E. (1973) *Isothermal and thermokinetic diagrams of overcooled austenite decomposition*: Refer. Book. Moscow: Metallurgiya.
5. Shorshorov, M.Kh., Belov, V.V. (1972) *Phase transformations and variations of steel properties in welding*: Atlas. Moscow: Nauka.
6. Kulik, V.M., Savitsky, M.M., Novikova, D.P. et al. (2001) Argon-arc treatment of welded joints on 30KhGSA steel. *The Paton Welding J.*, **6**, 6–12.
7. Wendlandt, U. (1978) *Thermal methods of analysis*. Moscow: Mir.
8. Kulik, V.M., Savitsky, M.M. (2007) New procedure for evaluation of cold cracking resistance of hardening steel welded joints. *The Paton Welding J.*, **1**, 8–13.
9. Yatsenko, A.I., Repina, E.I., Grushko, P.D. (1988) Primary structure of peritectic steels. *Metallovedenie i Term. Obrab. Metallov*, **1**, 9–11.
10. Kolosov, M.M., Stroganov, A.I., Smirnov, Yu.D. et al. (1973) *Quality of killed steel ingot*. Moscow: Metallurgiya.
11. Prokhorov, N.N. (1986) *Physical processes in metals during welding*. Vol. 1. Moscow: Metallurgiya.



FEATURES OF MICROMECHANISM OF FRACTURE IN JOINTS OF ALUMINIUM-LITHIUM ALLOYS PRODUCED BY PLASMA WELDING

T.M. LABUR, A.A. GRINYUK, T.G. TARANOVA, V.A. KOSTIN and A.G. POKLYATSKY
E.O. Paton Electric Welding Institute, NASU, Kiev, Ukraine

Comparative analysis of fracture toughness of metal of welds in high-strength aluminium-lithium alloys 1420 and 1460 produced by plasma welding in the gravity position and with backing using serial welding wires SvAMg63 and Sv1201, has been carried out. Peculiarities of fracture micromechanism of welded joints in case of off-centre tension are determined on the basis of analysis of specimen fracture.

Keywords: plasma welding, aluminium-lithium alloys, welded joints, weld, fusion zone, technological backing, fracture resistance, fracture relief

Owing to a high specific strength and increased modulus of elasticity, application of aluminum-lithium alloys in structures of aerospace engineering allows reducing the weight of the latter by 8–15 % [1], this promoting increase of the payload and improvement of tactical and technical characteristics of welded structures --- elements of the load-carrying frame, frame rings, beams and wing spars. The above alloys are also applied in airframes, fuselage, and wings of the aircraft, their sheathing and panels.

Under the conditions of process heating, including the welding processes, the alloys with lithium additives become prone to embrittlement. Formation of nonuniform structure and softening in the heat-affected zone is observed in the metal of welded joints produced by different processes of arc (consumable and non-consumable electrode) and electron beam welding [2–4]. This is due to a multicomponent composition of the alloys and presence of strengthening phase inclusions located parallel to the rolling direction. Moreover, overheating of the metal in welding leads to development of nonuniformity in the joint by the content of alloying elements and impurities as a result of their segregation along the grain boundaries, as well as formation of brittle intergranular eutectic interlayers [5]. The associated increase of stress concentration on phase boundaries promotes crack initiation resulting from phase cracking or violation of the contact with the matrix, this lowering such integral indices as strength and toughness of the welded joints. It results in complication of the technology of sound fabrication of welded assemblies of structures and lowering of the reliability of item operation under the conditions of the impact of limit high loads and low temperatures [2, 6, 7].

Searching for rational thermophysical conditions of welding aluminium-lithium alloys is still conducted now. One of the technological solutions ensuring the reliability of joining the structural elements from alu-

minium-lithium alloys, is application of plasma arc welding. While providing a highly concentrated heat input into the weld pool, this welding process allows achieving a low overheating of the metal in the thermal cycle and a sound structure of weld metal [8, 9]. The welding process is performed using process backing with the forming grooves and without them (gravity welding with through-thickness penetration of the plasma jet).

To substantiate the effectiveness of performing plasma welding, it is necessary to determine the influence of the above technology variants on physico-mechanical properties and fracture mechanisms of the metal of welds in welded joints of aluminium-lithium alloys of different alloying systems --- 1420 (Al-Mg-Li) and 1460 (Al-Li-Cu). This is due to the fact that structure reliability following the principle of fault tolerance is determined not only by their strength limit, but also by the action of stresses causing cracking. Without investigation of the above properties of welded structures, assessment of their level and compliance with the service requirements, it is difficult to substantiate selection of materials and joining technologies.

Experimental procedure. Welded joints of aluminium-lithium alloys 1420 and 1460 of 4 and 3 mm thickness, respectively, were produced by plasma welding with a backing and in the gravity position [7]. Welding wires SvAMg63 and Sv1201 of 1.6 mm diameter were used as filler material (Table 1).

Before welding, the aluminium sheets and filler wires were subjected to chemical etching, and sheet edges --- to additional mechanical cleaning to the depth of not less than 0.1 mm. Use of asymmetrical square-wave current with prevalence of straight polarity current duration ensured an effective cathode breaking up of the oxide film during the thermal cycle of welding and high electrode resistance. Frequency of current polarity reversal was 100 Hz. Modes of plasma welding are shown in Table 2.

Plasma welding was performed using a system of process equipment of «Fronius» Company (Austria), which includes PT 450-02 WZ power source, KD 4000

**Table 1.** Composition of aluminium-lithium alloys 1420 and 1460 and filler wires used in welding, wt.%

Alloy and wire grade	Cu	Mg	Mn	Ti	Zr	Fe	Si	Other
<i>Alloys</i>								
1420	0.1	5.60	0.3	--	0.10	0.30	0.10–0.30	1.9 Li
1460	3.2	--	--	0.1	0.09	0.30	0.20	2.0 Li 0.1 Sc
<i>Welding wires</i>								
SvAMg63	0.1	6.30	0.5	0.1	0.20	0.05	0.05	--
Sv1201	6.1	0.02	0.3	0.1	0.15	0.15	0.08	0.1 V

feed mechanism for filler wire, PMW 350 plasmatron and FPA 2003 control system.

Fracture toughness indices were evaluated at off-center tension of samples using Kahn procedure, when uniaxial tension and bending are simultaneously applied to the metal, this simulating the operating conditions of the welded structure of load-carrying shell of a space rocket fuel tank [9]. Conditions of testing the welded joint samples corresponded to requirements of GOST 25.506. Loading rate did not exceed 2 mm/min ($3.3 \cdot 10^{-5}$ m/s). At off-center tension the load–deformation diagram was recorded in the oscillograph, where the moments of crack initiation and propagation in the studied sample up to its complete fracture were recorded. This allowed performing quantitative evaluation of stress intensity during deformation of welded joint samples and determining the specific work consumed in crack development. Experimental results were obtained on the base of testing five samples using an all-purpose RU-5 machine.

Proceeding from these results, the rated breaking stress σ_{fr} and critical coefficient of stress intensity K_c , as well as specific work of crack initiation (J_c -integral) and propagation (SWCP) were determined [2] (Table 3). Values J_c were evaluated by calculation of the function of the change of deformation energy, depending on crack length, using Merkle–Corten ratio [9–11]. Obtained data were compared with the respective values for the base metal.

Special features of the nature of fracture and crack initiation sections were determined by fractographic method in the JEOL scanning electron microscope JSM-840 with the system of microanalyzers at the accelerating voltage of 20 kV and electron beam current of 10^{-10} – 10^{-7} A in the secondary electron mode. The obtained information was systematized using modern computer technologies, including ImagePro 30 and Statistica 5.0 software. Comparative analysis of the results of studying the fracture relief of welds made

by two technology variants of plasma welding on alloys 1420 and 1460 and level of fracture resistance of welded joint samples allowed revealing the features of their microfracture at the stages of crack initiation and propagation.

Investigation results. Analysis of physico-mechanical properties of aluminium-lithium alloys 1420 and 1460 showed that they are characterized by close values not only of strength (337–360 MPa), but also of the critical coefficient of stress intensity both at longitudinal (28.1–33.2 MPa \sqrt{m}) and transverse (27.5–31.0 MPa \sqrt{m}) orientation of the samples relative to rolling direction (Table 3). In the first case, J_c values of both the alloys are equal to 4.1–5.0 J/cm², and in the second case --- 3.0–4.0 J/cm². SWCP of 1420 alloy varies in the range of 2.5–3.0 J/cm², and that of 1460 alloy --- 5.0–5.9 J/cm², which is indicative of the low ductility of the alloys with manganese. Presence of this element in the composition of 1420 promotes lowering of lithium solubility in the solid solution and thus ensures a considerable strengthening effect at heat treatment. However, the alloy ductility decreases [1].

Comparison of testing results of welded joints on aluminium-lithium alloys 1420 and 1460 made by plasma welding showed that samples made on a backing are characterized by a higher level of rated breaking stress σ_{fr} and energy value characterizing the work of crack initiation J_c than those made in the gravity position (Table 4). Increase of the rated breaking stress of samples of such welded joints is equal to 80–100 MPa, compared to those made without backing (322 MPa). Values of critical K_c , SWCP and KCV here are 1.5–2 times higher than in welded joints made in the gravity position. This may be an indication of more favourable thermophysical conditions for a sound

Table 3. Nature of variation of fracture resistance of aluminium-lithium alloys 1420 and 1460

Alloy grade	σ_{fr} , MPa	K_{fr} , MPa \sqrt{m}	J_c	J/cm^2	
				SWCP	KCV
1420	353/337	28.1/27.5	4.1/3.0	2.5/3.0	6.0/4.0
1460	360/339	33.2/31.0	5.0/4.0	5.0/5.9	8.0/6.0

Note. The numerator and the denominator give the data obtained at longitudinal and at transverse rolling direction, respectively.

Table 2. Modes of plasma welding of 1420 and 1460 alloys

Alloy grade	Welding speed v_w , m/h	Welding current I_w , A	Plasma gas flow rate Q_{pl} , l/min	Filler wire feed rate v_f , m/h
1460	36	180	0.1	123
1420	36	200	0.2	142



Table 4. Fracture resistance of welded joints in aluminum-lithium alloys produced by plasma arc welding

Alloy (wire) grade	Technology variant of welding	σ_{fr} , MPa	K_{Ic} , MPa \sqrt{m}	J_c	SWCP	KCV
				J/cm ²		
1420 (SvAMg63)	Gravity position	$\frac{303-341}{322}$	$\frac{45-50}{47.5}$	$\frac{6.8-7.3}{7.1}$	$\frac{9.6-10.7}{10.2}$	$\frac{7.2-7.6}{7.4}$
	On a backing	$\frac{379-428}{404}$	$\frac{26-35}{30}$	$\frac{5.3-12.4}{8.3}$	$\frac{5.3-7.5}{6.8}$	$\frac{4.4-7.9}{5.9}$
1460 (Sv2101)	Gravity position	$\frac{341-356}{322}$	$\frac{49-51}{50}$	$\frac{5.3-7.1}{7.1}$	$\frac{10.5-10.9}{10.7}$	$\frac{12.1-15.4}{13.8}$
	On a backing	$\frac{403-408}{403}$	$\frac{31-36}{35}$	$\frac{8.6-8.9}{8.8}$	$\frac{7.4-7.5}{7.5}$	$\frac{8.6-10.4}{9.5}$

weld formation in the studied aluminium-lithium alloys. In the metal of the welds made on alloy 1420, a homogeneous microstructure with a uniform arrangement of phase inclusions in the intercrystalline space forms, this ensuring the strength of welded joints on the level of 379–356 MPa and crack resistance of 26–35 MPa \sqrt{m} .

Proceeding from the values of strength and fracture resistance of welded joints of 1460 alloy, it is established that plasma arc welding both on the backing and without it can be used for its joining. A criterion for selection is the level of strength and coefficient of stress intensity required for the operation conditions. Use of the backing ensures weld metal strength on the level of 403–408 MPa. However, K_c values do not exceed 36 MPa \sqrt{m} , this, nonetheless, being close to

the value of this parameter for the base metal. When welding is performed without a backing, the strength of welded joint metal is equal to 341–356 MPa, and its crack resistance is 49–51 MPa \sqrt{m} .

Visual examination of fractures of broken base metal samples of alloys 1420 and 1460 revealed the presence of delaminations in it. The layers were located at an angle of 60–90° to the plane of the main crack. Relief microstructures of each individual layer had the shape of a chevron with a fine-folded (stepped or rippled) relief (Figure 1). Each of the studied layers contained both the areas of intergranular fracture, and quasi-cleavage fragments. Tough pits formed at fracture were small and underdeveloped, which is indicative of an insignificant plastic deformation of the metal at the moment of crack initiation. Pit edges are mostly

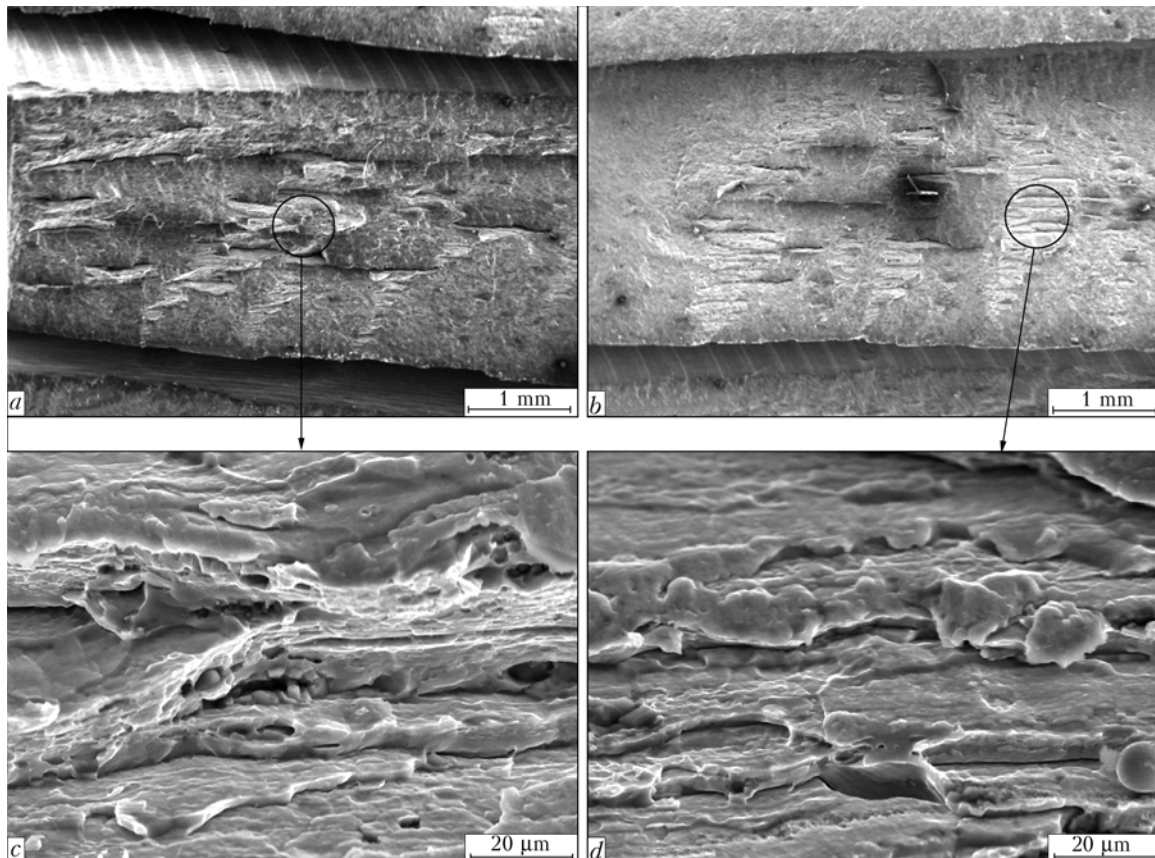


Figure 1. Delaminations on the fracture surface of alloys 1420 (a, c) and 1460 (b, d): a, c --- macroscopic image of the fracture; c, d --- steps on the delamination surface

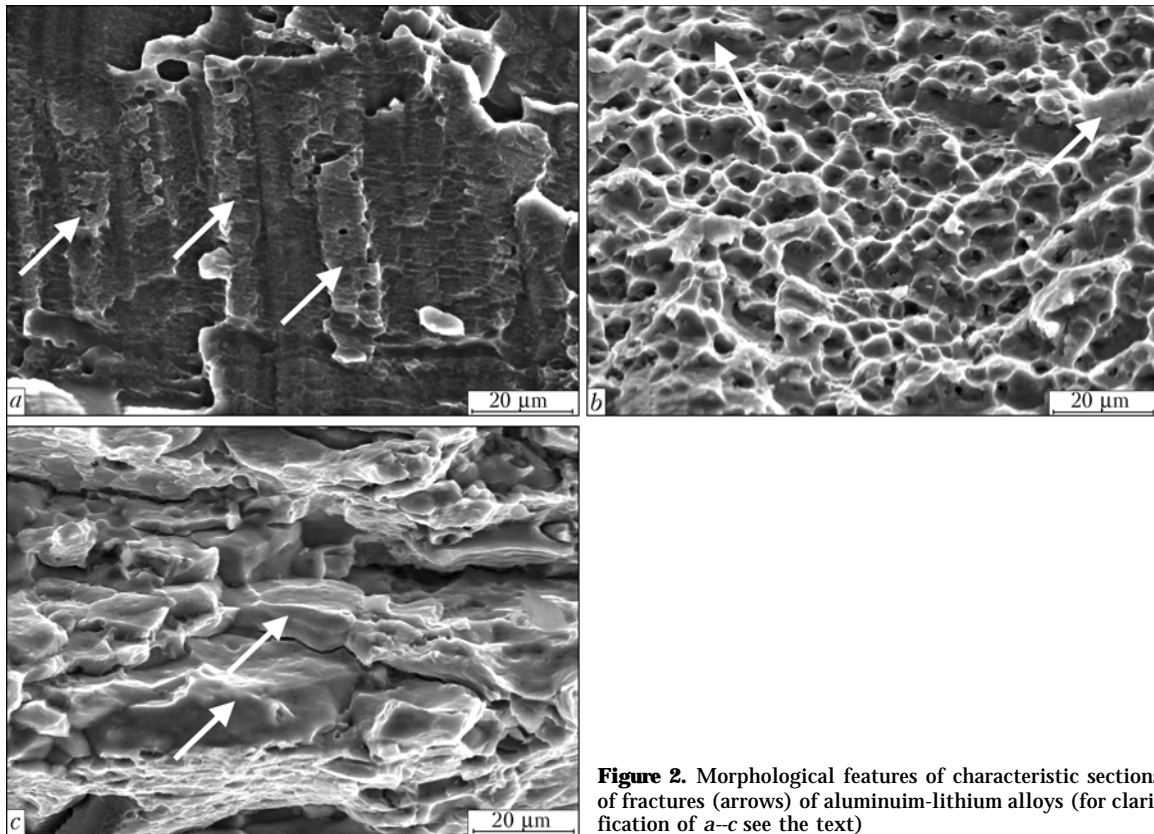


Figure 2. Morphological features of characteristic sections of fractures (arrows) of aluminum-lithium alloys (for clarification of a-c see the text)

oriented parallel to the semi-finished product rolling plane. Figure 2 shows the characteristic structural features of fracture of the studied alloys --- striated relief (Figure 2, a), pitted fracture with small flat areas (Figure 2, b), stone-like steps (2, c). Analysis of the features of the relief of base metal of alloys with lithium additives leads to the conclusion that the initial stage of their fracture depends on the volume fraction of phase precipitates. This is due to the complex composition of the alloys, level of the stressed state dependent on the mode of the metal heat treatment or machining, as well as the loading conditions in operation. Microcrack initiation in the alloys presumably proceeds as a result of running of several processes --- non-uniform plastic deformation in the grain bulk, its localizing near the boundary and interaction with the precipitates located in the intergranular space. As a result,

brittle particles of intermetallics phases crack and micropores develop in the form of shear pits, the shape of which is determined by the nature of the load impact at testing of alloys by off-center tension (Figure 3). The inner relief of the micropores differs from the main fracture by a more brittle structure. Quasi-cleavage prevails, which is related to multiaxial nature of the stressed state of the structure in the areas of the intermetallic phase location.

Microstresses developing in the metal on dissimilar phase boundaries make an additional contribution to the stressed state of the structure of both the alloys. They promote increased cracking of the most brittle areas of the structure and appearance of individual flat fragments forming as a result of transcrystalline rupture of the matrix-intermetallic phase boundaries, which also makes these structural sections the fracture sites. Microcrack coalescence and main crack formation occur at low SWCP values (see Table 3). The relief pattern has the form of step-like displacements caused by periodicity of the realized processes --- shear inside grains due to running of plastic deformation, and arresting of the microcrack front at the initial stage of its propagation along the grain boundaries (Figure 4).

A feature of the relief of 1420 alloy is a greater number of brittle fragments in the fracture compared to 1460 alloy, which is indicative of its lower ductility, which may be due to presence of magnesium lowering lithium and aluminium solubility and causing alloy oversaturation and susceptibility to nonuniform microplastic deformation of the structural components [1]. This is indicated by the presence of microtears in the fractures of 1420 alloy in the plane of contact of tougher phases with the matrix alongside the characteristic cracking of

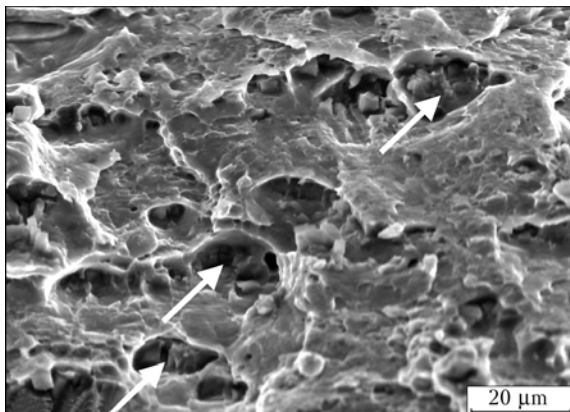


Figure 3. Micropores (shown by arrows) in the areas of fractured intermetallics phases in aluminum-lithium alloys

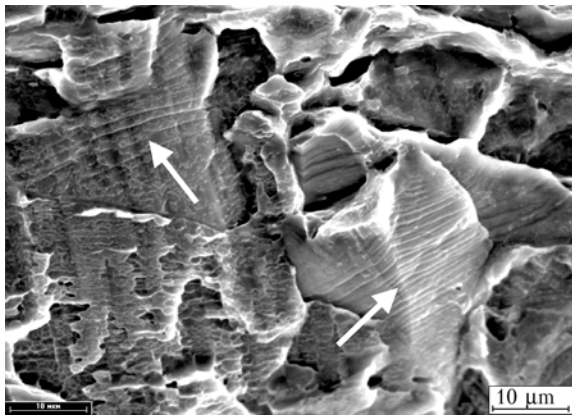


Figure 4. Bands of intensive deformations (shown by arrows) on the surface of fractures of alloy 1460

brittle inclusions of the intermetallics phases (Figure 5, *a*). Alloy fracture occurs predominantly through the bulk of brittle inclusions, and particularly in the points of grain junctions (Figure 5, *b*).

Analysis of fractures in welded joints of alloys 1420 and 1460 made on the technological backing shows that weld fracture runs by the tough mechanism, which is indicated by the presence of fine pits of 1.3 to 5.2 µm size (Figure 6, *a*, *b*). Ridges forming around them during plastic deformation of the metal are thinner in the joints of 1420 alloy. Flat sections of the relief characterizing the degree of weld structure embrittlement in welding take up approximately 30–35 % of the fracture area, which is by 10–15 % less than for alloy 1460. Cracks initiate on coarse phase particles and intermetallics inclusions located along the weld crystallite boundaries. Crack length is determined by the volume fraction of the structural component particles of the studied alloys in the initial state, as well as the conditions of the thermal cycle of welding. In both the alloys extended microcracks are observed in fractures of joints made on a backing. Such an effect can be related to formation of brittle intergranular interlayers of oversaturated phases during the thermal cycle, the appearance of which is due to an increased reactivity of the alloying elements and impurities at heating. This provokes development of a nonuniformity of their content along the weld crystallite boundaries, which creates prerequisites for a brittle initiation of microcracks.

Dimensions of facets in weld fractures in the joints made without using the technological backing vary between 3.1 and 11.5 µm (see Figure 2, *b*). The length of microcracks in the relief is 2–3 times smaller than in plasma arc welding on a backing. The fracture surface of the metal of a weld made on aluminium-lithium alloys has a much greater quantity of flat relief fragments. Note the significant differences in the structure of pits in fractures of welded joints produced by different variants of the technology. At fracture of welds of alloy 1420 made without a backing, the formed pits are shallow, and are limited by sharp ridges, which is indicative of realization of the quasicleavage mechanism during the main crack propagation, the formation of which requires low energy consumption and is ac-

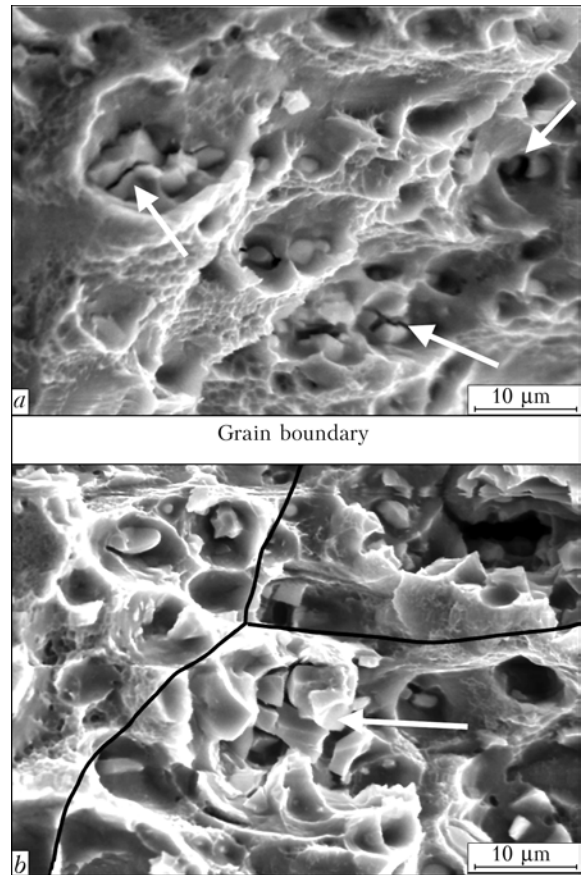


Figure 5. Intermetallic phases (marked by arrows) on the fracture surface of 1420 alloy (*a*) and in the points of junctions of three grains (*b*)

companied by low plastic deformation. The above fact can be due to overheating of the metal of alloy 1420 weld made by plasma arc welding without backing as a result of a low heat removal into the atmosphere. Deeper pits are found on the fractures of welded joints made on a backing, while the ridges at their edge are clear-cut. This is indicative of completion of plastic deformation of a sample at the stage of crack propagation and realisation of more rational thermophysical conditions with this variant of the technology, which are required for a sound formation of permanent joints.

Relief pits on fractures of 1460 alloy welded joints produced in welding both in the gravity position and on a backing, are mainly equiaxed with steps formed as a result of plastic shear at off-center tension (see Figure 3). Pit size varies from 1 to 10 µm. Ridges around the facets are better developed than with the same process of welding on a backing, their width being between 0.5 and 1.0 µm. Ridge orientation is of a random nature and is independent on the direction of the applied load. The area of flat regions of the welded joint produced by plasma welding in the gravity position is by 10–15 % less than with the same welding process on a backing. The length of microcracks formed during the main crack propagation, is 2 times smaller. The fracture relief of welded joints of 1460 alloy is typical for ductile materials, which are characterized by high-energy fracture by the tough mechanism [9–11].

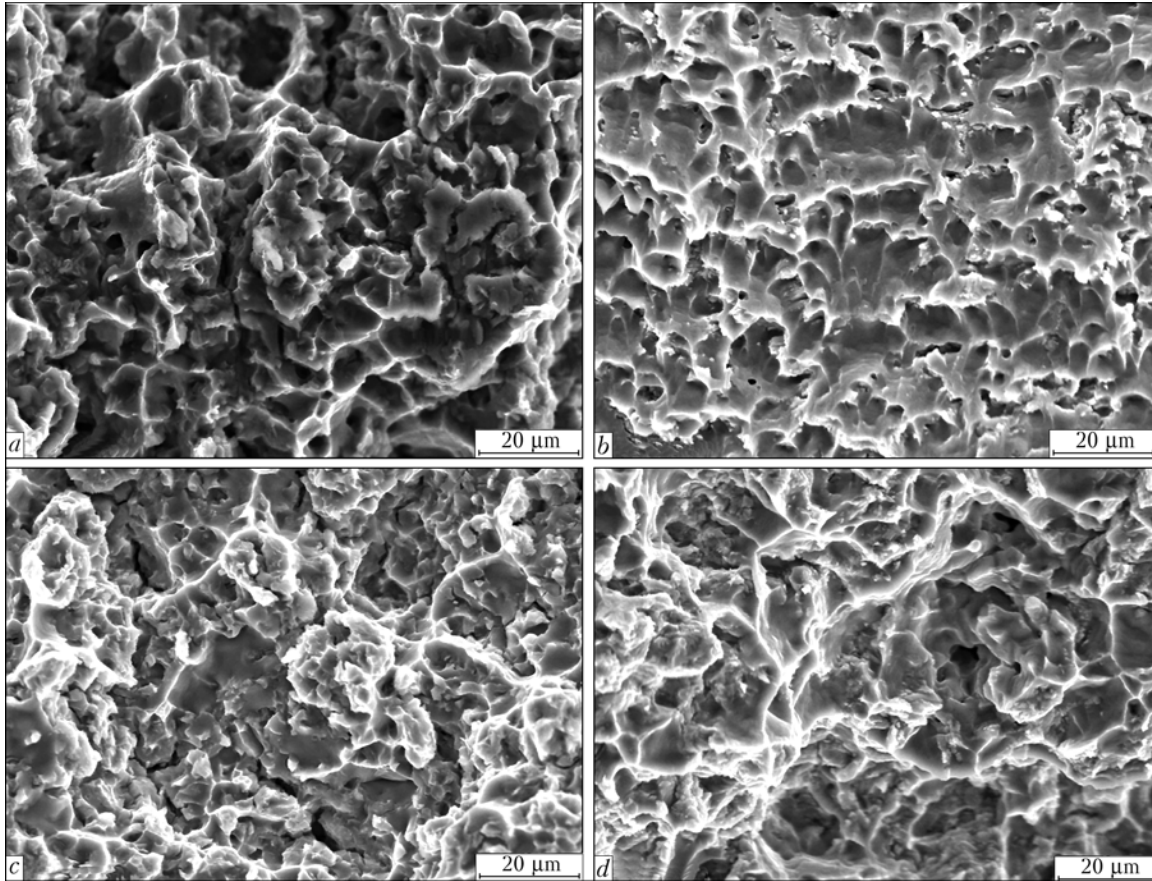


Figure 6. Fractograms of fracture surface of welded joints of alloys 1420 (a, b) and 1460 (c, d) produced by plasma welding on a backing (a, c) and in the gravity position (b, d)

CONCLUSIONS

1. It is established that aluminium-lithium alloys 1420 (Al-Mg-Li) and 1460 (Al-Cu-Li) are characterized by close values of the critical stress intensity factor both at longitudinal (28.1–33.2 MPa√m), and at transverse (27.5–31.0 MPa√m) orientation of the sample relative to the rolling direction. Nominal stresses, at which the base metal fracture occurs, are also close in value and are in the range of 337–360 MPa. At longitudinal orientation, J_c values of both the alloys vary in the range of 4.1–5.0 J/cm², and at transverse orientation — in the range from 3.0 to 4.0 J/cm². SWCP of alloy 1420 is equal to 2.5–3.0 J/cm², and that of alloy 1460 to 5.0–5.9 J/cm².

2. Use of technological backing in plasma arc welding of alloy 1420 enables formation of a more uniform structure of the weld metal, the quantity of brittle interlayers is reduced 2–3 times, which promotes an increase of strength by 80–100 MPa, and increase of K_c and J_c values by 15–20 %, and of KCV — by 1.5 times, compared to the weld made without backing. The sites of crack initiation are coarse phase particles and intermetallics inclusions located along the boundaries of weld crystallites.

3. For a joint of 1460 alloy it is recommended to use both of the studied technology variants of plasma welding. In the first case, the weld metal strength is equal to 403–408 MPa, and K_c values do not exceed 36 MPa√m; in the second case it is not more than

341–356 MPa, and crack resistance — 49–51 MPa√m. Irrespective of application of the technological backing, the fractures in both the variants of welding have a relief typical for ductile materials, which forms at high-energy fracture running by the tough mechanism.

1. Fridlyander, I.N., Chuistov, K.V., Berezina, A.L. et al. (1992) *Aluminium-lithium alloys. Structure and properties*. Kiev: Naukova Dumka.
2. Fridlyander, I.N., Bratukhin, I.N., Davydov, V.G. (1992) Aluminium-lithium alloys for welded aircraft structures. *Metally*, **3**, 117–119.
3. Rabkin, D.M., Lozovskaya, A.V., Sklabinskaya, I.E. (1992) *Metals science of welding of aluminium and its alloys*. Kiev: Naukova Dumka.
4. Labur, T.M., Bondarev, Andr.A., Lozovskaya, A.V. et al. (2001) Influence of welding process on fracture resistance of joints in aluminium-lithium alloys 1420 and 1460. *The Paton Welding J.*, **7**, 11–15.
5. Ryazantsev, V.I. (2005) Welded structures of aluminium alloys with lithium. *Aviats. Promyshlennost*, **2**, 32–41.
6. Khertsberg, R.V. (1989) *Deformation and fracture mechanics of structural materials*. Ed. by M.L. Bernshtejn, S.P. Efimenko. Moscow: Metallurgiya.
7. Labur, T.M. (2003) Increase in reliability of welded joints of aircraft engineering structures from aluminium-lithium alloys. *Tekhnol. Sistemy*, **2**(18), 71–79.
8. Poklyatsky, A.G., Grinyuk, A.A. (1999) Stability of the process of plasma welding of aluminium alloys by penetrating arc. *Avtomatich. Svarka*, **4**, 42–46.
9. Bogdanov, G.Ya., Eryshev, O.N., Kozlov, L.M. et al. (2001) Specifics of plasma-arc welding of hull aluminium alloys at direct current of reverse polarity. *Voprosy Materialovedeniya*, **1**(25), 35–45.
10. Nott, J. (1979) Fracture micromechanism and crack resistance of structural alloys. In: *Fracture mechanics*. Vol. 17. Moscow: Mir.
11. (1973) *Fracture*. Vol. 17: Microscopic and macroscopic principles of fracture mechanics. Ed. by G. Libovits. Moscow: Mir.



MATHEMATICAL MODELLING OF THERMAL STRAIGHTENING OF CYLINDRICAL SHELLS AND SHAFTS WITH DISTORTIONS ALONG THEIR LONGITUDINAL AXIS

O.V. MAKHNENKO and A.F. MUZHICHENKO
E.O. Paton Electric Welding Institute, NASU, Kiev, Ukraine

Numerical study of the deformed state of cylindrical shells in local heating was performed using thermoplastic analysis and finite element method. Calculation algorithms and procedure for determination of parameters of thermal straightening, based on the approximate method of shrinkage function, were developed. The procedure was used for thermal straightening of long cylindrical shells with general distortion deformations of their longitudinal axis caused by circumferential butt welds, as well as straightening of long auger shafts with longitudinal deflection deformations.

Keywords: welded cylindrical shells, deformations, thermal straightening, numerical study, calculation algorithms, procedure

Inadmissible general distortion deformations of longitudinal axis may result from welding heating in manufacture of long cylindrical shells, or from the effect of different factors in operation. These deformations are caused either by a local effect, e.g. deflection of the shell axis due to welding of the circumferential weld, or by an effect distributed along the length of the shell, which leads to its uniform bending. Thermal straightening can be used as one of the methods for decreasing such deformations down to a permissible level [1, 2]. This method has been little studied as yet for structures of cylindrical shells, and has not been used in practice.

Numerical study of the deformed state (residual plastic strains and general shape changes) of cylindrical shells in local heating using thermoplastic analysis and finite element method (FEM) was carried out to investigate the possibility of applying thermal straightening to cylindrical structures, and to determine optimal heating parameters [3].

However, prediction of general distortion deformations of axis of a long cylindrical shell as a result of local heating, based on a general approach of the theory of thermoelastoplasticity and FEM, is now a very complicated problem, which requires development of a 3D mathematical model and substantial computation facilities to find a solution. But as selection of parameters of the heat effect in thermal straightening should be done promptly and, desirably, in real-time, the calculation algorithms and procedure were developed for determination of parameters of thermal straightening, based on the approximate method of shrinkage function [4].

The above procedure was applied to advantage in practice of thermal straightening of long cylindrical shells, having general distortion deformations along the longitudinal axis, which were caused by circum-

ferential butt welding, as well as of long auger shafts, having longitudinal deflection deformations.

Numerical study of the deformed state of cylindrical shells in local heating. The study was carried out for conditions of thermal straightening of long auger shafts with longitudinal deflection deformations. As the shafts under investigation are hollow, a cylindrical shell (Figure 1) with inside diameter corresponding to that of a shaft ($D_{in} = 50$ mm), and outside diameter set to be equal to the average diameter of the auger profile ($D_{out} = 92$ mm), was selected as a mathematical model. To reduce the calculation time, length of the model of a cylindrical shell, made from stainless steel 20Kh13, was limited to 100 mm. Heating of a strip on the outside surface of the shell was simulated by a heat flow distributed along the strip length. The maximal temperature of heating was 650 °C.

To illustrate, Figure 2 shows the results of calculations of distribution of temperature on the outside surface of the shell (Figure 2, a) and across the section through the wall thickness (Figure 2, b) at the moment of the end of heating a strip with length $L_q = 90$ mm and width $B_q = 10$ mm. Power of a distributed heat source was $P_q = 27$ kW, heating time was $t_q = 30$ s, and its maximal temperature was $T_{max} = 600$ °C. Because of a substantial wall thickness (21 mm) of the

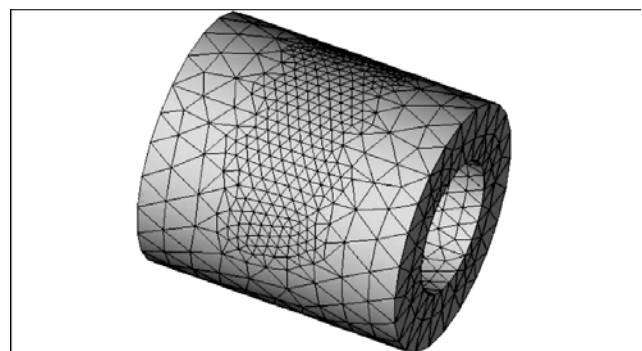


Figure 1. Model of cylindrical shell with finite element mesh deposited on it

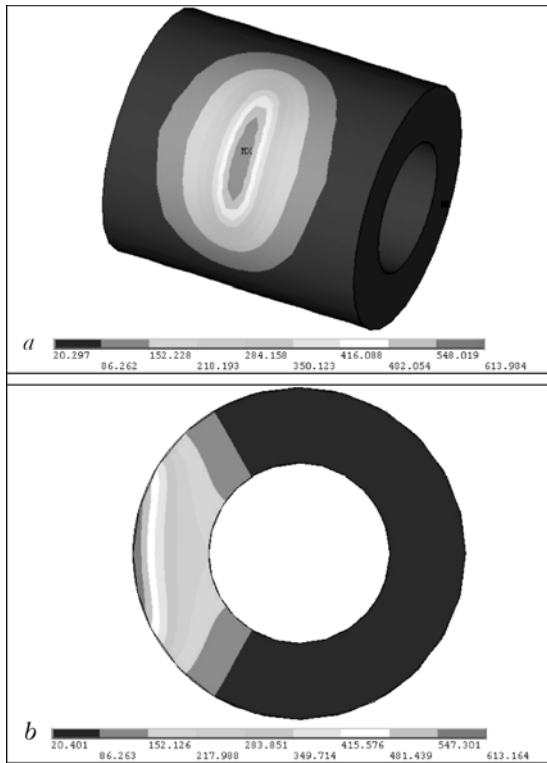


Figure 2. Distribution of temperature at the end of heating strip on outside surface of shell (a) and in its cross section through wall thickness (b)

shell, the distribution of temperature through the wall thickness was non-uniform (see Figure 2, b). Accordingly, as shown by experiments, residual stresses (Figure 3, a) and plastic strains (Figure 3, b) in a cross section of the cylindrical shell were also distributed non-uniformly: they were formed mostly in the surface layer of the shell wall. Total residual deflection of the shell with a certain assumption can be determined on its outside surface on the opposite side of heating (Figure 4). This deflection is insignificant (up to $W = -0.001$ mm), which is explained by high rigidity of the shell and small length of the model. Corresponding bend angle of the shell axis, $\alpha = 2 \arcsin (W/50) = 4 \cdot 10^{-5}$ rad, can be estimated from the deflection. Along the length of the shaft equal to 2000 mm, this heating provides a 0.02 mm decrease in the total deflection.

Series of calculation experiments was conducted to determine residual bend angle α of axis of a cylindrical shell depending upon length L_q and width B_q of the strip, as well as time t_q of heating to maximal temperature $T_{max} \approx 650$ °C. The calculation results given in Table 1 prove that the bend angle of the shell axis grows much with increase in the heating length and width, as well as the time of heating to the maximal temperature. The calculation results obtained were used to carry our thermal straightening of long auger shafts with general longitudinal deflection deformations.

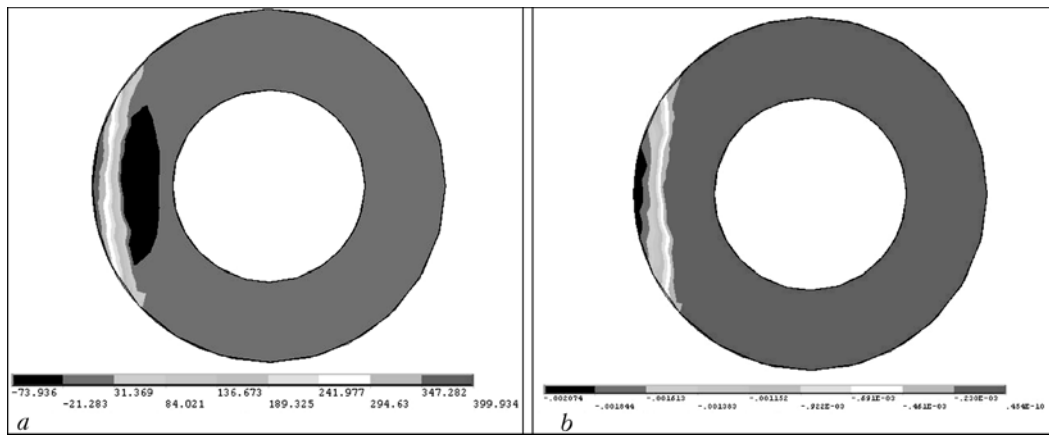


Figure 3. Distribution of residual stresses (a) and plastic strains (b) along the heating strip across the shell section

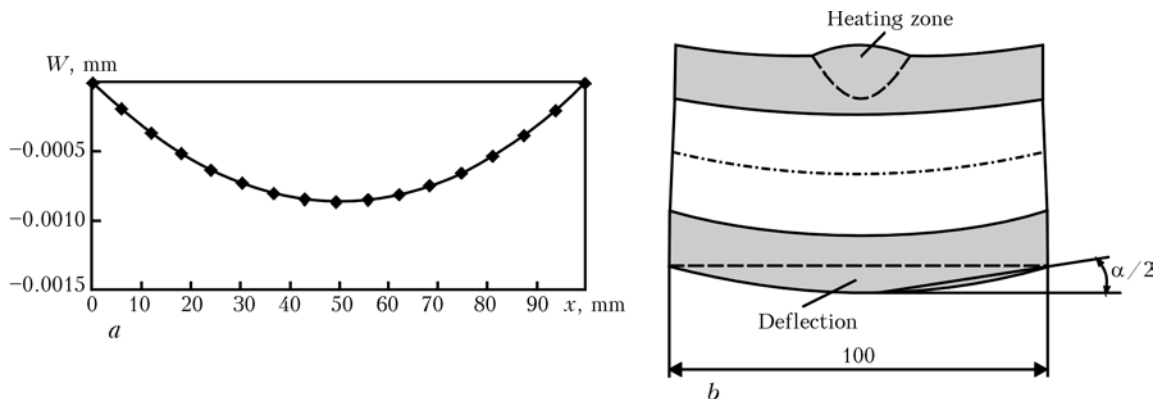


Figure 4. Curve of general deflection W of cylindrical shell on its outside surface on the opposite side of heating (a), and schematic of general deflection of the shell model (b): x — coordinate along generating line of the shell



Table 1. Results of calculation of bend angle α of shell axis in different modes of thermal straightening

Straightening No.	β , deg	L_q , mm	B_q , mm	P_q , kW	t_q , s	T_{max} , °N	$W_{max} \cdot 10^3$, mm	$\alpha \cdot 10^5$, rad
1	25	40	10	1.280	30	640	0.16	0.64
2	38	62	10	2.340	10	649	0.21	0.84
3	38	62	10	1.500	30	667	0.45	1.80
4	38	62	10	1.500	60	642	0.67	2.70
5	56	90	10	2.520	30	640	0.35	1.40
6	56	90	10	2.025	61	632	0.72	2.90
7	56	90	20	2.700	61	650	1.00	4.00

Note. β --- angle determining length of a heating strip.

Calculation procedure for determination of thermal straightening parameters based on the approximate method of shrinkage function. Figure 5 shows schematic of unclosed circumferential heating of a long cylindrical thin-walled shell with radius R and wall thickness δ . Here AB is the heating strip providing transverse shrinkage due to the heating strip, Δ_{tr} , in a free state. The dashed line designates the zone with width D , where the transverse shrinkage tensile forces are effective:

$$N_{xx} = \int_{-\delta/2}^{\delta/2} \sigma_{xx} dz, \quad N_{xx} = \frac{E}{1+\nu} [\varepsilon_{xx} + \nu \varepsilon_{\beta\beta} - \varepsilon_{xx}^P], \quad (1)$$

where ε_{xx} and $\varepsilon_{\beta\beta}$ are, respectively, the strains along axis x and on the circumference on a mean surface of the shell, $z = 0$; E is the Young modulus; and ν is the Poisson ratio;

$$\varepsilon_{xx}^P \approx -\frac{\Delta_{tr}}{b} \quad (2)$$

is the free shrinkage deformation on a base of width b of the plastic deformation zone.

If we ignore the $\nu \varepsilon_{\beta\beta}$ value and use the hypothesis of flat sections, i.e.

$$\varepsilon_{xx} = \varepsilon_{xx}^0 + \chi R \cos \beta, \quad (3)$$

where ε_{xx}^0 is the deformation of the mean surface, and $\chi = -\partial^2 W / \partial x^2$ is the curvature of the shell axis, then the equations of equilibrium for section $x = \text{const}$ will have the following form:

$$\int_0^{2\pi} N_{xx} d\beta = \frac{E}{1+\nu} [2\pi \varepsilon_{xx}^0 - 2\alpha \varepsilon_{xx}^P] = 0;$$

$$\int_0^{2\pi} N_{xx} R \cos \beta d\beta = 2 \frac{E}{1+\nu} [\chi R^2 \frac{\pi}{2} - \varepsilon_{xx}^P R \sin \beta] = 0.$$

Hence,

$$\varepsilon_{xx}^0 = \varepsilon_{xx}^P \frac{\beta}{\pi}, \quad \chi = \frac{2\varepsilon_{xx}^P \sin \beta}{\pi R}. \quad (4)$$

Curvature χ of the shell axis is a function of coordinate x .

Therefore,

$$\chi = \chi(x) = -\frac{\partial^2 W}{\partial x^2}. \quad (5)$$

Unknown bend angle α of the shell axis is

$$\alpha = \frac{\partial W}{\partial x} = -\int_{-D}^D \chi(x) dx = \frac{-2\varepsilon_{xx}^P \sin \beta}{\pi R} 2D. \quad (6)$$

Using dependence (2) for ε_{xx}^P and assuming that $b = \delta K_1$ and $D = \delta K_2$, yield

$$\alpha = \frac{2\Delta_{tr} \sin \beta}{\delta K_1 \pi R} 2\delta K_2 = \frac{4\Delta_{tr} \sin \beta}{\pi R} K_3, \quad (7)$$

where $K_1 - K_3 = K_2 / K_1$ are the calculation-experimental coefficients.

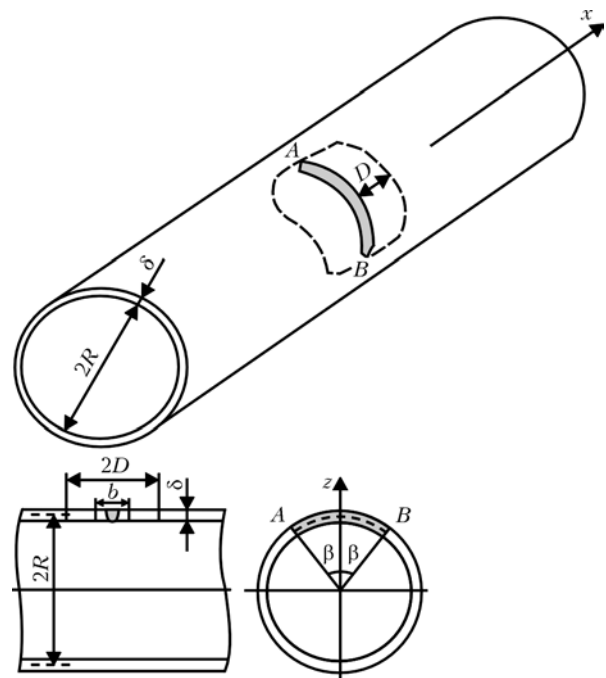


Figure 5. Schematic of unclosed circumferential heating of cylindrical thin-walled shell (see explanations in the text)

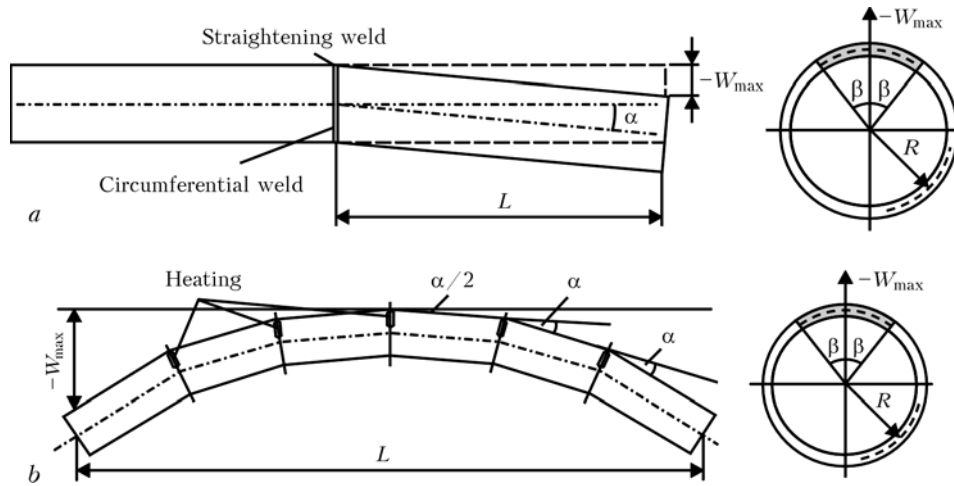


Figure 6. Schematic of thermal straightening of cylindrical shell by heating in locations of deflection, which is uniform along the length of deformation of longitudinal bend (a), and stepwise deflection, consisting of N heating strips (b)

Algorithm for selection of heating parameters in thermal straightening. If the cylindrical shell has a longitudinal bend caused by any local effect (Figure 6, a), e.g. deflection of the shell axis due to circumferential welding, straightening should be performed by heating a strip in the location of deflection of the axis. Position of this heating is selected so that the angular coordinate of the centre of heating is equal to the coordinate of maximal flexure of the shaft, $-W_{max}$. Length of the heating strip is determined through angle β using the following relationship:

$$\sin \beta = \frac{\pi R}{4\Delta_{tr}K_3} \alpha, \quad (8)$$

where $K_3 \approx 1-2$, and $\alpha = W_{max}/L$.

If the cylindrical shell has a bend that is uniform along the length, with deflection W_{max} (Figure 6, b), straightening should be performed using a set of N heating strips uniformly distributed along length L of the shell. In this case, length of the heating strips is determined through angle β using the following relationship:

$$\sin \beta = \frac{\pi R}{4\Delta_{tr}K_3} \frac{4W_{max}}{L(1 + (N - 1)N)}. \quad (9)$$

Thermal straightening of cylindrical shell. Experiments on thermal straightening of distortion de-

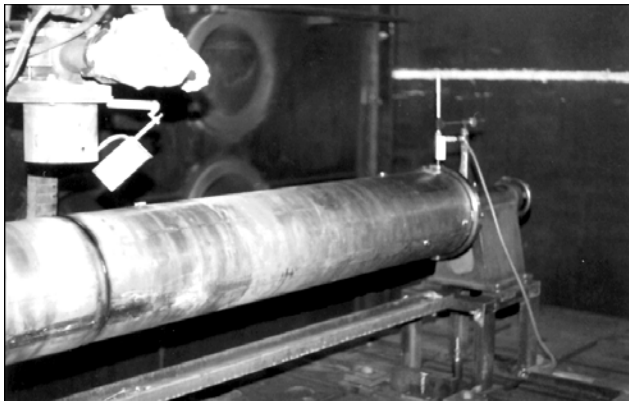


Figure 7. Thermal straightening of long shell of alloy VT-1 with distortion deformations of longitudinal axis

formations of axis of a cylindrical shell made from titanium alloy VT-1 and assembled of three sections 2 m long, 350 mm in diameter and with a wall thickness of 6 mm (Figure 7), were conducted using electron beam welding (EBW) and the developed calculation algorithm. As distortion deformations along the axis may be induced by circumferential butt welding, it was decided to straighten the shell by depositing unclosed beads on the location of a circumferential weld. Firstly, this does not add any new melting zones and heat-affected zones to the shell. Secondly, as determined by experimental measurement of the deformations formed in EBW of plates, the subsequent weld beads have the transverse shrinkage close to that of the first bead, i.e. repeated heating does not practically decrease the efficiency of thermal straightening.

The purpose of the experiments was to verify the developed procedure for thermal straightening of general distortion deformations of axis of a long cylindrical shell, and experimentally check the values of coefficient K_3 in the developed calculation algorithm for the given shell and EBW conditions.

In this connection, unclosed circumferential welds of different lengths were made in the location of a circumferential butt weld. Half-length of the weld in straightening was set by angle β . Location of these welds was chosen on the basis of the results of measurements of distortion deformations of axis of the shell: the angular coordinate of the centre of a weld bead was equal to the coordinate of maximal deviation of the shell with a minus sign. The higher-power EBW parameters were chosen for these welds, compared with standard welding parameters for making a circumferential butt weld, so that the size of HAZ was not in excess of the already existing zone formed in making the circumferential butt weld. Based on the results of the measurements of flat specimens, the chosen EBW parameters correspond to transverse shrinkage $\Delta_{tr} = -0.15$ mm in thermal straightening.

The system allowing measurements of distortion deformations of axis directly in a vacuum chamber was developed to check accuracy of the welded cylindrical shell. Measurements of the deformations, as



Table 2. Experimental data on thermal straightening of cylindrical shell

Straightening No.	β , deg	W, mm (before straightening)	W, mm (after straightening)	Variation in deflection ΔW , mm	K_3
1	15	1.26	0.50	0.76	1.49
2	15	2.04	1.16	0.88	1.72
3	30	3.16	1.90	1.26	1.28
4	30	2.36	0.79	1.57	1.60
5	60	3.21	0.55	2.66	1.56
6	60	0.75	-2.20	2.95	1.72
7	75	4.14	1.00	3.14	1.65
8	85	4.85	2.04	2.81	1.45

well as the thermal straightening process, were displayed on the monitor screen. Deviation of the shell from straightness was measured at a distance of 1800 mm from the circumferential weld. The measurements were conducted before making the straightening weld, and after complete cooling of the shell. Their results are given in Table 2.

Results of the experiments showed the high efficiency of the new method for thermal straightening of distortion deformations of axis of a long cylindrical shell, and proved the assumption made in the developed calculation algorithm that $K_3 \approx 1-2$. Table 2 gives experimental values of coefficient K_3 , obtained by using formula (8) for the welds of different lengths in straightening. It can be seen from these values that for a given shell and chosen welding parameters the coefficient in straightening can be assumed with a sufficient accuracy to be equal to $K_3 = 1.5$. Therefore, the developed calculation algorithm can be effectively applied to determine the required length of a weld for straightening the measured distortions along the axis of a shell.

The experimental results are characterised by a sufficient accuracy of repeatability. The developed thermal straightening procedure allows substantial distortion deformations of axis of long shells to be decreased to the required level, and in one try in the majority of cases. However, if as a result of the first try the distortions are not decreased to the required level, deposition of subsequent weld beads, the length of which should allow for variations in the distortions, will provide a successful completion of the straightening process.

Thermal straightening of long shafts. General deflection deformations of long (2000 mm) auger shafts, caused by non-uniform heating as a result of emergency interruption of the technological process, were decreased to a permissible value of deflection (1 mm) using thermal straightening, which was realised by making several heating strips (600–650 °C) of a certain length, uniformly distributed along the length of the shaft (see Figure 6, b). Position of heating was chosen on the basis of the results of measurements of deflec-

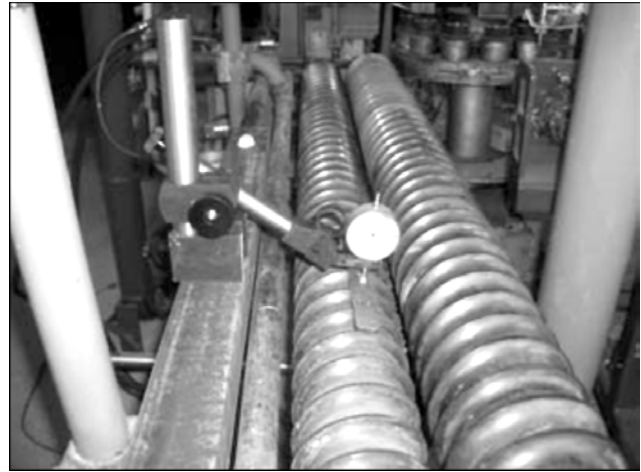


Figure 8. Variations in deflections of auger shafts 2000 mm long, made from stainless steel 20Kh13

tion deformations of axis of the auger, so that the angular coordinate of the centre of heating was equal to the coordinate of maximal deflection of the shaft, $-W_{max}$. Length of the heating strips can be very effective at $L_q \approx (0.1-0.2)2\pi R$, but providing that it is no more than half the length of the shaft circumference ($L_q < \pi R$).

After performing a series of heatings, deflection of the shaft (Figure 8) should be measured only after it fully cools down. If as a result of the first try of thermal straightening the deflection deformations of axis of the shaft do not decrease to the required value, the straightening process can be successfully completed by the method of progressive approximation through additional heatings.

Thermal straightening of two auger shafts 2000 mm long, having maximal deflections of 4.0 and 2.8 mm (Figure 9), was performed using the developed procedure. The gas-flame torch was used as a heat source. The values of transverse shrinkage for a 40 mm thick flat specimen of stainless steel, resulting from corresponding heating with the gas-flame torch, were obtained from approximation formulae taken from study [1]. They were $\Delta_{tr} \approx -0.02$ mm. According to



Figure 9. Unclosed circumferential heating with gas-flame torch in thermal straightening of auger shaft

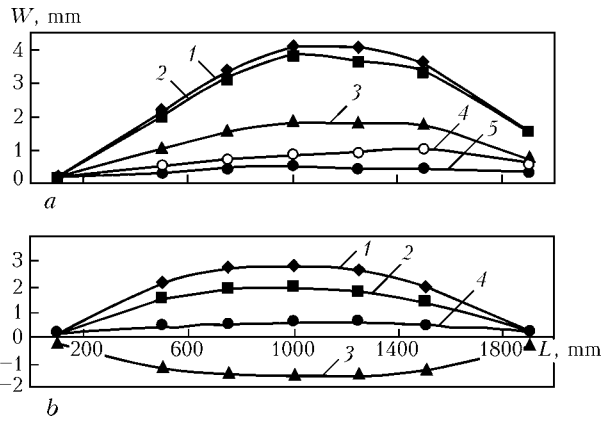


Figure 10. Results of measurements of deflections along the length of shafts 1 (a) and 2 (b): 1 — before straightening; 2 — after the first series of heating (5 heatings); 3 — after the second series of heating (10 heatings); 4 — after the third series of heating (8 heatings); 5 — after the fourth series of heating (5 heatings)

the developed procedure and formula (9), for straightening of a shaft 2000 mm long, having deflection of about 3–4 mm, it is necessary to perform several dozens of such heatings. Results of thermal straightening of the shafts proved in practice the efficiency of the developed procedure.

Figure 10 shows the results of measurements of deflections along the length of the shafts before and after thermal straightening. After the latter, the values of deflections decreased to 0.5 and 0.7 mm, respectively, which corresponded to the allowance (1 mm) for deflection of an auger shaft.

CONCLUSIONS

1. Numerical study of the deformed state (residual plastic strains and general shape changes) of cylindrical shells in local heating, performed by using thermoplastic analysis and finite element method, showed the possibility of successful application of thermal straightening for cylindrical structures with general distortion deformations of longitudinal axis of a shell. However, determination of optimal heating parameters by this method is labour- and time-consuming.

2. The developed calculation algorithm and procedure for determination of optimal parameters of thermal straightening on the basis of the approximate method of shrinkage function make it possible to decide in real time on the choice of parameters of the heat effect in performing thermal straightening to eliminate distortion deformations of axis of a cylindrical shell.

3. Experimental verification of thermal straightening to eliminate general distortion deformations of axis of long cylindrical shells and auger shafts proved efficiency of the developed thermal straightening procedure.

1. Kuzminov, S.A. (1974) *Welding strains of ship hull structures*. Leningrad: Sudostroenie.
2. Mikhajlov, V.S. (1972) *Straightening of welded ship hull structures*. Leningrad: Sudostroenie.
3. Makhnenko, V.I. (1976) *Calculation methods for investigation of kinetics of welding stresses and strains*. Kiev: Naukova Dumka.
4. Makhnenko, V.I., Velikoivanenko, E.A., Pochinok, V.E. et al. (1999) Numerical methods for the predictions of welding stresses and distortions. In: *Welding and Surfacing Rev.*, Vol. 13, Part 1. Harwood A.P.

EXPERT SYSTEM FOR DESIGN OF MECHANISED ELECTRIC ARC SURFACING TECHNOLOGIES



Selection of group of parts on the basis of their service conditions and types of wear

Purpose. The system is intended for design of surfacing technologies for a wide range of parts subject to repair because of wear or requiring initial deposition of coatings. The system allows selection of surfacing consumables, methods, procedures and parameters for parts of the types of bodies of revolution or parts with a flat surface, depending upon their dimensions, service conditions and types of wear. Recommendations on the surfacing technology offered by the expert system to a user are based on the expertise of highly skilled specialists in electric arc surfacing.

The system software includes an off-line database editor, which allows a user to update the databases of surfacing consumables, information on their welding-technological properties and chemical composition of deposited metal. Results of design of a surfacing technology are documented in the form of a flow sheet and stored in a databank of technical designs, thus generating the bank of technologies for surfacing of parts from a range of those manufactured by a given engineering enterprise.

The system is intended for a wide range of users dealing with development of surfacing technologies for machine-building enterprises, design bureaus and educational institutions.

Application. The system is intended for design of surfacing technologies for machine parts and mechanisms operating in different industries, such as mining, metallurgical, chemical, transportation, agricultural, etc. It can be used in an educational process.

Contacts: Prof. Makhnenko V.I.
E-mail: d34@paton.kiev.ua



MATHEMATICAL MODEL OF TRANSPORTATION OF HYDROGEN BY EDGE DISLOCATION*

A.V. IGNATENKO

E.O. Paton Electric Welding Institute, NASU, Kiev, Ukraine

Suggested is the model of transportation of hydrogen atoms by edge dislocation, based on the theory of diffusion. An equation of hydrogen diffusion in the field of a moving edge dislocation is proposed, which allows calculation of the amount of hydrogen transported by the dislocation depending upon the metal temperature, velocity of the edge dislocation, and concentration of free hydrogen. As shown by numerical calculations, transfer of hydrogen by the edge dislocation has maximum at a temperature close to the normal one. The results obtained are in good agreement with peculiarities of reversible hydrogen-induced brittleness.

Keywords: arc welding, high-strength steels, welded joints, reversible hydrogen brittleness (RHB), transportation of hydrogen, edge dislocations, temperature and velocity dependence of RHB

Hydrogen is known to have a negative effect on strength of steel welded structures. Reversible hydrogen brittleness (RHB) is a special case among other types of hydrogen-induced embrittlement of welded joints in high-strength low-alloy steels. For welding, it is important that RHB starts showing up as early as at very low hydrogen concentrations ($< 10 \text{ cm}^3/100 \text{ g}$) and leads to a substantial decrease in strength and reliability of the entire welded joint. Also, RHB is characterised by an experimentally established [1, 2] temperature and velocity dependence of the degree of hydrogen-induced embrittlement of metal. RHB is most pronounced at metal temperatures close to the normal temperature. Decrease or increase of temperature causes mitigation of the negative effect of hydrogen. Another necessary condition for RHB to occur is the presence of plastic deformation formed in a welded joint under the effect of external or residual stress. As shown by experiments, increase in the rate of deformation of metal leads to decrease in the negative effect of hydrogen, while at high deformation rates the metal fractures at the same stress as without hydrogen.

Studies [1–3] suggest the model of reversible brittleness, the key point in the mechanism of which is behaviour of an embryo sub-microcrack that interacts with hydrogen. The main role in this case is played by dislocations, the movement of which is an elementary event of plastic deformation that leads to initiation of a sub-microcrack and, at the same time, is the most effective way of transportation of hydrogen into this crack. This process is very difficult to study experimentally. Therefore, it is necessary to employ numerical methods to gain a better insight into the processes occurring in RHB.

*The study was performed under the supervision of Prof. I.K. Pokhodnya, Academician of the NAS of Ukraine.

The term «transportation of hydrogen by dislocations» is often used in literature. The point of this term is as follows. The presence of an edge dislocation increases solubility of hydrogen in a certain region of metal. Movement of the dislocation causes movement of the region of increased solubility. Trying to fill up the formed potential pit, hydrogen starts diffusing following the dislocation. This results in a diffusion of hydrogen atoms in a direction of movement of the edge dislocation. For short, the edge dislocation is usually considered to transport hydrogen.

Interaction of hydrogen with fixed edge dislocation. Further developing the Cottrell's study on interaction of hydrogen with a fixed edge dislocation, M.A. Krishtal and V.V. Davydov refined it by conducting computerised numerical integration. The computation method they used allowed for the fact that components of normal and tangential stresses at any point of crystal are a sum of corresponding stresses induced by the elastic fields of dislocation and impurity atom. With this approach, potential of the hydrogen–edge dislocation interaction can be regarded as a sum of potential of the dislocation field, impurity atom field and field of their interaction. Based on the numerical calculations, they suggested a new dependence for the potential of elastic interaction between the impurity atom and fixed edge dislocation [4, 5]:

$$u_D = B \ln \left[\frac{30b \sin(e \sin \alpha)}{r} \right], \quad (1)$$

where B is the constant determined experimentally; e is the base of the natural logarithm; b is the modulus of the Burgers vector; and α is the angle between axis X and radius-vector r .

Figure 1 shows potential of elastic interaction $u_D(x; y)$ atom–edge dislocation, and Figure 2 shows a 3D image of potential field $u_D(x; y)$.

Diffusion of interstitial atoms in external force field. Frenkel suggested a simplified microscopic theory for diffusion of interstitial atoms in interstices of the crystalline lattice of solid body. At different time moments, while moving inside a solid as a result of interaction with the crystalline lattice, an atom has

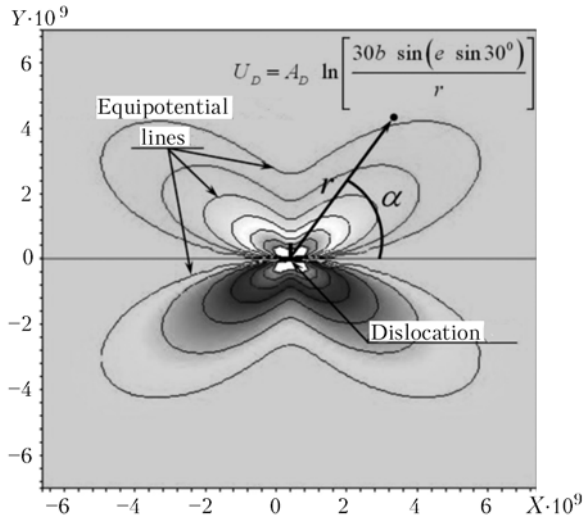


Figure 1. Equipotential lines of potential of interaction $u_D(x; y)$ atom–edge dislocation obtained by M.A. Krishtal and V.V. Davydov using the numerical integration method

different potential energy u_M (which is minimal at interstices). Consider in more detail transition of the atom from one interstice to the other (Figure 3). Let the atom at the beginning be in the first interstice

(point 1). To move from the first to second interstice (point 2), the atom has to overcome a potential barrier with energy u_B (point 3). Energies u_M and u_B are the result of interaction of the atom with the crystalline lattice, which is in the non-deformed state. According to the microscopic theory of diffusion, probability W of transition of an interstitial atom to a certain neighbouring interstice per unit time is equal to [6]

$$W = \frac{1}{\tau_0} \exp \left[\frac{(u_B - u_M)}{kT} \right] = \frac{1}{\tau_0} \exp \left[- \frac{\Delta u_B}{kT} \right], \quad (2)$$

where τ_0 is the constant of the time length, which has an order of magnitude of a period of oscillation of a hydrogen atom in the interstice; difference $\Delta u_B = (u_B - u_M)$ is the height of the potential barrier; T is the temperature of a specimen; and k is the Boltzmann constant.

The diffusion equation derived from (2) coincides with the phenomenological diffusion equation obtained on the basis of the law of conservation of matter and the experimental fact that the flow of matter of one of the components due to diffusion is directly proportional to the gradient of its concentration.

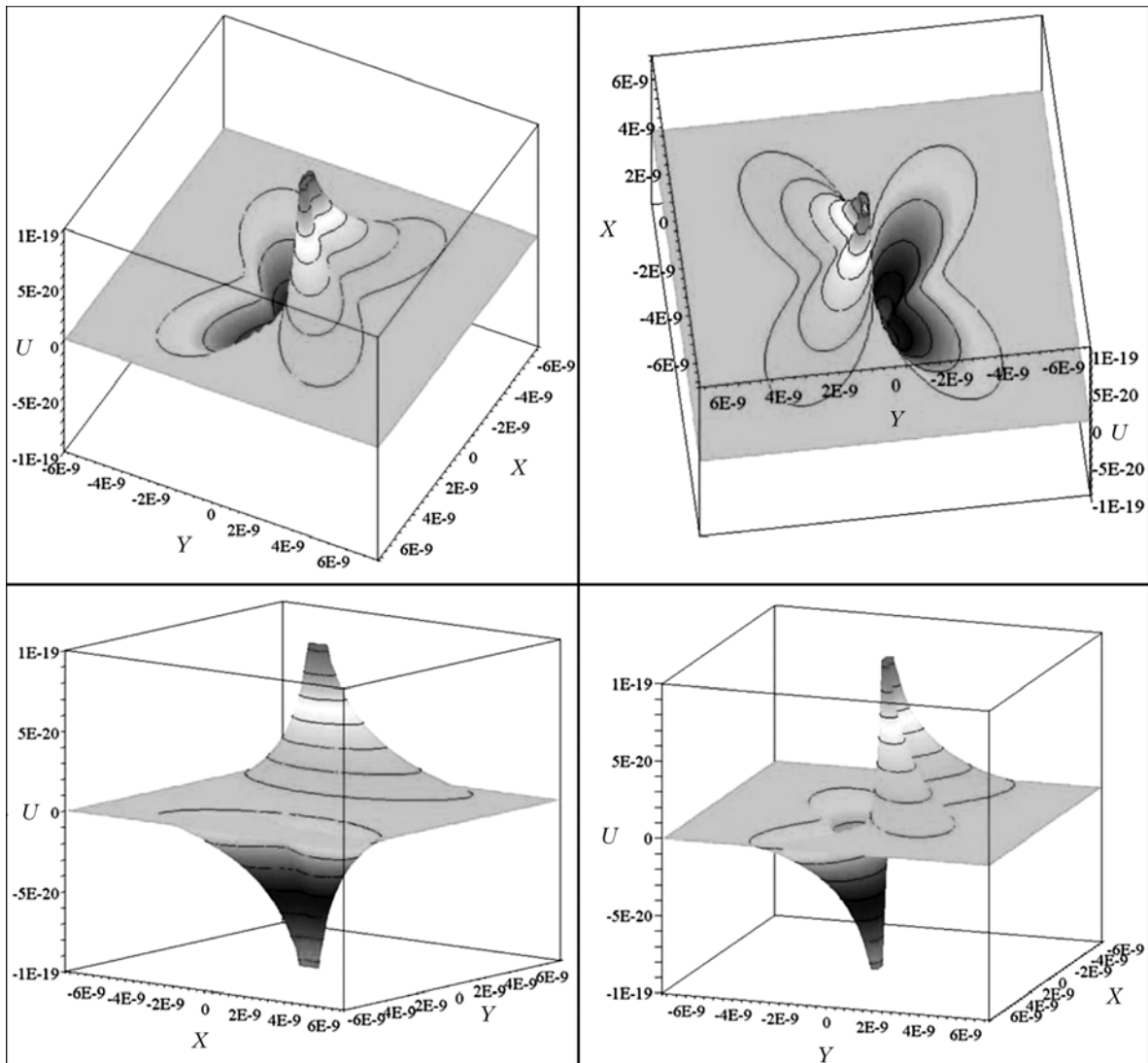


Figure 2. 3D image of potential field $u_D(x; y)$ formed by edge dislocation, according to V.V. Davydov, at $E = 0.6 \text{ eV} = 9.6 \cdot 10^{-20} \text{ J}$



Estimation of the amount of transported hydrogen is a more complicated problem, as it requires that interaction of hydrogen atoms between each other and with a moving dislocation be also allowed for. Consider a general case, where an interstitial atom is in a range of the effect by certain external force field U (e.g. in the edge dislocation affected range). Probability W of transition of such an atom to the neighbouring interstice is equal to

$$W = \frac{1}{\tau_0} \exp \left[- \frac{(u_B - u_M + U_3 - U_1)}{kT} \right] = \frac{1}{\tau_0} \exp \left[- \frac{\Delta u_B + \Delta U_{13}}{kT} \right], \quad (3)$$

where U_1 is the value of the external field in the first interstice; U_3 is the value of the external field at point 3; and $\Delta U_{13} = U_3 - U_1$.

For the simplicity of calculations, consider a case where diffusion proceeds only along axis X and where $U = U(x)$. Allowing for the extent of filling of interstices, flow j_{12} of interstitial atoms from the first to second interstice and opposite flow j_{21} are equal, respectively, to

$$j_{12} = Wp(x) [1 - p(x + dx)] = \frac{1}{\tau_0} \exp \left[- \frac{(\Delta u_B + \Delta U_{13})}{kT} \right] p(x) [1 - p(x + dx)], \quad (4)$$

$$j_{21} = \frac{1}{\tau_0} \exp \left[- \frac{(\Delta u_B + \Delta U_{23})}{kT} \right] p(x + dx) [1 - p(x)], \quad (5)$$

where $p(x)$ and $p(x + dx)$ are, respectively, the probabilities of location of an atom in the first and second interstices; $\Delta U_{23} = U_3 - U_2$; and U_2 is the value of the external field in the second interstice.

The resultant flow from the first to second interstice is $j = (j_{12} - j_{21})$. Using the expansion of functions according to the Taylor's formulae yields

$$p(x + dx) = p(x) + \frac{dp(x)}{dx} dx, \quad \exp \left[- \frac{\Delta U_{13}}{kT} \right] = 1 - \frac{\Delta U_{13}}{kT},$$

$$\exp \left[- \frac{\Delta U_{23}}{kT} \right] = 1 - \frac{\Delta U_{23}}{kT}.$$

Then the expression for the resultant flow through a unit plane normal to axis X has the following form:

$$j_0 = -\alpha \exp \left[- \frac{\Delta u_B}{kT} \right] \times \left[\frac{1}{kT} \frac{\Delta U_{13} - \Delta U_{23}}{\Delta x} p(x)(1 - p(x)) + \frac{dp}{dx} \right], \quad (6)$$

where α is the coefficient that depends upon the form and geometrical dimensions of the crystalline lattice, as well as the type of interstices through which the diffusion propagates.

According to [6]

$$D = \alpha \exp \left[- \frac{\Delta u_A}{kT} \right]. \quad (7)$$

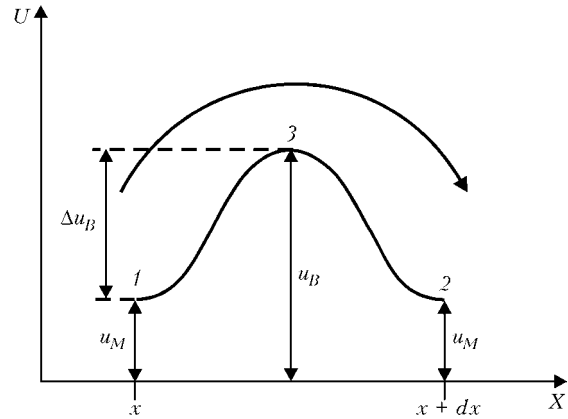


Figure 3. Diagram of diffusion of interstitial atom in interstices (see designations 1-3 in the text)

In the case of unidimensional diffusion, equation (6) can be re-written as follows:

$$j_0 = -D \left[\frac{1}{kT} \frac{dU}{dx} p(x)(1 - p(x)) + \frac{dp}{dx} \right]. \quad (8)$$

In a stationary case, where dislocations are quiescent and flow j_x is equal to zero, equation (8) coincides with the equation that is obtained using the Fermi-Dirac statistics and applied to calculate the concentration of hydrogen about the quiescent edge dislocation [2, 7].

If diffusion of interstitial atoms propagates along axis X and Y , this will yield the following system of equations:

$$\begin{cases} j_0^X = -D \left[\frac{1}{kT} \frac{dU(x, y)}{dx} p(x, y)(1 - p(x, y)) + \frac{dp(x, y)}{dx} \right], \\ j_0^Y = -D \left[\frac{1}{kT} \frac{dU(x, y)}{dy} p(x, y)(1 - p(x, y)) + \frac{dp(x, y)}{dy} \right]. \end{cases} \quad (9)$$

Model of transportation of hydrogen by moving edge dislocation, based on diffusion equation.

Write down the system of equations for a case where hydrogen is in the field of an edge dislocation that uniformly moves along the slip plane at velocity v_0 . As the force field depends upon the two coordinates, the system of equations can be written down as follows:

$$\begin{cases} \tilde{j}_X = -D \left[\frac{du_D}{dx} p(1 - p) + \frac{dp}{dx} \right] C_M, \\ \tilde{j}_Y = -D \left[\frac{du_D}{dy} p(1 - p) + \frac{dp}{dy} \right] C_M \end{cases} \quad (10)$$

where \tilde{j}_X and \tilde{j}_Y are the hydrogen flows along axes X and Y , respectively; and p is the hydrogen concentration related to the quantity of interstices: $p = C/C_M$ (C_M is the quantity of interstices per unit volume). Unknown variables \tilde{j}_X , \tilde{j}_Y and p are the functions of not only coordinates $(x; y)$, but also of time t .

Now we pass on to the system of coordinates which is related to the edge dislocation moving at velocity v_0 . The process will set in some time after the beginning of movement. New functions j_X , j_Y and p will depend only upon the coordinates $(x; y)$. System (10),

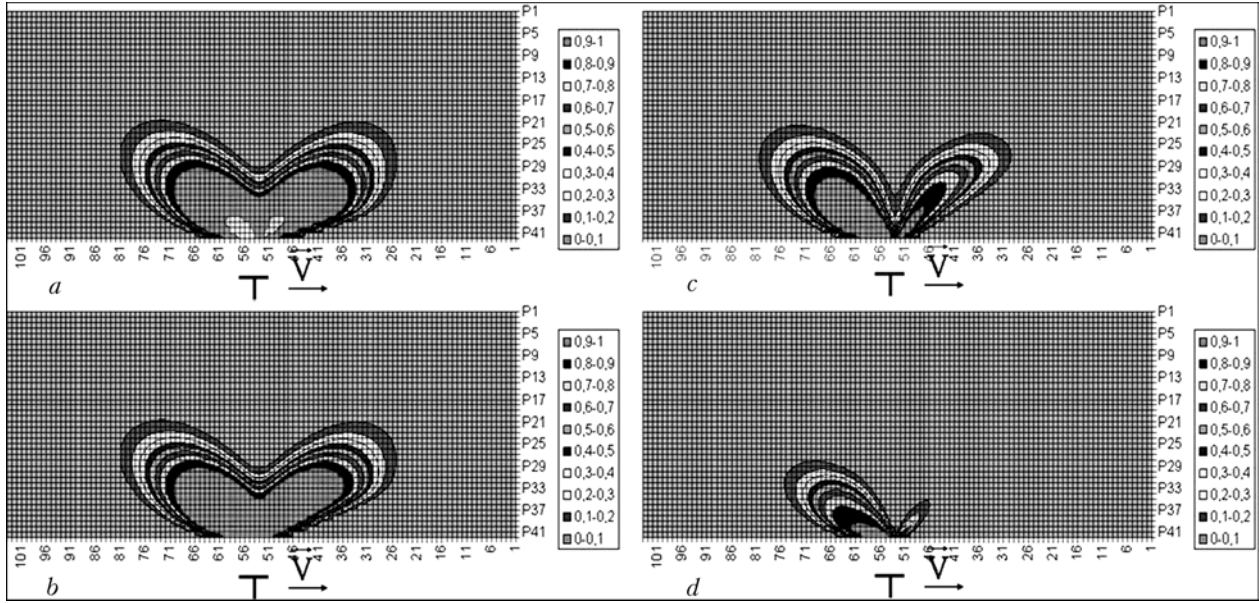


Figure 4. Hydrogen concentration field about a moving dislocation at different velocities v_0 : a — 0.0001; b — 0.01; c — 1; d — 10 m/s

allowing for the continuity equation, can be written down in the following form:

$$\begin{cases} j_x = -D \left[\frac{du_D}{dx} p(1-p) + \frac{dp}{dx} \right] + v_0 p, \\ j_y = -D \left[\frac{du_D}{dy} p(1-p) + \frac{dp}{dy} \right], \\ \frac{d(j_x)}{dx} + \frac{d(j_y)}{dy} = 0 \end{cases} \quad (11)$$

with the infinity condition: $p = p_0 = C_0 / C_M$; $j_x = v_0 C_0 / C_M = v_0 p_0$; and $j_y = 0$ at $(x^2 + y^2) \rightarrow \infty$.

Because of high gradients of potential $u_D(x; y)$ near the centre of the dislocation, system (11) in a general case is very complicated for numerical calculations. Therefore, to simplify and speed up the calculation, it can be re-written as follows for a unidimensional case:

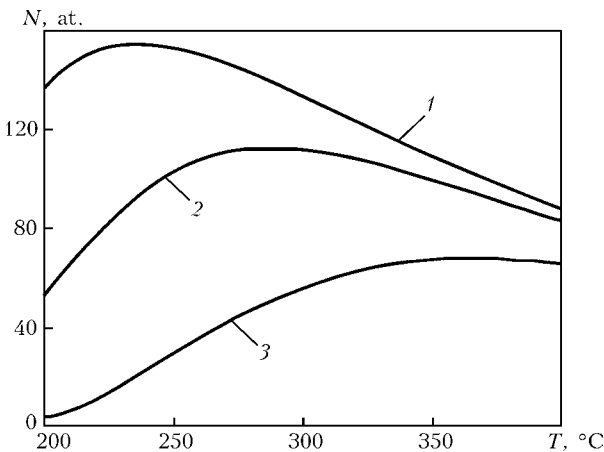


Figure 5. Amount of hydrogen, N , transported by unit length of edge dislocation depending upon the temperature of specimen, T , at different velocities v_0 : 1 — 10^{-1} ; 2 — 10^{-2} ; 3 — 10^{-3} m/s

$$\begin{cases} j_x = -D \left[\frac{du_D}{dx} p(1-p) + \frac{dp}{dx} \right] + v_0 p, \\ j_x = \text{const} \end{cases} \quad (12)$$

Calculation of the amount of hydrogen transported by edge dislocation. The following characteristics of metal: $b = 2.56 \cdot 10^{-10}$ m and $E = 0.6$ eV, were used to calculate the amount of hydrogen transported by a length of the dislocation equal to the modulus of the Burgers vector. The relative concentration of free hydrogen was assumed to be $C = 2.5 \cdot 10^{-4}$ (approximately 5 cm³ of hydrogen per 100 g of metal). The distance at which the dislocation still affected a hydrogen atom was limited by forty Burgers vectors. The coefficient of diffusion of hydrogen was estimated from equation $D = 1.6 \cdot 10^{-7} \exp[-(19640/RT)]$, m²/s.

Figure 4 shows calculation of the hydrogen concentration field about a moving edge dislocation using the Davydov's equation. It can be seen that low velocities of the edge dislocation have a low effect on the hydrogen concentration field, which remains almost symmetrical. As the velocity increases, the concentration of hydrogen near the dislocation gradually decreases, and the concentration field becomes asymmetrical. At high velocities, almost all hydrogen loses contact with the dislocation.

Figure 5 shows the results of calculations of the amount of hydrogen, N , transported by a unit length of the edge dislocation depending upon the temperature of a specimen, T , for different dislocation velocities v_0 . The calculation results obtained are attributable to a complex character of interaction of hydrogen with the edge dislocation. Friction force F (resistance force) on the side of the crystalline lattice of metal starts affecting a hydrogen atom transported by the dislocation at velocity v_0 . At low temperatures, the concentration of hydrogen about the quiescent edge



dislocation increases, but friction force F affecting the transported hydrogen atom also increases because of a low coefficient of diffusion of hydrogen. Hence, during movement, almost the whole of the hydrogen cloud under the effect of force F detaches from the edge dislocation, and the latter becomes capable of transporting a comparatively small amount of hydrogen. As the temperature increases, friction force F decreases, and the edge dislocation transports more hydrogen, other conditions being equal. At a certain temperature close to the normal one, the amount of hydrogen transported by the edge dislocation reaches its maximum. As the temperature further grows, the concentration of hydrogen about the edge dislocation falls because of a thermal motion of hydrogen atoms. Therefore, the amount of transported hydrogen decreases in a range of the increased temperatures. According to [1–3], RHB of metal occurs if dislocations transport a sufficient amount of hydrogen to a sub-microcrack. The most favourable temperature range is that close to the normal temperature, which is in agreement with the calculated temperature dependence for transportation of hydrogen by the edge dislocation.

As seen from Figure 5, in addition to temperature, velocity of the edge dislocation also has a substantial effect on the amount of transported hydrogen. According to the results obtained, as velocity v_0 decreases,

the amount of transported hydrogen increases, and maximum of the dependence moves to a range of lower temperatures. Velocity v_0 of the edge dislocation is proportional to relative strain rate ε of metal [3, 8]. Therefore, as follows from the calculations, decrease in strain rate ε leads to increase in the degree of RHB and shift of the peak of hydrogen-induced brittleness to a range of lower temperatures. If the value of ε becomes very high, the amount of transported hydrogen decreases to a great degree. In this case, RHB of metal may not show up at all. The results obtained are in good agreement with the RHB peculiarities studied earlier [1, 2].

1. Pokhodnya, I.K., Yavdoshchin, I.R., Shvachko, V.I. et al. (2004) *Metallurgy of arc welding. Interaction of gases with metals*. Ed. by I.K. Pokhodnya. Kiev: Naukova Dumka.
2. Kolachev, B.A. (1985) *Hydrogen brittleness of metals*. Moscow: Metallurgiya.
3. Pokhodnya, I.K., Shvachko, V.I., Utkin, S.V. (2002) Effect of hydrogen on equilibrium of dislocation sub-microcrack in α -iron. *Fiz.-Khim. Mekhanika Materialiv*, **1**, 1–8.
4. Krishtal, M.A., Golovin, S.A. (1976) *Internal friction and structure of metals*. Moscow: Metallurgiya.
5. (1972) *Problems of metals science and diffusion of metals*. Tula: TPI.
6. Smirnov, A.A. (1982) *Theory of diffusion in interstitial alloys*. Kiev: Naukova Dumka.
7. Hirth, J.P., Carnahan, B. (1978) Hydrogen adsorption at dislocation and cracks in Fe. *Acta Met.*, **26**, 1795–1803.
8. Vladimirov, V.I. (1984) *Physical nature of metal fracture*. Moscow: Metallurgiya.

TECHNOLOGIES FOR MELTING TITANIUM INGOTS FROM UNDERSEPARATED TITANIUM SPONGE IN SECTIONAL MOULD USING HIGH-FREQUENCY HEATING

Cutting down of costs in production of titanium sponge and its remelting into ingots is a major technical challenge. One of the methods to handle it is to shorten by 20–30 % the time of the processes of magnesium-thermic reduction of titanium from its chlorides with subsequent topping of the reaction products in vacuum (separation). This allows a 20 % decrease in consumption of power supplies and extension of service life of expensive equipment used for production of titanium sponge. The sponge produced by the shortened cycle contains up to 1 wt.% of chlorine compounds, instead of 0.08 wt.% required by the standard. Titanium sponge with an increased content of chlorides can be remelted into ingots using the process of induction melting in a sectional mould. The method is based on the fact that the zone with a high-intensity magnetic field is formed in the cooled copper mould using a small-height inductor, and that melting and refining of metal fed in portions during melting occur in this zone. To provide the incremental formation of an ingot, the zone is moved along the mould or left fixed, and then the ingot is drawn from the mould.

Purpose and application. Melting of titanium ingots from gas-saturated titanium sponge, lumpy scrap, wastes of pipe and plate rolling, chips.

State and level of development. Pilot plant is available for melting ingots of commercial titanium from underseparated titanium sponge. The metal meets specification requirements for chemical composition.

Proposals for co-operation. Building of the melting facilities and transfer of the technology to enterprises producing titanium.

Principal performers and developers: Shapovalov V.A., Dr. of Techn. Sci.; Shejko I.V., Dr. of Techn. Sci.; Konstantinov V.S., Cand. of Techn. Sci.

Contacts: Prof. Shapovalov V.A.
E-mail: shapovalov@paton.kiev.ua

MECHANIZED REPAIR WELDING OF METALLURGICAL COMPLEX UNITS USING FLUX-CORED WIRE

V.N. SHLEPAKOV¹, V.N. IGNATYUK¹, A.S. KOTELCHUK¹ and Yu.M. GITIN²

¹E.O. Paton Electric Welding Institute, NASU, Kiev, Ukraine

²F.E. Dzerzhinsky Dneprovsky Metallurgical Works, Dnepropetrovsk, Ukraine

Technological parameters and welding productivity in case of application of the wire of three types were determined on the basis of experimental investigations of the welding technique of typical joints of the metallurgical complex units using self-shielded flux-cored wire. Advisability of using the double-layer wire in welding of the metal of medium and high thickness in downhand and horizontal positions of the welds is shown. It is expedient to use tubular wire of small diameter in fulfillment of welds in vertical and overhead positions. Technology for welding of typical metal structures was developed.

Keywords: arc welding, repair of metal structures, low-alloy steel, metallurgical complex, flux-cored wire, development of composition

At present increase of the service life and operation safety of structures and machines is urgent task in fulfillment of the repair-renovation welding of metal structures from low-alloy steels under workshop conditions and during erection of the metallurgical equipment. One of the efficient ways of its solution is application of the high-productivity and quality mechanized welding using self-shielded flux-cored wire.

Bodies of blast furnaces, converters and ladles are produced from low-alloy steels, in particular the 09G2S steel, and requirements to the welding material properties meet the E50A type according to DSTU (GOST 9467-75). Typical are the butt joints with grooves beveled at 50° (for downhand and vertical design positions) and 45° (for horizontal position with a one-side bevel-

ing). Thickness of the metal is 12–60 mm, of the base one — 30 mm. The joints are mounted with a 1–3 mm slot in the weld root (Figure 1).

It was necessary to develop a self-shielded flux-cored wire, which could be used in welding of various types of joints in different spatial positions of the work performance, whereby necessary parameters of strength and viscoplastic properties of the welded joint metal and high parameters of the welding productivity had to be ensured.

Investigation of crack resistance of welded joints by the calculation methods, taking into account class of the steels, type of the wire and welding conditions. As far as formation and development of cracks, initiated by hydrogen, is determined, mainly, by the class of a steel welded, type of the welding material, welding conditions, shape and geometric size of the joint, the following four conditions, in case of

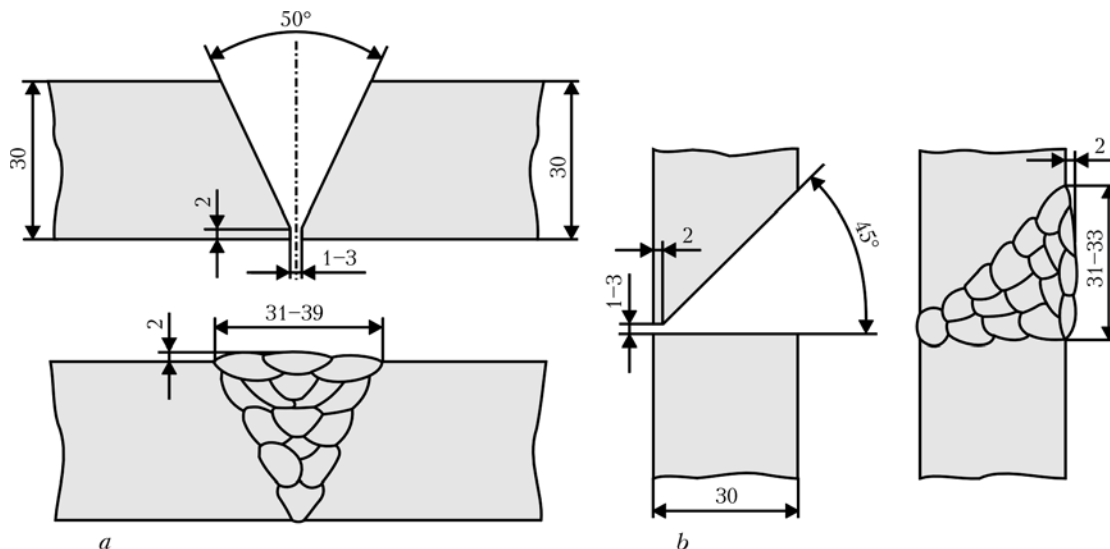


Figure 1. Types of butt joints on vertical plane of bodies of industrial ladles and units of metallurgical complex: *a* — downhand design position; *b* — horizontal position with one-side beveling

*The article is prepared on the basis of results of fulfillment of a targeted comprehensive program of the NAS of Ukraine «Problems of service life and operation safety of structures and machines» (2004–2006).



occurrence of which probability of origination and development of the hydrogen cracks increases, are accepted for forecasting hydrogen embrittlement of a welded joint:

- presence of a tensile stressed state in the welded joint area, occurring as a result of the welding thermal cycle and determined by the character of joining of the welded parts, their thickness, and application of external stresses;

- maximum level of hydrogen content in the weld metal, which is adsorbed in the process of welding by the weld pool from the arc atmosphere and is able to diffuse into the HAZ metal (it is determined by the residual moisture content in the flux-cored wire core, presence of contamination or lubricating oil, used in drawing, and other thermally unstable compounds of hydrogen on surface of the wire or the metal being welded);

- formation of microstructure in the HAZ metal or a weld sensitive to origination or distribution of the initiated by hydrogen cracks (it is mainly determined by chemical composition of the base and weld metal and thermal deformation cycle of welding);

- thermal cycle of the welding proper, i.e. time interval, sufficient for diffusion of hydrogen from critical zones of the welded joint (HAZ or weld metal) during cooling down to the temperature, at which sharply increases risk of hydrogen embrittlement (it is determined by the welding conditions, heating temperature, shape of the joint, and thickness of the material being welded) [1–3].

In case of application of a welding material with increased content of alloying elements possibility of crack formation in the very weld increases.

There are three main approaches to prevention of formation of hydrogen cracks.

Firstly, deceleration of cooling within the martensite transformation temperature range, i.e. increase of the time period, necessary for diffusion of hydrogen from the weld and HAZ metal, reduction of hardness of the latter and, respectively, reduction of the microstructure sensitivity to formation of cracks. In practice this approach is implemented by local heating or welding at increased heat input.

Secondly, reduction of the deposited metal hardness (probability of origination of cracks in more plastic microstructures is lower) by application of the base metal or welding material, which ensure lower carbon equivalent of the built-up metal.

Thirdly, reduction of the amount of hydrogen, which is introduced into the weld metal, because the lower are levels of the latter the lower is risk of formation of cracks. In practice this approach is implemented by application of the technological processes, which control level of the introduced hydrogen, or by application of the low-hydrogen welding material, and drying and roasting of the welding materials and fluxes before welding [2].

Estimation of the hydrogen embrittlement probability in welding with a flux-cored wire of the joints

from a metal of different thickness at various values of heat input of welding was carried out using the PREHEAT software. Probability of formation of microstructures, sensitive to origination and distribution of the induced by hydrogen cold cracks, is forecasted in the program by the hydrogen embrittlement index --- carbon equivalent (CE or P_{cm}) of the metal.

For estimating sensitivity of steels to cold cracks the following expressions were used [4, 5]:

1) formula, adopted by the International Institute of Welding for carbon steels, containing more than 0.18 wt.% C, or in cases, when slow cooling is possible (cooling time from 800 to 500 °C is more than 12 s):

$$CE_{IIW} = C + \frac{Mn}{6} + \frac{Ni + Cu}{15} + \frac{Cr + Mo + V}{5}; \quad (1)$$

2) formula for P_{cm} , proposed by Y. Itoh and K. Bessio:

$$P_{cm} = C + \frac{Si}{30} + \frac{Mn + Cu + Cr}{20} + \frac{Ni}{60} + \frac{Mo}{15} + \frac{V}{10} + 5B \quad (2)$$

or for CE_{MW} (Durain):

$$CE_{MW} = C + \frac{Si}{25} + \frac{Mn + Cu}{20} + \frac{Cr}{10} + \frac{Ni}{40} + \frac{Mo}{15} + \frac{V}{10}. \quad (3)$$

Formulas (2) and (3) were used for steels, containing less than 0.22 wt.% C, and in case of quick cooling (cooling time from 800 to 500 °C is less than 6 s);

3) formula of N. Yurioka:

$$CEN = C + A(C) \times \left(\frac{Si}{24} + \frac{Mn}{6} + \frac{Cu}{15} + \frac{Ni}{20} + \frac{Cr + Mo + Nb + V}{5} + 5B \right) \quad (4)$$

where $A(C) = 0.75 + 0.25 \tanh\{20(C - 0.12)\}$, for estimation of the steels, containing up to 0.25 wt.% C.

Formula (4) is easily transformed into the expression, similar for CE_{IIW} , P_{cm} or CE_{MW} for steels with increased content of carbon, as depending upon content of the latter changes the correcting factor $A(C)$;

4) in order to take into account influence of oxygen on the microstructure, formula of D.L. Olson may be used:

$$P_{cm}^O = C + \frac{Si}{30} + \frac{Mn + Cr + Cu}{20} + \frac{V}{10} + \frac{Mo}{15} + \frac{Ni}{60} + 5B - \frac{3}{4}O. \quad (5)$$

It is used for estimation of carbon equivalent of the weld metal.

The results obtained may be interpreted using the following parameters: minimal temperature of the joint being welded; heat input of welding; maximal carbon equivalent of the base metal; permissible level of the diffusion hydrogen content.

On the basis of the experimental data concerning main parameters of the welding process, type of the joint, base metal and its thickness, value of one of

$[H]_{dif}, \text{cm}^3/100 \text{ g}$

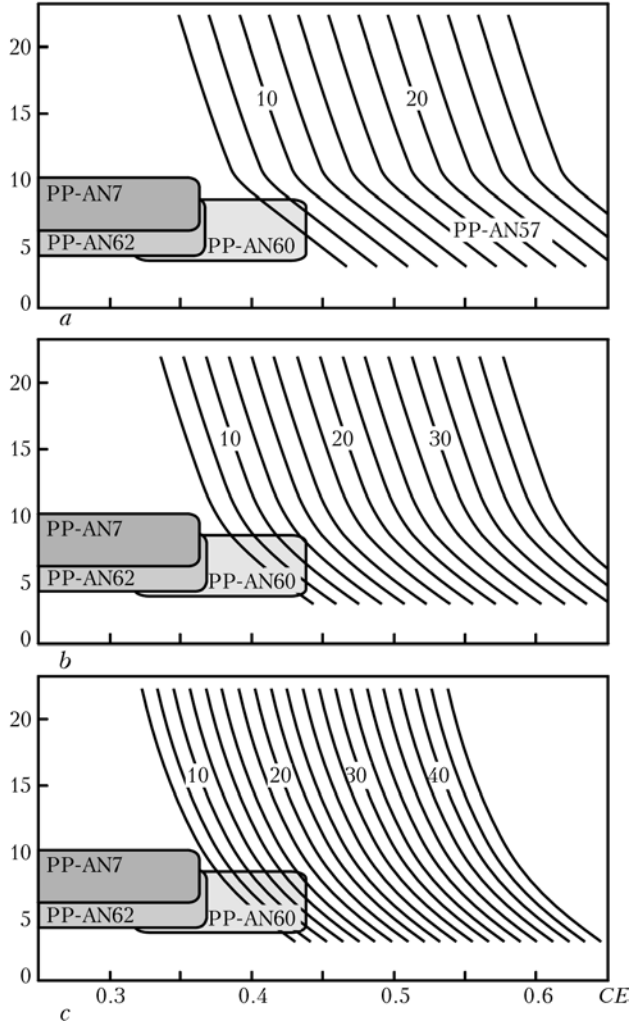


Figure 2. Diagrams of safe heat input levels Q depending upon carbon equivalent of metal (curves) in welding of butt joints of different total thickness: a — 33; b — 44; c — 60 mm

four characteristics is determined. So, safe combinations of the heating temperature, heat input, carbon equivalent of the base metal (the weld metal) and allowable level of the diffusion hydrogen, at which formation of hydrogen cracks in the HAZ metal or the weld is improbable, can be quickly estimated.

In Figure 2 diagrams of safe levels of heat input Q in welding of butt joints of different total thickness of the welded plates are presented. On the diagram the areas are indicated, which correspond to the typical chemical composition of the weld metal and level of content in it of the diffusion hydrogen for a number of self-shielded flux-cored wires, given in Table 1.

When selection of the base metal or welding process is limited by the metallurgical or economic requirements and technical and technological possibilities of

the used equipment, risk of the hydrogen crack formation may be reduced by prolongation of the time, necessary for diffusion of hydrogen from the welded joint zone during cooling down to the temperature, which is hazardous from the viewpoint of increased risk of formation of the induced by hydrogen cracks. In practice this task is solved by selection of respective welding conditions, which ensure higher heat input, or application of the technological welding processes with local heating. These actions decelerate separately or jointly rate of cooling within the range of martensite transformation temperatures in a weld and HAZ metal. In addition, in case of application of these methods the microstructure in many cases is more favorable and, as a result, less sensitive to formation of cracks.

The most efficient method for preventing formation of cold cracks is reduction of hydrogen amount, which can get into the welding zone. In practice it means application of the low-hydrogen welding processes, such as welding by a non-consumable electrode or in the inert gases with cleaning of the welding site. Use of the welding with application of a flux-cored wire may cause saturation with hydrogen in rather big volumes. Substantiated selection of the wire composition and application of its heat treatment prior to welding allows ensuring necessary low level of the diffusion hydrogen content in the weld metal.

Butt joints of low-alloy steels, welded with application of the flux-cored wire, were analyzed by the calculation methods. Such steels as 10KhSND and 09G2S were considered as the base metal. The calculations were performed for butt joints with the base metal thickness of 12–80 mm. As a consumable material experimental version of the designed for welding self-shielded flux-cored wire of the PP-AN60 type was considered. Diameter of the wire was 1.6 mm; welding conditions were as follows: $U_a = 24\text{--}28 \text{ V}$; $I_w = 200\text{--}300 \text{ A}$; $v_w = 20\text{--}40 \text{ cm/min}$; $Q = 7.2\text{--}25.2 \text{ kJ/cm}$. Content of the diffusion hydrogen was not more than $10 \text{ cm}^3/100 \text{ g}$.

Carbon equivalent of the 10KhSND steel: $CE_{b,m1} = 0.38\text{--}0.46$ ($CE_{b,m1}^{av} = 0.43$); the 09G2S steel: $CE_{b,m2} = 0.32\text{--}0.44$ ($CE_{b,m2}^{av} = 0.38$). Carbon equivalent of the deposited metal: $CE_{d,m} = 0.33\text{--}0.45$ ($CE_{d,m}^{av} = 0.39$). Total thickness of the joint $TT = 24, 40, 120$ and 160 mm .

Results of the calculation investigations are presented in Table 2. Local heating has to be used directly before welding. The base metal temperature should achieve minimal recommended temperature of heating at the distance not less than 75 mm on both sides of the joint. Temperature has to be measured on opposite

Table 1. Chemical composition of metal, wt.%, deposited with application of self-shielded flux-cored wire

Grade of wire	C (max)	Si	Mn	Ni	Al	Ti	Zr	S (max)	P (max)
PP-AN60	0.15	0.10–0.15	1.1–1.3	0.9–1.0	0.65–0.75	--	0.010–0.015	0.005	0.01
PP-AN-62	0.15	0.05–0.10	1.0–1.3	--	0.2–0.3	0.05–0.10	--	0.01	0.025
PP-AN72	0.15	0.3–0.4	0.9–1.2	--	--	--	--	0.03	0.03

**Table 2.** Minimal heating temperatures, °C, at different heat input of welding and chemical composition of metal for butt joints

Q, kJ/mm	Base metal --- 09G2S steel of total thickness, mm			Base metal --- 10KhSND steel of total thickness, mm			Weld metal of total thickness, mm		
	24	40	120-160	24	40	120-160	24	40	120-160
0.7	40	112	149	83	128	167	65	121	159
0.8	0	102	146	51	119	163	27	110	155
0.9	--	86	143	17	109	159	0	100	150
1.0	--	65	139	0	98	155	--	84	147
1.1	--	39	136	--	83	151	--	64	144
1.2	--	15	133	--	63	148	--	39	141
1.3	--	0	129	--	39	145	--	16	137
1.4	--	--	126	--	17	142	--	0	134
1.5	--	--	122	--	0	139	--	--	131
1.6	--	--	119	--	--	136	--	--	128
1.7	--	--	115	--	--	133	--	--	125
1.8	--	--	112	--	--	129	--	--	121
1.9	--	--	108	--	--	126	--	--	118
2.0	--	--	105	--	--	123	--	--	114
2.2	--	--	101	--	--	120	--	--	111
2.5	--	--	92	--	--	115	--	--	106

from the applied heating source side of the plates being welded. In case of a limited access to the item, it is necessary to let temperature to equalize over the base metal section (about 2 min for each 25 mm of thickness).

Investigations and development of self-shielded flux-cored wire samples for repair welding of metallurgical equipment. For repair welding of metallurgical equipment the PP-AN60 and PP-AN62 self-shielded flux-cored wires of 1.6 mm diameter, designated for welding in all spatial positions of structures from carbon and low-alloy steels [6–8], as well as the PP-AN7 self-shielded flux-cored double-layer wire of 2.0 mm diameter for horizontal welding, were developed at the E.O. Paton Electric Welding Institute. In Table 3 main characteristics of these wire grades are presented.

In case of welding by the PP-AN60 and PP-AN62 wires, resistance of the weld metal to formation of the pores, caused by nitrogen, is achieved by doping of the weld metal by aluminium, which is introduced in the form of a powder into the core of the self-shielded flux-cored wire. The PP-AN60 flux-cored wire has the core of oxide-fluoride type with high

basicity of the slag; PP-AN62 is wire of oxide type with low basicity. Both wires form slag during welding, which quickly hardens.

Results of metallographic investigations of distribution and composition of the non-metal inclusions in metal of the welds, performed by wires of fluoride and oxide types, are presented in Figure 3. For metal of the welds, performed by the PP-AN60 wire of fluoride type, a relatively uniform distribution of the disperse particles of non-metal inclusions, which mainly represent aluminium nitrides and oxides, is characteristic. Non-metal inclusions in metal of the weld, performed by the PP-AN62 self-shielded wire of oxide type, represent mainly aluminium oxides, and only a small portion (less than 5 vol.%) --- silicon and manganese oxides. Volume share of non-metal inclusions in the welds, produced with application of the PP-AN60 wire of fluoride type, equals on average 0.3 %, and in the welds produced with PP-AN62 wire of oxide type --- 0.85 %.

The metal, built up by the PP-AN60 wire, has low content of sulfur (0.003–0.008 wt.%), which is significantly lower than in metal of the welds performed by wires of general designation (~ 0.015–0.025 wt.%).

Table 3. Main characteristics of self-shielded flux-cored wires

Wire grade	Type of standard		Slag base	Welding current polarity
	GOST 26271	EN758		
PP-AN60	PS49-A3U	T 50 3 1Ni YN 1 H10	CaO--MgO--Al ₂ O ₃ --R ₂ O--BaF ₂ --LiF	Straight
PP-AN62	PS44-A2U	T 46 2 SN 1 H10	MgO--R ₂ O--MnO _x --FeO--Al ₂ O ₃	Reverse
PP-AN7	PS44-A2G	T 42 2 VN 3 H10	CaO--TiO ₂ --SiO ₂ --Na ₂ O--CaF ₂ --NaF	Same

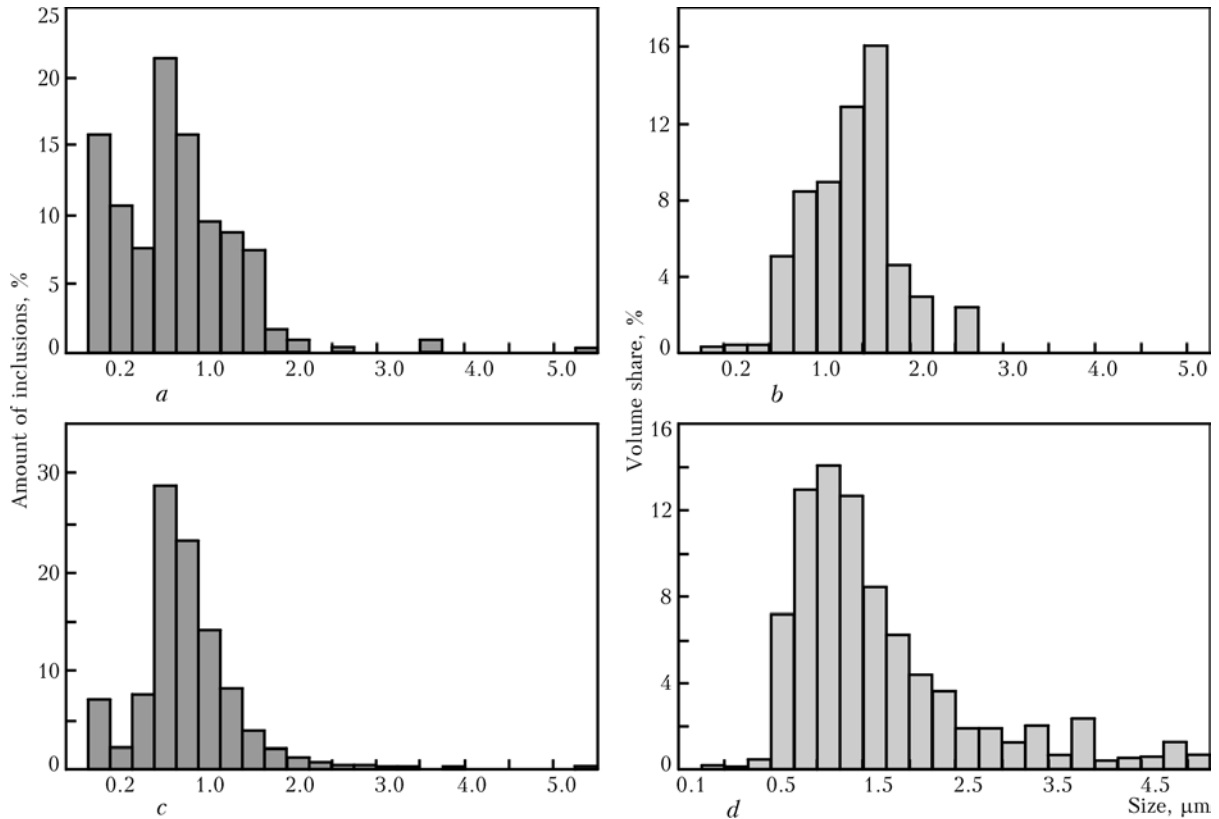


Figure 3. Distribution of non-metal inclusions by their size in welding with flux-cored wires of fluoride (a, b) and oxide (c, d) types

This is explained by application in the core of active desulfurizers.

Typical mechanical properties of the metal of welds and welded joints, performed by self-shielded flux-cored wires of three types --- fluoride (PP-AN60), oxide (PP-AN62) and carbonate-fluorite (PP-AN7) ones, are presented in Table 4. In relation to the welding-technological properties the wires are characterized by good separation ability of the slag crust, favorable shape of the welds, and possibility of welding of a wide range of thicknesses of the metal welded; they allow performing welding of metal structures under the erection site conditions in different spatial positions.

Testing of flux-cored wire according to requirements of repair erection welding under conditions of metallurgical production. The program for testing

flux-cored wires in repair and erection welding was preliminarily coordinated with metallurgical enterprises of «F.E. Dzerzhinsky Dneprovsky Metallurgical Works», Metallurgical Works «Azovstal» (Mariupol) and «NDVP Krivorozhstalonkonstruktsiya», producer of the erection-welding works at the «Azovstal». The programs included selection of typical welding objects, previous tests with determination of the welding equipment types (semi-automatic machines) for the erection conditions, and practical training of the welders in order to familiarize them with technology of welding with application of a self-shielded flux-cored wire at the metallurgical enterprises.

For fulfillment of the program experimental-commercial (according to separate agreements) and commercial lots of the self-shielded flux-cored wire of three grades were produced at SE «PWI Pilot Plant



Figure 4. General view of air heater erection

Table 4. Mechanical properties of welded joints performed using flux-cored wires

Grade of wire	Tensile strength σ_t , MPa	Yield strength σ_y , MPa	Elongation δ , %	Temperature, at which impact toughness KCV is not less than 35 J/cm ² , °C
		not less than		
PP-AN60	580-620	490	22	-30
PP-AN62	550-580	490	22	-20
PP-AN7	500-650	440	20	-20

Note. Welding conditions: $I_w = 250-270$ A, $U_a = 21-22$ V; PP-AN60 --- straight, PP-AN62 and PP-AN7 --- reverse polarity current.

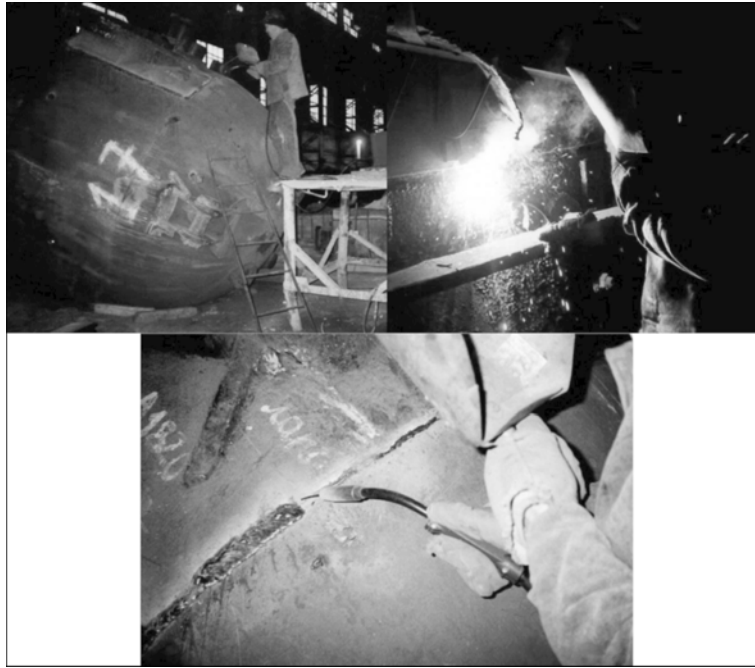


Figure 5. Repair welding of metallurgical equipment at Dneprovsky Metallurgical Works using PP-AN7 flux-cored wire

of Welding Materials». The previous tests showed that the PP-AN7 wire of 2.4 mm diameter met to the greatest degree the productivity requirements, established for erection welding of the selected objects.

The main object of erection welding at the «Azovstal» was construction (reconstruction) of the blast furnace air heater (Figure 4). The base metal was the 09G2S steel. The main volume of welding with application of the flux-cored wire was connected with making of horizontal and vertical joints during erection of the dome. The PSh-107V modified semi-automatic machines were used. Quality of the produced welds met the established requirements. The remarks mainly concerned unstable operation of the semi-automatic machines, which were powered from the welding current source. For remedying this shortcoming the power supply scheme was changed, and an independent power source was used, which ensured stable operation of the semi-automatic machines. As a result productivity and quality of welded joints, performed with application of the flux-cored wire, improved in the welding-erection works.

At the «F.E. Dzerzhinsky Dneprovsky Metallurgical Works» bodies of the converters, jackets of the blast furnaces, metal structures of bridge cranes, pipelines, and bodies of ladles were selected as welding objects (Figure 5). The greatest volume of welding at the initial period was connected with repair welding of the objects with making of welds in downhand, horizontal and vertical positions (shields, reinforcement chords, cover plates, etc.). During welding with application of the self-shielded flux-cored wire on open sites, where speed of wind did not exceed 8 m/s, any noticeable influence of wind on quality of the welded joints was not detected. That's why permission

on application of the process at speed of wind up to 7 m/s was introduced into the welding regulations, which exceeds several times possibilities of welding in erection with application of the solid wire.

On the basis of the results of experimental-commercial tests the decisions were made to expand volumes of mechanized welding of metal structures and equipment of metallurgical enterprises with application of the self-shielded flux-cored wire. The measures were determined for technical and technological preparation of the enterprises for expansion of the nomenclature of the objects, recommended for introduction of welding with application of the flux-cored wire. Preliminary economic calculations were made, which confirmed efficiency of the new technology introduction in repair-renovation welding under conditions of metallurgical enterprises.

1. Hrivnyak, I. (1984) *Weldability of steels*. Ed. by E.L. Makarov. Moscow: Mashinostroenie.
2. Coe, F.R. (1973) *Welding steels without hydrogen cracking*: The Welding Institute Report. Abington.
3. Devletian, J.H., Fichtelberg, N.D. (2001) Controlling hydrogen cracking in shipbuilding. *Welding J.*, **11**, 46–52.
4. De Meester, B. (1990) Note on the carbon equivalent. *Welding in the World*, **28(2–4)**, 48–54.
5. Pokhodnya, I.K., Yavdoshchin, I.R., Shvachko, V.I. et al. (2004) *Metallurgy of arc welding. Interaction of metal with gases*. Ed. by I.K. Pokhodnya. Kiev: Naukova Dumka.
6. Shlepakov, V.N., Naumejko, S.M. (2004) Self-shielded flux-cored wire of small diameter for welding of metal structures of carbon and low-alloy steels in erection conditions. *Svarshchik*, **1**, 35.
7. Shlepakov, V.N., Naumejko, S.M. (2004) Self-shielded flux-cored tubular wires with core on the base of acid systems. In: *Welding Consumables. Development. Technology. Production. Quality*: Proc. of 3rd Int. Conf. on Welding Consumables in the CIS Countries (Dnepropetrovsk, 1–4 June, 2004), 123–131.
8. Shlepakov, V.N., Naumejko, S.M. (2005) Self-shielded flux-cored wires for welding low-alloy steels. *The Paton Welding J.*, **4**, 28–30.

EXTENSION OF LIFE OF LARGE-SIZE CONCENTRATED SULPHURIC ACID STORAGE TANKS*

K.A. YUSHCHENKO¹, L.V. CHEKOTILO¹, G.F. NASTENKO¹, Yu.B. DANILOV², V.A. KACHANOV², A.I. KABASHNY², S.N. IVANUNA², V.R. DORN³, V.V. ILIENKO³, N.V. AMBROZYAK³, B.P. KISLY³ and T.M. KHODAN³

¹E.O. Paton Electric Welding Institute, NASU, Kiev, Ukraine

²OJSC «Ukrainian Research and Development Institute for Chemical Engineering», Ukraine

³SC «Eastern Ore Mining and Processing Enterprise», Ukraine

Possible causes of accelerated corrosion of elements of large-size concentrated sulphuric acid storage tanks with a capacity of up to 3000 m³, made from steel St3, are considered. Specifications and technology developed for repair of the tanks, allowing extension of their service life, are reviewed.

Keywords: arc welding, repair of process equipment, carbon steels, welded joints, corrosion, quality inspection, extension of life

Mining and smelting enterprises use a large amount of sulphuric acid for production of rare metals, e.g. uranium concentrates, used to manufacture fuel cells for nuclear power stations. Sulphuric-acid plants (SAP) and sulphuric-acid factories (SAF) produce, as a rule, the concentrated acid with a main product content of 94.5–98.5 %.

As reported [1–3], the concentrated sulphuric acid has low reactivity with respect to conventional carbon steels at temperatures of up to 40–80 °C. Therefore, the major part of the SAP equipment operating at the above temperatures (rail tank cars [4], truck cars, acid storage tanks, etc.) is made at SAF from carbon steels of the St3 grades of different deoxidation and strength categories according to GOST 14637–89 and DSTU 2651–94 (GOST 380–94), steels 10, 15 and 20 according to GOST 1050–74, etc. Some components of stop valves, bends, branch pipes, etc. are made from grey and malleable cast iron. Advantages of these ma-

terials are a good corrosion resistance, low cost and good (for steel) or satisfactory (for cast iron) weldability. SAP available at the Eastern Ore Mining and Processing Enterprise (VostGOK) is equipped with the concentrated sulphuric acid storage tanks with a diameter of 20 m, height of 9.54 m and capacity of 3000 m³ (Figure 1). The tanks are welded from plate steel St3S (Poland, analogue of steel St3sp2 (killed), according to GOST 14637–89) 16 mm thick (lowering), 14, 12, 10 and 8 mm thick (upper ring). The rings are 2 m high, and thickness of the bottom is 25 mm. The cover has a hemispherical shape, it is a welded component, and has a hatch for maintenance. Pressure inside a tank is atmospheric. The tanks are located in open air. Welding of the tanks was performed using electrodes ER346 based on a low-carbon wire of the Sv-08 type with a covering of the rutile-carbonate type [5] (analogue of electrodes of the ANO-4 and MR3 grades according to GOST 9466–75 and GOST 9467–75).

The tanks are painted on their outside surface. The inside surface, which is in contact with the concentrated acid, experiences general uniform corrosion and local corrosion of the pitting type (Figure 2). The rate of general corrosion of the shells and bottom is comparatively low (Figure 3 and Table 1). For example, after 16 years of operation, the depth of corrosion of the upper (fifth) ring of tank # 1 was 0.2–0.5 mm, that of the lower (first) ring --- 1.8–2.3 mm, and bottom --- 0.8–1.9 mm, which on the average is 0.01–0.03, 0.11–0.14 and 0.05–0.12 mm/year, respectively. The depth of pits was 0.1–1.0 mm, and diameter ranged from 0.5 to 2.0 mm. Also, there were pits of a larger diameter --- up to 5–8 mm.

Corrosion resulting from contact of carbon steel with sulphuric acid causes formation of ferric sulphate FeSO₄ and an equivalent amount of hydrogen by the following reaction [2]:

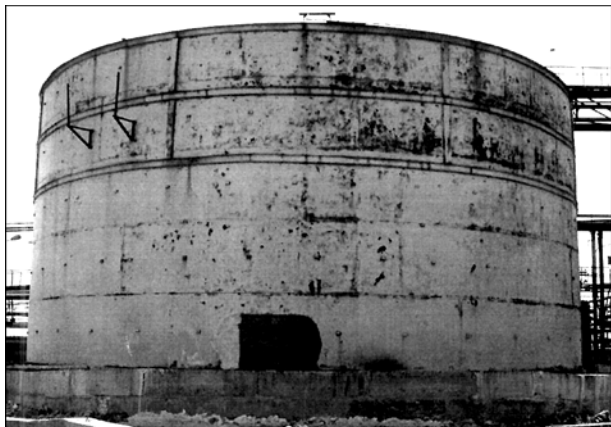


Figure 1. Large-size sulphuric acid storage tank of steel St3S with a capacity of 3000 m³

*The article is based on the results of the target program of the NAS of Ukraine «Problems of Life and Safe Operation of Structures, Constructions and Machines» (2004–2006).

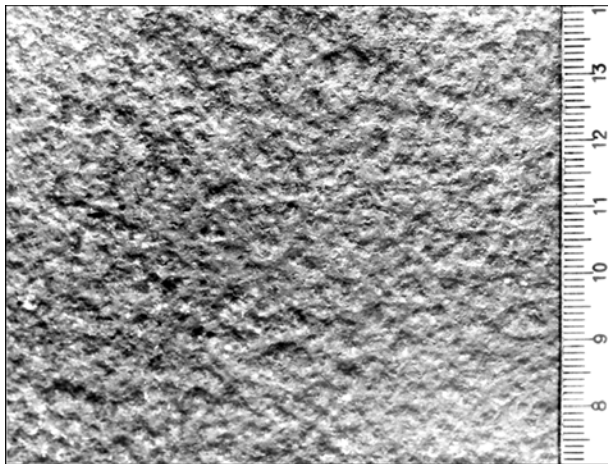
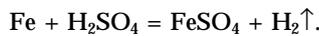


Figure 2. Appearance of inside surface of a concentrated sulphuric acid storage tank of steel St3S after operation for 16 years



Because of low solubility in the acid, ferric sulphate FeSO_4 is deposited in a thin layer on the tank surface and inhibits a corrosion damage of metal. Acting as an oxide reagent, sulphuric acid causes passivation of the metal surface. Hydrogen evolved during the reaction partially diffuses into metal, and is accumulated in the location of defects, non-metallic inclusions and at grain boundaries. This may lead to formation of a high level of stresses, buckling of metal and corrosion cracking (CC) [6, 7]. The higher the purity of steel used to manufacture equipment, the lower the probability of cracking of the CC type. Note

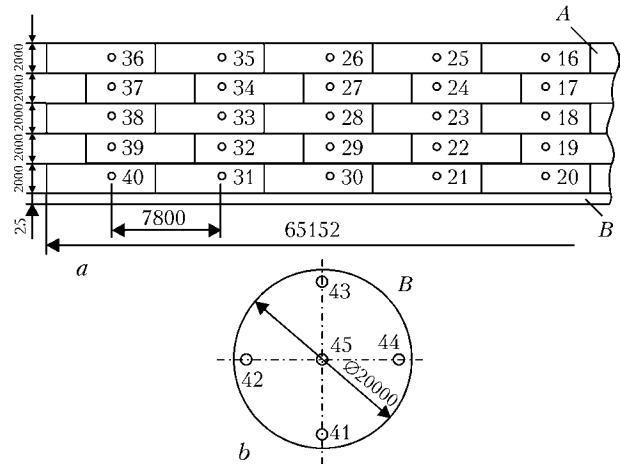


Figure 3. Fragment of scanning of shell (a) and scheme of bottom (b) of concentrated sulphuric acid storage tank # 1 of steel St3S with numbering of reference points for thickness measurement

that cracks of the CC type are rarely formed in the tanks of carbon steel St3S, which operate under the above conditions. Only two cases of formation of cracks of this type were fixed for 22 years of operation of the tanks at VostGOK. One of them was a crack in the bottom of tank # 4. A longitudinal through crack about 70 mm long formed in the weld and propagated to the base metal on the right and left side of the weld to a distance of about 50 mm. No defects of the type of buckling were fixed in the shells and bottoms of the tanks. Components of conventional low-alloy cast iron are less sensitive to cracking of the CC

Table 1. Variations in thickness of wall and bottom of sulphuric acid tank # 1* at VostGOK in years

Number of shell ring	Thickness of shell wall, mm	Number of point of measurement of shell thickness	Measured thickness of shell, mm				Number of point of measurement of shell thickness	Measured thickness of shell, mm			
			1994	1996	2000	2002		1994	1996	2000	2002
5	8	36	7.6	7.6	7.6	7.5	26	7.8	7.8	7.7	7.5
4	10	37	9.0	9.0	9.0	8.7	27	9.4	9.4	9.3	9.0
3	12	38	10.5	10.5	10.3	10.0	28	10.6	10.4	10.0	9.7
2	14	39	12.4	12.3	11.9	11.6	29	12.7	12.6	12.3	12.0
1	16	40	14.2	14.2	13.7	13.4	30	13.9	13.9	13.7	13.4

Table 1 (cont.)

Number of point of measurement of shell thickness	Measured thickness of shell, mm				Number of point of measurement of bottom thickness	Measured thickness of shell, mm		
	1994	1996	2000	2002		1994	1996	2002
16	7.8	7.7	7.6	7.5	41	24.2	24.0	23.5
17	9.5	9.3	9.2	9.0	42	23.5	23.4	23.3
18	10.5	10.4	10.2	10.0	43	24.7	24.3	24.2
19	12.3	12.2	12.2	12.0	44	23.5	23.3	23.1
20	14.2	13.8	13.7	13.6	45	23.2	22.9	23.5

* Tank # 1 is in operation since quarter III of 1984 until now.



type, which is attributable to a high carbon content [6, 7] and low ductility of the cast iron.

The hydrogen evolved is also accumulated in the upper part of a tank. Therefore, the tank should be thoroughly purged to perform technological operations (welding, cutting, heating, etc.).

During operation of the tanks, corrosion damage may result in formation of discontinuities in the tank covers, through which moisture, rain or snow may get into a tank. In this case, zones with a low-concentration sulphuric acid, which leads to an accelerated local corrosion damage of metal, may form on the filling mirror. In particular, this case was fixed in operation of one of the tanks at VostGOK.

During many years' operation of the concentrated sulphuric acid storage tanks, corrosion products (residue) based on ferric sulphates are accumulated in a lower part of the SAP tanks. For example, during 16 years of operation at VostGOK, about 120 t of the residue were accumulated in tank # 1, and about 100 t --- in tank # 15. In 2000, further operation of these tanks became practically impossible. Removal of the residue through hatches in the tank cover is a labour-consuming process. Moreover, it is prohibited by safety requirements [8]. It is recommended to remove the residue from a tank immediately after discharge of the acid, as an accelerated corrosion of the shell wall occurs in the upper part of the residue. That caused a corrosion damage of the shell in tank # 5. As a result, it was necessary to replace the lower part of the lower ring 700 mm high on the entire perimeter of the tank.

To make cleaning of the tanks from the residue more convenient, a process window 850–1050 mm high and 850 mm wide was cut out in the lower ring by the gas-oxygen method. Cutting out of such a window made it easier and faster not only removal of the residue from the tanks, but also performance of other operations, such as deactivation of the tanks, washing,

purging, checking of the corrosion state of the inside surface of the tanks, and repair operations by welding and cladding of the zones damaged by corrosion.

The E.O. Paton Electric Welding Institute, Open Joint Stock Company «Ukrainian Research and Development Institute for Chemical Engineering» (UkrNIIKhimash) and VostGOK developed specifications and technology for repair of the above tanks. Prior to repair, the tanks were subjected to technical diagnostics in compliance with requirements of DSTU 4046--2001 and GSTU 3-020--2001 [9, 10]. Thickness of the shells and bottoms of the tanks was measured at the reference points (see Table 1), horizontality of the bottoms and verticality of the shell walls was checked, defective locations were cleaned by the abrasive method, and all the welds and zones damaged by corrosion were thoroughly examined by the visual and optical methods. Completeness of removal of the zones of corrosion damage, welding defects (undercuts, pores, etc.) and cracks in metal of the questionable locations was checked by the dye penetrant and ultrasonic inspection methods. Test specimens were welded of steel St3S cut from a process window, inserts of steel St3sp2 welded into the window in the shell, and bottom regions subject to repair. Tests of the specimens proved correctness of the selected welding parameters (steel grade St2sp2 for inserts into the windows to repair defective zones in the shells and bottoms, types of weld edges, grades of welding electrodes, welding and cladding conditions, etc.) used in the repair specifications (Table 2).

Preparatory operations for welding, cladding and repair were performed by keeping to the standards in force in the industry [10, 11]. Treatment of edges of the S21 type, according to GOST 5264--80, for welding of inserts into the process windows and for repair of defective zones in the shells was identical on the entire contour with opening to the external part of a tank. Welding of an insert into a shell in replacement of

Table 2. Mechanical properties of base metal and welds in check welded joints of steel St3S and St3sp2 made with electrodes UONII-13/55 at room temperature

Test specimens	Static tension					Impact toughness	
	Yield stress, MPa	Tensile strength, MPa	Elongation, %	Reduction in area, %	Location of fracture in specimen	Location of U type notch in specimen	Impact toughness KCU, J/cm ²
Steel St3S, 13 mm thick	240.0 237.5	423.5 414.5	38.3 36.7	65.9 62.0	--	Across rolling direction	246.3 250.0
Steel St3sp2, 16 mm thick	252.8 260.8	463.1 461.1	35.7 32.7	57.2 59.8	--	Same	300.0 244.3
Welded joint St3sp2 + St3S, 16 + 13 mm thick	--	411.0 419.0	--	--	In less strong steel St3S	At weld centre	283.9
Specimens of weld metal	399.8 365.9	520.1 521.8	28.3 31.3	75.6 73.9	--	Across weld length	270.0
Requirements of GSTU 3-17-191--2000 to weld metal	--	Not lower than σ_r of less strong steel	Not lower than 18 %	--	--	--	Not less than KCU = 50 J/cm ²



part of the lower ring in tank # 5 was performed in a similar way. Welding in replacement of part of the bottom in tank # 5 and repair of the bottom in the CC zone in tank # 4 was performed on a permanent backing. Metal in the weld root inside the tank was machined with a grinder. Completeness of removal of a non-penetrated metal was checked by the dye penetrant method. And the weld root was welded in one-two passes. Electrodes of the UONII-13/55 grade were used for repair. To prevent separation of the deposited metal, cladding of the bottom regions and welds damaged by corrosion was carried out by depositing a sub-layer using the UONII-13/45 electrodes, followed by depositing layers using the UONII-13/55 electrodes. After repair, the welded joints and cladding regions were subjected to visual-optical examination, ultrasonic inspection, and tightness testing (kerosene test) [12]. Where necessary, certain welded joints and cladding regions were tested by the dye penetrant inspection method.

Four tanks were repaired: in 2000 --- # 1 (replacement of an insert in the process window because of formation of a crack of the CC type in the weld), # 2 (replacement of a wavy part of the shell), # 4 (repair of the bottom in the CC zone), and in 2005 --- # 5 (replacement of part of the shell and bottom). The life of the tanks was extended with a requirement to perform annual re-examinations.

CONCLUSIONS

1. Specifications were developed, and repair was performed on four large-size concentrated sulphuric acid

storage tanks of steel St3S (analogue of steel St3sp2), with a capacity of 3000 m³.

2. Service life of the tanks was extended with a requirement to perform annual re-examinations of their corrosion state.

3. The technology and recommendations can be applied to other carbon steel tanks for storing corrosive products.

1. Dyatlova, V.N. (1964) *Corrosion resistance of metals and alloys*. Moscow: Mashinostroenie.
2. Tomashov, N.D., Chernova, G.P. (1986) *Corrosion theory and corrosion-resistant alloys*. Moscow: Metallurgiya.
3. Sukhotin, A.M., Zotikov, V.S. (1975) *Chemical resistance of materials*. Leningrad: Khimiya.
4. Gladyshevskaya, S.A. (1964) Extension of service life of sulphuric acid tank wagons. *Zheleznodorozhn. Transport*, **6**, 77-79.
5. (1972) *Elektrody do Elektrycznego Lukowego spawania. Producenta*. Huta Baildon.
6. Archakov, Yu.I. (1985) *Hydrogen corrosion of steel*. Moscow: Metallurgiya.
7. Vasylenko, I.I., Shulte, O.Yu., Radkevich, O.I. (1990) Influence of chemical composition and technology of production of steels on their sensitivity to hydrogen cracking and sulphur-hydrogen corrosion cracking. Review of foreign researches. *Fiz.-Khim. Mekhanika Materialiv*, **26(4)**, 8-22.
8. (1980) *Safety rules for productions of main chemical industry*. Moscow: Nedra.
9. *DSTU 4046-2001: Technological equipment of petroleum refining, petrochemical and chemical productions. Technical diagnostics. General technical requirements*.
10. *DSTU 3-020-2001: Fusion welding of metallic materials in chemical and petroleum machine-building*.
11. (1988) *Rules of technical service of vessels and recommendations for their repair*. Moscow: Nedra.
12. *DNAOP 1.3. 00-8.02-93: Performance of operations on evaluation of remaining serviceability of technological equipment for petroleum refining, petrochemical and chemical productions*. Kiev.

WELDABLE HIGH-CHROMIUM NICKEL-FREE STEEL 04Kh19AFT OF GENERAL PURPOSE

Basic technology of processing of thick- and thin-walled ferrite steel 04Kh19AFT and also the technology of its welding have been developed. The industrial production of hot-rolled thick-sheet steel of 0.8-2.0 mm thickness has been mastered. Corrosion resistance of the new ferrite nickel-free steel was investigated in the media of baking, sugar and alcohol production.

It is recommended to use steel 04Kh19AFT instead of Cr-Ni steel in food machine building.

Purpose and application. The new nickel-free steel 04Kh19AFT is designed for manufacture of products and technological equipment of food, processing, chemical, automotive industry, home appliances, consumer's good, etc. Steel has passed tests at the enterprises of Ukraine under the industrial conditions in manufacture of tanks for dough kneading, dough mixing machines, table sets, fermenting tubs.

Experimental-industrial production of hot- and cold-rolled sheet 04Kh19AFT has been mastered, the technology of automatic, semi-automatic, and also manual arc welding of this steel has been developed.

Status and level of development. Experimental-industrial production.

Proposals for co-operation. Signing of contract for mastering the manufacture of welded structures.

Main developers and performers: Prof. Yushchenko K.A., Dr. Morozova R.I.

Contacts: Prof. Yushchenko K.A.
Tel./fax: (38044) 287-10-88



MODIFICATION OF WELD METAL IN ELECTROSLAG WELDING OF KhN77TYuR REFRACTORY ALLOY

E.N. ERYOMIN

Omsk State Technical University, Omsk, Russia

For manufacturing of annular billets, used in the aviation engine building, it is proposed to use electroslag welding by a combined electrode with modification of the weld metal by disperse particles of titanium carbonitride. Results of the weld metal investigation in welding of the KhN77TYuR alloy are presented. Advantages of new welding technology are demonstrated.

Keywords: electroslag welding, refractory nickel alloy, modification, structure, mechanical properties

Special-purpose items, manufactured from refractory alloys, are widely used in the aviation engine building. Manufacturing of billets of such items in a welded version allows significant increasing utilization factor of expensive alloys. However, such alloys are characterized by low weldability, and because of this reason the billets are produced mainly by different methods of hot conversion --- forging, piercing and rolling, which ensure high labor input in their production and significant consumption of metal in machining. Application of mentioned technological processes is a forced solution, which is resorted to because of low quality of welded joints. That's why search of the technology for manufacturing of such billets in welded version is rather urgent task.

In this relation application of electroslag welding (ESW), by means of which a single-pass welding of structures of different thickness is performed, has good prospects. However, the advantageous ESW methods, in which plate, wire and plate-wire electrodes were used, not always ensured necessary quality of welded joints of the refractory nickel alloys.

For the purpose of improvement of the technology, ESW was performed by a «split» combined electrode with application of a specialized installation equipped with the TShS-3000-1 power source [1, 2]. Simultaneous introduction into the slag pool of a non-consumable and a consumable electrode was performed, whereby the devices, indicating melting of the weld root and withdrawal of the shrinkage cavity, were used.

Technology of the ESW process with application of a combined electrode was developed on specimens

of the EI-437BUVD (KhN77TYuR) alloy of 22--43 mm thickness. A tungsten bar of 10 mm diameter was used as a non-consumable electrode. The EP-533 wire of 3 mm diameter was used as a consumable electrode.

As it is known, fluxes exert great influence on the weld quality and formation. The lowest melting loss of titanium and aluminium --- main alloying elements of a refractory alloy forming γ -phase --- is ensured by the ANF-7 and ANF-1 fluxes. In this connection they are more frequently used in welding of the alloys doped by these elements [3]. However, the ANF-7 flux is hygroscopic, that's why frequent calcination at high temperatures is necessary. The ANF-1 flux has high melting point, which causes lack of fusion of the edges being welded. In this relation the ANF-21 flux of the $\text{CaF}_2\text{-Al}_2\text{O}_3\text{-TiO}_2$ system, designated for electroslag remelting of the titanium-containing steels, has good prospects for welding as well: it is not hygroscopic, has a reduced melting point, and ensures high temperature of the slag pool [4].

Estimation of chemical composition of the weld metal in relation to main alloying elements, responsible for properties of the alloy, was performed on the ARG-MET-930SP optical-emission analyzer.

Results of chemical analysis of the electrode and the weld metal in welding of the KhN77TYuR alloy using the ANF-21 flux presented in Table 1, showed expediency of using this flux, because in this case chemical composition of the weld metal in correspondence with requirements of the specifications and quality formation of the weld are ensured.

The shortcomings of welding of refractory nickel alloys are low mechanical properties of the weld metal and its high-temperature strength. In this connection investigation of quality of the welded joints using metallography and mechanical and high-temperature strength tests were carried out. The specimens were subjected to heat treatment according to the specifications established for the base metal: tempering at 1080 °C for 8 h, cooling in air; ageing at 700 °C within 16 h, cooling in air.

Results of the tests showed that metal properties of the weld, produced with application of the EP-533 wire, did not meet any parameter requirements of the

Table 1. Content, wt.%, of main alloying elements in KhN77TYuR alloy

Object of investigation	Al	Ti
Electrode	0.86	2.76
Weld	0.65-0.77	2.50-2.54
According to specifications	0.6-1.0	2.5-2.9

**Table 2.** Test results of metal of ES-welded joints of KhN77TYuR alloy

Weld metal	σ_t , MPa	σ_y , MPa	δ , %	ψ , %	KCU, MJ/m ²	τ_{350}^{750} , h
Non-modified weld	$\frac{830-856}{843}$	$\frac{676-689}{684}$	$\frac{9.2-9.8}{9.6}$	$\frac{12.3-13.1}{12.8}$	$\frac{0.22-0.29}{0.26}$	$\frac{31-42}{36}$
NWZ metal	$\frac{934-940}{936}$	$\frac{718-726}{722}$	$\frac{12.2-13.4}{12.7}$	$\frac{14.8-16.1}{15.6}$	$\frac{0.32-0.38}{0.35}$	$\frac{46-51}{48}$
Modified weld (TIN)	$\frac{982-1012}{996}$	$\frac{756-769}{762}$	$\frac{19.2-19.7}{19.4}$	$\frac{20.2-21.4}{20.7}$	$\frac{0.78-0.85}{0.81}$	$\frac{92-98}{94}$
NWZ metal	$\frac{928-936}{931}$	$\frac{743-752}{748}$	$\frac{13.8-14.5}{14.2}$	$\frac{15.9-16.8}{16.4}$	$\frac{0.39-0.47}{0.44}$	$\frac{50-57}{53}$
KhN77TYuR alloy according to specifications	≥ 950	≥ 650	≥ 12.0	≥ 14.0	≥ 0.30	≥ 50

specifications. In addition, the weld metal had low high-temperature strength at temperature 750 °C and 350 MPa load, which constituted 60–70 % of the required one. Properties of the near-weld zone (NWZ) metal exceeded properties of the weld metal. That's why fracture always occurred over the weld --- the weakest place of the welded joint.

As state authors of a number of works [3, 5, 6], it is most expedient to use in welding metallurgical methods for increasing properties of the welded joints. To the main metallurgical method should be attributed suppression of the columnar character of solidification and refining of the crystalline structure using alloying by the elements-modifiers [7, 8]. In addition, in case of formation of equilibrium structure of the weld, the possibility appears to increase speed of welding at the same heat input [9].

In this connection modification of the metal pool by disperse inoculators was used for improving properties of the weld metal [10]. A modifier was used, composition of which included particles of titanium carbonitride (0.04 wt.%) [11]. Introduction of the components was performed by remelting of an additional nickel-base tubular electrode, internal cavity of which was filled with a powder modifier.

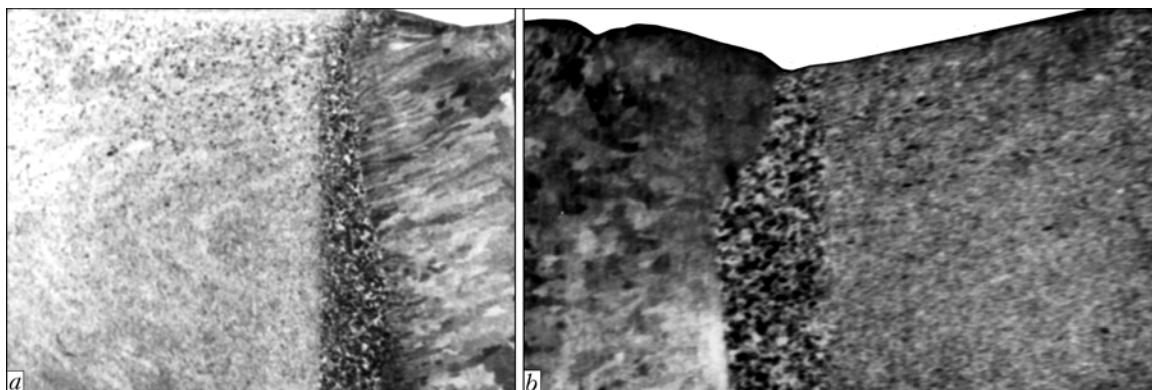
Results of the tests of the specimens from the KhN77TYuR alloy are presented in Table 2.

Place of the failure, size of the grains, distribution of non-metal inclusions and character of precipitation of the strengthening phases were investigated by metallographic method. Results of the microstructure in-

vestigation showed that failure of all specimens was of the intergrain character. Macrostructure of specimens of the non-modified weld metal is characterized by the developed transcrystallization from the fusion zone to the axis (Figure 1, a). In middle portion of the weld metal the zone, in which meet two solidifying fronts, is observed. Here columnar crystals have radial-axial direction with a small angle of inclination. Grain boundaries with such arrangement are the most vulnerable places of the weld. This is well seen on relief of surfaces of the weld metal fracture, which have a glossy stone-like appearance with zones of complete breaking, which characterizes the fracture as a brittle one (Figure 2, a).

It was established in investigation of fracture places of the specimens of the non-modified weld metal after long-term high-temperature strength tests that the fracture always occurs in the area of a directed crystallization. Especially low high-temperature strength has the weld metal, boundaries of crystallites in which are arranged perpendicular or at a small angle to the action of main stresses (Figure 2, b). This may be explained by the fact that important factors, which determine quality and service properties of the refractory alloys, are phase composition, state of the grain boundaries, size of the grains, degree of homogeneity, and morphology and topography of the inclusions [10, 12].

In macrostructure of the modified weld metal the grains are contained, boundaries of which are located approximately at the same distance from the center

**Figure 1.** Fragments of macrostructure of welded joints produced by ESW without (a --- $\times 0.5$) and with (b --- $\times 1.0$) modification

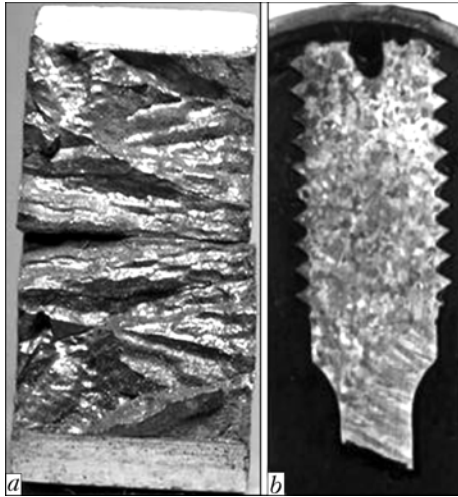


Figure 2. Character of fracture of specimens of non-modified weld metal after impact toughness (a) and high-temperature strength (b) tests

(see Figure 1, b), whereby size of the grains reduces down to 1–2 mm. Defects of the weld metal were not detected on any metallographic sections. Modification of the weld metal causes significant change of macrorelief of fractures of the impact specimens, in which side zones and zones of complete breaking appear, and the surface gets fine-grained and dull (Figure 3, a). Failure of the specimens in the long-term tests occurs in the area of equiaxial relatively fine grains (Figure 3, b). Formation of such structure, which removes the «slack» area of over the weld axis, causes increase of the technological strength that allows increasing speed of welding 2 times.

Microstructure of the non-modified weld metal is characterized by significant volume shares of the row carbides, sometimes of acicular shape, boride eutectic phases on the boundaries, and fine non-metal inclusions near the boundaries (Figure 4, a). Similar picture is observed in NWZ. Boride eutectics, which have low melting point, enable appearance of the crystallization cracks in welding.

Results of investigation of microstructure of the modified weld metal (Figure 4, b) showed that carbides are in this case coagulated and have a compact orbicular shape. They are mainly located on grain

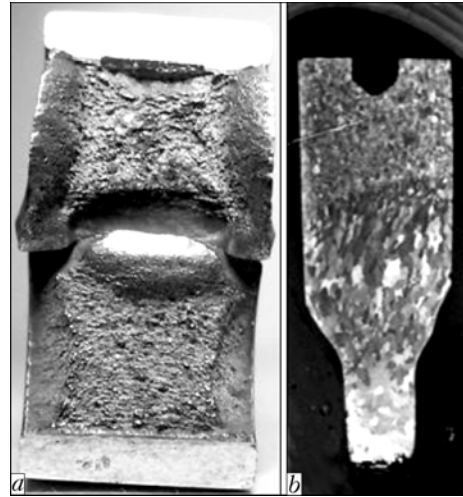


Figure 3. Character of fracture of specimens of modified weld metal after impact toughness (a) and high-temperature strength (b) tests

boundaries — the fact, which evidently enables their strengthening and stipulates increased high-temperature strength of the metal. Content of non-metal inclusions in this case is insignificant. The NWZ structure is similar to the one described above, but because of a higher welding speed it has a smaller size of the grains, which somewhat increases properties of the welded joint as a whole.

Change of gradient of temperatures and speed of movement of the solidification front in case of modification exert significant influence of the dendrite structure, size of the components, and phase composition of the refractory alloys.

Dendrite structure is used to be characterized by dispersity (mean distance between axes of the dendrites of second order) and density, which in this work was determined by ratio of total lengths of segments of axes and interaxial spaces, detected by the method of X-ray microspectral analysis. Non-simultaneity of the metal solidification in the interaxial spaces creates its segregation inhomogeneity in regard to the chemical composition.

Investigation of the alloy dendrite structure showed that after introduction of the modifier distance between dendrites of second order reduced from 43 to

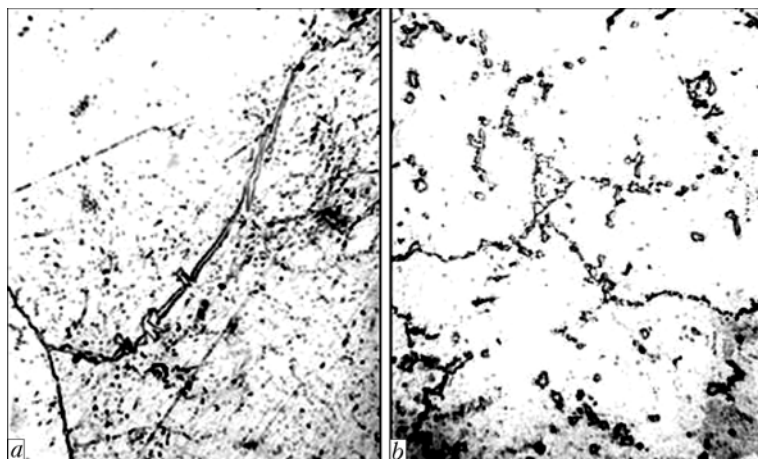


Figure 4. Microstructure of metal of weld produced without (a — $\times 240$) and with (b — $\times 520$) modification

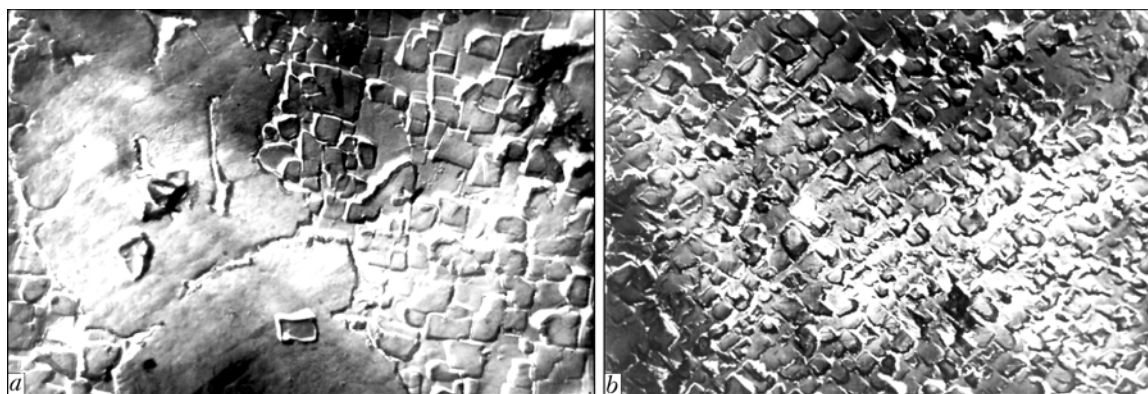


Figure 5. Microstructure of weld metal with γ -phase without (a) and with (b) ($\times 8000$) modification

21 μm , density of the dendrite structure increased from 1.3 to 1.9, and dispersity increased 2.3 times.

In this connection one has to expect lower development of the dendrite segregation. Usually segregation in complex alloys is sufficiently objectively estimated by the ratio of concentrations of the elements within a dendrite cell --- $K_s = C_i / C_a$, where C_i is the concentration of the element in the interaxial space, C_a --- in the dendrite axis.

Values of the segregation coefficient K_s of main doping elements of the KhN77TYuR alloy, determined by means of the X-ray microanalyser Cameca MS-46, are presented in Table 3. It follows from the Table that dendrite segregation of aluminium, chromium and nickel is insignificant, and they are uniformly distributed among axes and interaxial spaces, while segregation of titanium is sufficiently high.

Table 3. Segregation coefficients of main alloying elements of KhN77TYuR alloy

Weld metal	Al	Ti	Cr	Ni
Non-modified	1.06	1.94	0.92	1.11
Modified	1.03	1.15	0.96	1.08

If a doping element has $K_s > 1$, it is concentrated in the interaxial spaces and, vice versa, axes of dendrites are enriched with the doping elements at $K_s < 1$. In correspondence with this the γ -forming elements such as aluminium and titanium are forced back into the interaxial spaces, while chromium is mainly concentrated in axes of dendrites. Precipitation of phases in the interaxial space integrates their composition, which also enables reduction of high-temperature strength of the alloys [13]. In addition, due to significant segregation of the elements and their accumulation in carbides and borides of the eutectic, the solid solution gets depleted and content of γ -phase reduces down to 46 vol.%, which also significantly reduces high-temperature strength.

After modification titanium, which has high propensity to segregation, is redistributed more uniformly, ensuring noticeable equalization of composition among dendrite axes and interaxial spaces, whereby the trend to formation of a more homogeneous

structure in comparison with a non-modified alloy is observed. This is explained by the fact that modification activates diffusion processes in the melt and thus enables more complete removal of segregation.

Investigation of γ -phase (Figure 5) showed that precipitates of the strengthening phase formed in disintegration of the solid solution are even in cast state sufficiently fine and uniformly distributed for the modified weld metal solidified at relatively high rates.

In structure of the non-modified weld metal extensive precipitates of secondary phases are observed, which occupy significant share of γ -matrix; in this connection content of γ -phase here is significantly lower than in the modified weld metal.

So, application of improved ESW technology will allow significant saving of material and monetary resources due to increased quality and reduction of labor input in manufacturing of annular billets from refractory alloys in the aviation engine building.

1. Eryomin, E.N. (2005) Application of a combined electrode in electroslag welding of thin materials. *The Paton Welding J.*, **12**, 48–49.
2. Eryomin, E.N. (2005) Device for formation of weld in electroslag welding. *Ibid.*, **9**, 46–47.
3. Medovar, B.I. (1966) *Welding of heat-resistant austenitic steels and alloys*. Moscow: Mashinostroenie.
4. Medovar, B.I., Tsykulyenko, A.K., Shevtsov, V.L. et al. (1986) *Metallurgy of electroslag process*. Kiev: Naukova Dumka.
5. Khimushin, F.F. (1969) *Heat-resistant steels and alloys*. Moscow: Metallurgiya.
6. Shorshorov, M.Kh. (1973) *Hot cracks in welding of heat-resistant alloys*. Moscow: Mashinostroenie.
7. Zemzin, V.N. (1972) *High-temperature strength of welded joints*. Leningrad: Mashinostroenie.
8. Bashnin, Yu.A., Isakova, V.N., Maslenkova, E.A. (1991) *Influence of remelting processes on structure and properties of steels*. Moscow: Metallurgiya.
9. Dudko, D.A., Sidoruk, V.S., Tyagun-Belous, G.S. (1982) Means of decrease in heat input in welded metal during electroslag welding of thick-walled structures. *Avtomatich. Svarka*, **10**, 48–50.
10. Saburov, V.P. (1998) Strengthening modification of steel and alloys. *Litejnoe Proizvodstvo*, **9**, 7–8.
11. Eryomin, E.N. (2005) Application of electroslag remelting for generation of waste of heat-resistant alloys. *Advances in Electrometallurgy*, **2**, 20–23.
12. Logunov, A.V., Petrushin, N.V., Kuleshova, E.A. et al. (1981) Prediction of influence of structure factors on mechanical properties of heat-resistant alloys. *Metallovedenie i Term. Obrab. Metallov*, **6**, 16–20.
13. Kishkin, S.T. (1980) Specifics of structure transformations of heat-resistant nickel alloy during high-temperature heating. *Izvestiya AN SSSR. Metall.*, **6**, 190.

STRENGTH OF JOINTS ON SHEET ALUMINIUM ALLOYS PRODUCED BY FRICTION STIR WELDING

A.G. POKLYATSKY, A.Ya. ISHCENKO and M.R. YAVORSKAYA
E.O. Paton Electric Welding Institute, NASU, Kiev, Ukraine

The paper deals with the features of weld formation in fusion welding of aluminium alloys under the impact of high-temperature heating, and friction stir welding, ensuring weld formation due to plastic deformation of the metal in the welding zone. Technological sequence of friction stir welding process is given and the main principles of its implementation using the designed laboratory unit are described. Strength and ductility indices of welded joints on sheet (1.8–2.4 mm) high-strength aluminium alloys produced by nonconsumable-electrode argon-arc and friction stir welding have been analyzed.

Keywords: friction stir welding, aluminium alloys, non-consumable electrode argon-arc welding, hardness, bend angle

Development of modern mechanical engineering industries leads to ever higher requirements being made of the reliability of welded joints. In Ukraine arc and beam welding processes are used for manufacturing welded structures from aluminium alloys in most cases. They allow producing permanent joints through formation of welds as a result of melting of the edges being welded under the impact of a high-temperature heat source. Because of irreversibility of the physico-chemical processes running in aluminium alloys in fusion welding, phase transformations occur and zones of different structure form in the welding zone. Differences in the structure of weld metal and HAZ lead to a non-uniform distribution of residual deformations and stresses and lower the service properties of the joints. Presence of surface-melted grain boundaries and coarse phase inclusions in the metal structure limits plastic deformation and leads to increase of local stresses in the sections located between the grain boundaries. The overall stressed state of welded joints can exceed the yield point and lead to initiation of

microcracks, which lower the structure strength and initiate fatigue cracks, thus lowering the residual life and performance of weldments.

It is also characteristic that the current level of engineering development requires application in welded structures of different alloys developed on the basis of more complex alloying systems and produced using advanced technologies. Such materials are characterized by the necessary set of physico-mechanical characteristics and are often difficult-to-join by fusion welding. Therefore, friction stir welding (FSW) is highly promising for making permanent joints of aluminium alloys, when weld formation is due to localizing the heat evolution and plastic deformation of the metal in the welding zone [1, 2].

No macroscopic melting of the metal occurs with the above welding process, that is why the degree of structural-phase transformations in the weld metal and HAZ is much lower than in fusion welding. This enables obtaining higher physico-mechanical properties of welded joints and a lower level of residual stresses. The probability of microcrack initiation decreases, thus promoting an improvement of the life and performance of welded joints [3, 4].

FSW technology (Figure 1) developed in 1991 by W. Thomas from the Welding Institute (TWI) includes three main stages [5, 6].

At the first stage the rotating tool 1 is lowered into the butt of parts 4 and 5 to be joined so that the working surface of lip 2 of the tool contacted their surface. Heat evolves in the place of contact of the lower surface of the rotating tip of the tool with the parts. This leads to plastic flow of the metal from under the working tip, resulting in its gradual immersion, thus increasing the area of the contacting surfaces and amount of heat evolving through friction. After complete immersion of the working tip to the full thickness of the metal being welded, friction develops between the surfaces of the lip and the parts. As a result of heating the metal goes into the plastic state, which is followed by the second stage of welding, namely displacement of the rotating tool along the butt line. Linear displacement of the tool leads to plastic flow of the metal from the tool lip front to its

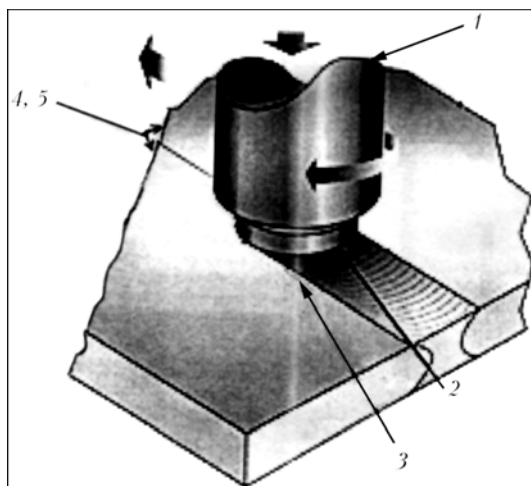


Figure 1. Schematic of FSW of aluminium alloys: 1 — rotating tool; 2 — working surface of tool lip; 3 — weld; 4, 5 — parts being welded

opposite side, where the metal cools down and forms the weld 3. Such a weld is non-symmetrical relative to its longitudinal axis, as the material is ousted by the working tip from the one (frontal) side to the other (rear) side. At the final stage of the welding process (at the end of the weld), the tool is raised till its tip completely moves out of the butt and its rotation is stopped. The parts being welded are rigidly fastened and clamped to the backing to avoid their displacements or bending out during welding [5, 7].

A laboratory set-up (Figure 2) was developed for implementation of FSW of sheet (1.8–2.5 mm) aluminium alloys. The set-up allows making butt and overlap joints with up to 400 mm weld length. The set-up consists of a mobile table moving at up to 40 m/h speed, on which the parts to be welded are fastened, and a rigid frame on which an asynchronous motor is fastened. Vertical displacement of the motor is provided by a support, the tool working tip being lowered into the metal being welded at the start of the weld and removed from the metal at completion of the welding process. A tool rotating at the frequency provided by the electric motor is fastened directly on the electric motor shaft.

The designed set-up was used to produce butt joints from aluminium alloys of the main alloying systems of 1.8–2.4 mm thickness. Mechanical properties of the studied alloys are given in Table 1.

FSW was performed by a special tool with lip diameter of 12 mm and conical working tip of 3.5 mm diameter at the base. Weld root was formed on a flat backing from stainless steel without a groove. At the tool rotation frequency of 2880 rpm sound welded joints of the studied aluminium alloys were produced at the welding speed of 233 mm/min (Figure 3). Welds were located parallel to the direction of sheet rolling.

The produced welded joints were used to make standard samples for mechanical testing, which were ground from the weld face side to achieve equal thickness of the base metal and the weld, and from the root side --- to avoid possible defects in the form of lacks-of-fusion. In addition, hardness distribution in the metal of welds and HAZ was studied, and their struc-

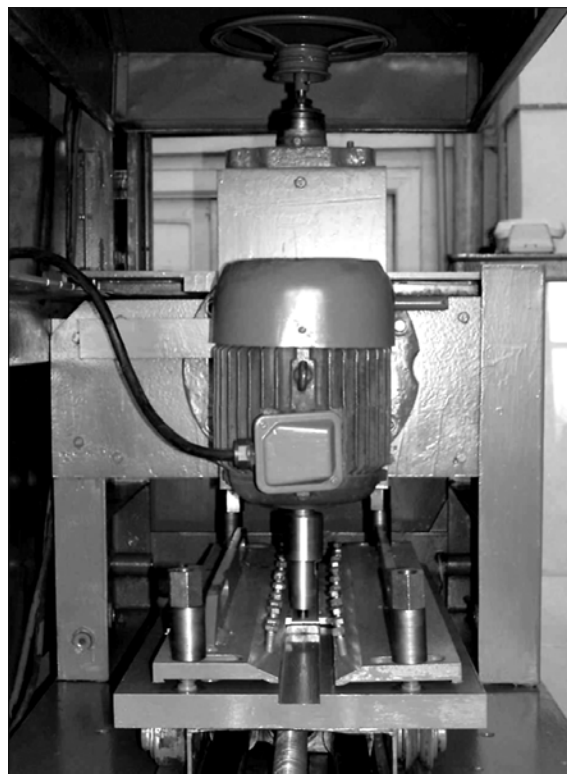


Figure 2. Appearance of laboratory set-up for FSW of sheet (1.8–2.5 mm) aluminium alloys

tural features were evaluated. Results of mechanical testing of the samples are given in Table 2.

Analysis of the results showed that the strength of aluminium alloy welded joints produced by FSW is on a sufficiently high level, and is higher than the values achieved in TIG welding in argon. For instance, in welded joints of alloys AMg6 and 1420 the ultimate strength is higher by 30–40 MPa, and that of alloys 1201 and 1460 --- by 15–20 MPa. The bend angle of welded joints is also not lower than that of fusion welded joints. In addition, FSW was used to successfully weld alloys AMg6 + 1201 and AMg6 + 1460. In their fusion welding hot cracks, which are due to a critical content of manganese and copper in the alloys being welded, quite often form at molten metal solidification.

Table 1. Mechanical properties of aluminium alloys

Alloy grade	Tensile strength σ_t , MPa	Yield point $\sigma_{0.2}$, MPa	Relative elongation δ , %	Bend angle α , deg
AMg6	370	228	21.2	180
	359	220	22.3	96
1420	459	322	11.4	50
	486	311	15.4	52
1201	427	303	11.9	60
	423	308	11.9	73
1460	504	460	8.9	36
	486	445	17.7	37

Notes. 1. Here and in Table 2 average parameter values are given from the results of testing three samples. 2. The numerator gives the values of samples cut out along the rolling direction, and the numerator --- across rolling.

Table 2. Strength and ductility properties of welded joints of aluminium alloys made by FSW and TIG welding in argon

Grades of welded alloys	σ_t , MPa		α , deg	
	FSW	TIG	FSW	TIG
AMg6 + AMg6	343 (ñ)	313 (b)	180	180
1420 + 1420	362 (b)	320 (b)	96	82
1201 + 1201	294 (b)	280 (b)	180	180
1460 + 1460	325 (b)	305 (b)	180	174
1460 + 1201	310 (b)	285 (b)	180	176
AMg6 + 1201	229 (ã)	--	180	--
AMg6 + 1460	323 (b)	--	180	--

Note. a, b, c --- sample fracture locations in weld metal, in the zone of weld fusion with the base metal and in the base metal in HAZ, respectively.

The curves of hardness distribution in the welded joints given in Figure 4 showed that when a high-temperature heat source applied in fusion welding is used, a significant heating of the metal and its considerable softening in the welding zone occur. The cast weld metal hardness is minimum. However, as the weld section is increased due to reinforcement, fracture of all the studied samples should proceed in the zone of weld fusion with the base metal, which was confirmed by the results of mechanical testing. In FSW no macroscopic melting of the metal occurs --- it is heated only to the plastic state. Therefore, hardness distribution in the welded joint metal made by FSW is

indicative of a lower heat impact on all its zones. In addition, the weld metal is subjected to plastic defor-

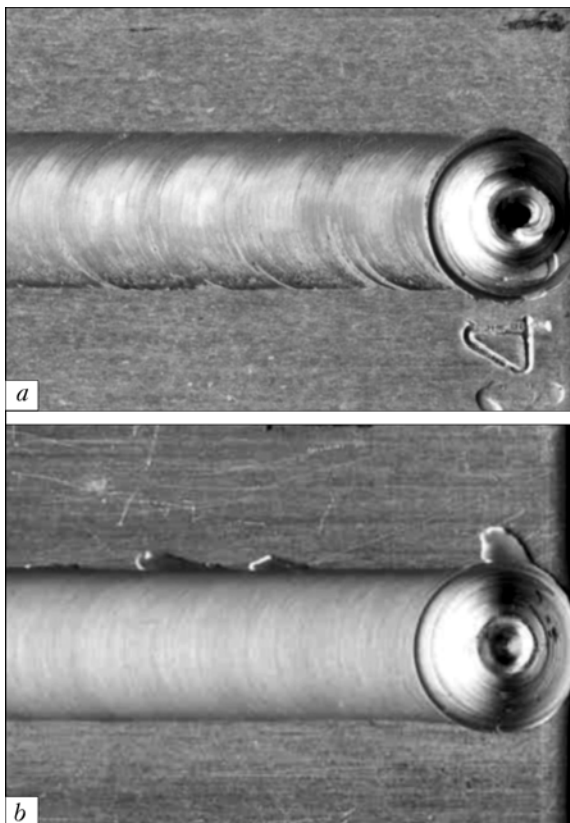


Figure 3. Appearance of FSW welds made on aluminium alloys 1460 2.2 mm thick (a) and AMg6 1.8 mm thick (b)

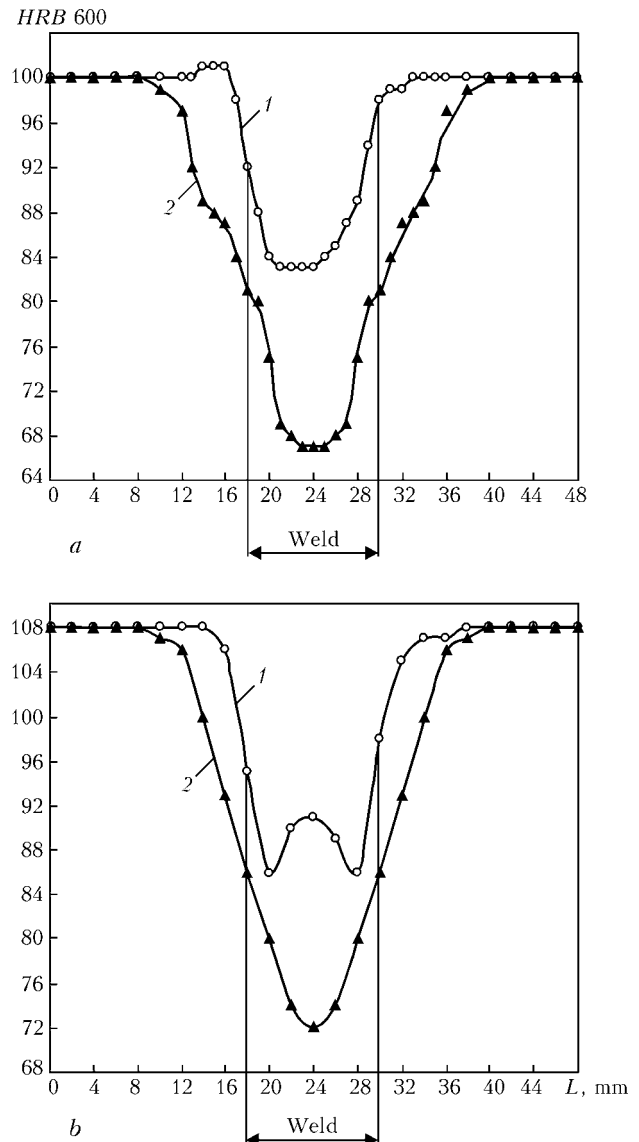


Figure 4. Hardness distribution in butt joints of 1201 alloy 2.0 mm thick (a) and 1460 2.2 mm thick (b) produced by FSW (1) and TIG welding (2)

mation due to the tool working surface pressing to the surfaces of sheets being welded, thus ensuring its higher hardness than in fusion welding.

A characteristic feature of FSW welds is their non-symmetrical location relative to the longitudinal axis, which is indicated by the curves of hardness distribution (Figure 4), as well as transverse macrosections. This can be especially clearly seen in macrosections of welds made by FSW on dissimilar aluminium alloys (Figure 5). Such a weld shape is produced as a result of the metal being ousted by the tool working tip on the one side (frontal) and being transferred to the other (rear) side.

Thus, the developed laboratory set-up for FWS allows producing sound welded joints of sheet aluminium alloys. Application of this welding process ensures a higher level of the joint mechanical properties than in TIG welding. The process of formation of a weld without macroscopic melting of the metal characteristic for other arc welding processes, allows joining difficult-to-weld aluminium alloys by fusion welding and widens the possibilities of application of dissimilar alloys in fabrication of welded structures for different mechanical engineering industries.

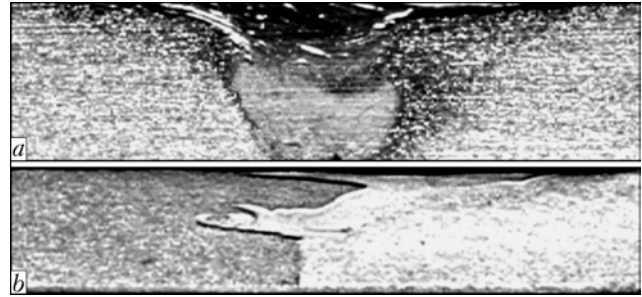


Figure 5. Transverse macrosections of FSW welds on aluminium alloys 1420 + 1420 2.4 mm thick (a) and AMg6 + 1420 2.0 mm thick (b)

1. Thomas, W.M., Nicholas, E.D., Needham, J.C. et al. *Friction stir welding*. Pat. 5460317 US. Publ. Oct. 1995.
2. Kninstrom, K.-E., Pekkari, B. (1997) A novel joining process — friction stir welding. *Svetsaren*, **1/2**, 49–52.
3. Larsson, H., Karlsson, L. (2000) Friction stir welding of AA5083 and AA6082 aluminium. *Ibid.*, **2**, 6–10.
4. Lanciotti, A., Vitali, F. (2003) Characterisation of friction stir welded joints in aluminium alloy 6082-T6 plates. *Welding Int.*, **8**, 624–630.
5. Tretyak, N.G. (2002) Friction stir welding of aluminium alloys (Review). *The Paton Welding J.*, **7**, 10–18.
6. Dawes, C.J., Thomas, W.M. (1996) Friction stir process welds of aluminum alloys. *Welding J.*, **3**, 41–45.
7. Stepanov, V.V., Konkevich, V.Yu., Frolov, V.A. (2003) Formation of joints in friction stir welding process. *Tekhnologiya Lyog. Splavov*, **1**, 58–67.

SYSTEM OF AUTOMATIC CONTROL AND MONITORING OF RESISTANCE SPOT WELDING

V.S. GAVRISH, P.M. RUDENKO and N.V. PODOLA
E.O. Paton Electric Welding Institute, NASU, Kiev, Ukraine

Virtual technology of the process of resistance spot welding is described. It enables automation of the process of selection of welding equipment, electrodes and welding modes, allowing for the grade and thickness of the alloy being welded and features of the structures being welded.

Keywords: resistance spot welding, computer control system, mathematical model, neural network

Current state of resistance spot welding technology enables widening the field of its application while obtaining higher quantitative and qualitative results. This is due to the broad range of welding machines with diverse technical characteristics and design, various electrode materials, differing by their physical properties and application features. Currently available control systems for resistance spot welding machines allow realizing complex cyclograms of metal heating and application of electrode compression force, stabilizing various parameters of the process, performing their reciprocal monitoring and evaluation of welded joint quality. However, full use of the available capabilities is related to the need for processing large volumes of technical information, and ability to make an effective use of it. This is not a simple task, as the required knowledge is at the junction of differ-

ent areas of science and technology. So, for instance, in order to perform setting up of the modern regulator for resistance spot welding, it is necessary to assign 20 and more parameters describing the welding mode, algorithms of stabilization of welding process parameters in real time, monitoring the welded joint quality and compensation of electrode wear.

The posed task is considerably simplified when virtual technology (VT) is used. For the case of resistance welding technology, VT is a PC program designed for rendering assistance to designers and technologists in design and fabrication of welded structures. The program allows selection of welding modes, welding machine type, method of process adjustment and welded joint quality control for a particular grade of material and its thickness, surface condition, required strength or diameter of weld nugget, as well as assessment of the welded joint quality by mathematical models. The technological chart for welding a particular item is printed out. Furtheron, welding

of two or three samples is required for practical verification of the technology.

The basis of VT is an expert system, consisting of the following main modules:

- data base containing the parameters of the welding mode for various grades of materials being welded and thickness of parts being welded, physical properties of the used electrodes, as well as technical characteristics of welding equipment;
- knowledge base including the rules and algorithms, which are used to select from the data base the welding mode parameters, electrodes and type of welding machine, depending on the grade and thickness of material being welded, as well as welding conditions;
- inference engine --- a subprogram allowing application of particular algorithms and rules from the knowledge base, depending on the user requirements;
- means of communication in terms of welding terminology --- subprogram ensuring a connection between VT and user through a multiscreen interface for input of data, which pertain to materials being welded and welding conditions;
- explanation subsystem --- subprogram, which is based on the principle of retrospective reasoning and explains how the system has come to a specific decision, describes the rule or rule sequence leading to this decision;
- subsystem for knowledge acquisition designed for entering new facts and rules into the system to complement or correct the knowledge base.

Data base is divided by the functional principle into several sections: «Equipment», «Welding modes», «Electrode alloys».

«Equipment» section includes about 70 types of welding machines with the following parameters: rated power of the welding machine, rated long-term secondary current, rated and maximum secondary current, rated and maximum clamping force, extension, opening, secondary circuit resistance, productivity, water flow, air flow, overall dimensions, and weight.

The «Welding modes» data base for parts from 0.3 to 4.0 mm thickness includes the following parame-

ters: welding current, welding duration, welding clamping and forging forces, electrode diameter, electrode sharpening radius, welding nugget diameter, and shear force.

«Electrode alloys» section contains data on 12 electrode alloy grades with the parameters of their physical properties.

The knowledge base includes the rules, by which selection of welding modes and welding equipment occurs. Selection of the type of welding machine is performed from the conditions of rated value of current, clamping force and power, corresponding to the machine certificate data. Depending on the dimensions of the item being welded, the possibility of its welding in the selected machine is checked by the maximum extension and opening of the machine contour. In addition, the process productivity (number of spot welds per minute) is calculated, proceeding from the welding cycles recommended by the system, and it is compared with the rated productivity of the welding machine. If it is impossible to achieve the calculated productivity, recommendations for selection of a higher power machine are given.

After selection of machine type by its technical characteristics, the system can give recommendations on welding machine connection to the mains, taking into account the maximum admissible current, duty cycle (in %), as well as the admissible voltage drop in the line. The required cross-section of the cable is recommended, depending on its length. At significant oscillations of the mains voltage, regulators are recommended, which ensure voltage stabilization in the welding transformer primary winding. Possibility of using the transformer of specified power at connection of single-phase peak load is checked based on ensuring a voltage drop of not more than 10 % of mains voltage for the machine the most removed from the substation.

Depending on the certificate data of the selected machine type, proceeding from water and air flow rate, recommendations are given for selection of inner diameter of hoses of the water and air supply system.

Rules of selection of the welding mode contain algorithms and formulas, by which the selected welding mode is corrected, allowing for the part surface preparation, requirements to splashes and dents from the electrodes. In addition, depending on welding modes, recommendations are given on electrode dressing after welding of a certain number of spots. The algorithms of welding mode correction use the data given in publications [1, 2], and incorporate the experience of the authors accumulated during performance of technological work on resistance welding together with enterprises of automotive, aircraft, radioelectronic industry operating the welding equipment.

VT work is based on the dialogue mode of the computer program (Figure 1). The dialogue starts with the proposed list of different materials, from which the material to be welded should be selected. VT includes the data on low-carbon, medium-carbon,

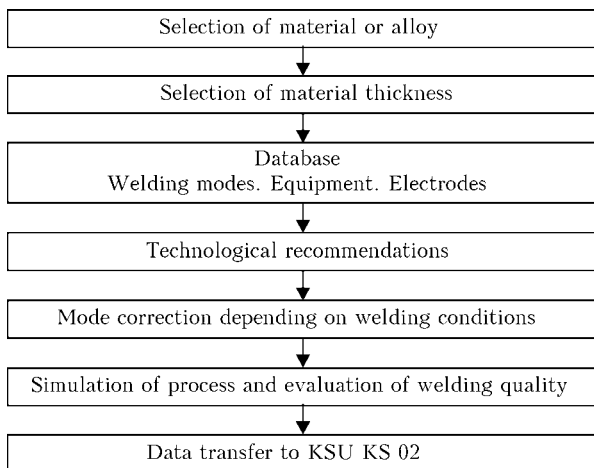


Figure 1. Algorithm of expert system operation together with KSU KS 02

low-alloyed, alloyed and corrosion-resistant steels, titanium and aluminium alloys. After selection of the material being welded, it is necessary to indicate its thickness (from the range of 0.3–4.0 mm), as well as the number of parts in the pack. Proceeding from the entered data on the material and thickness of the parts being welded, the system determines the basic mode, which is further on corrected, depending on the welding conditions. Analysis of the recommended welding modes showed that a tendency to application of more «stringent» modes is currently observed. In this connection, the parameters of welding modes allowing for recommendations of [1, 2] are included into the system. Then the condition of the surface of parts to be welded is indicated, and if it was subjected to treatment, also the treatment method is specified. VT issues recommendations on electrode grade and periodicity of their dressing, and also allows evaluation of the possibility of replacement of the recommended welding machine with the necessary correction of the mode. In addition, it is possible to obtain information on the technical characteristics of the recommended welding machine, applied electrodes, as well as a brief explanation of the prerequisites leading to particular decisions ---- recommendations issued to the welding-technologist.

The basic welding mode recommended by VT (Figure 2) can be corrected, depending on the welding conditions in a specific production. In welding of parts covered with scale, modulation of the first pulse of welding current and application of several current pulses separated by a pause, are recommended. The electrode life becomes longer and metal splashes in welding are reduced.

Basic welding mode is also corrected depending on the requirements made of the appearance of the joints, presence of splashes and dents caused by electrodes.

After the performed corrections comes the question of how does the obtained mode satisfy the requirements to the welded joint quality, allowing for the possible violations of the technological process, for instance, as a result of current shunting by earlier welded spots, introduction of ferromagnetic masses into the machine contour, etc. In order to conduct the necessary studies in VT, it is necessary to assign the ranges of parameter variations, which are connected with these disturbances and, on the other hand, are characteristic for the considered production by their value (Figure 3).

Investigation of the influence of disturbances is performed using mathematical models of the process, and is presented to the technologist in the graphic form (Figure 4). As was noted, the modern control systems for spot welding machines enable performance of welding process control with stabilization of individual parameters. In order to evaluate the effectiveness of application of these algorithms, it is possible to conduct studies of the influence of disturbances at I_w , U , P stabilization (Figure 4). From the data of

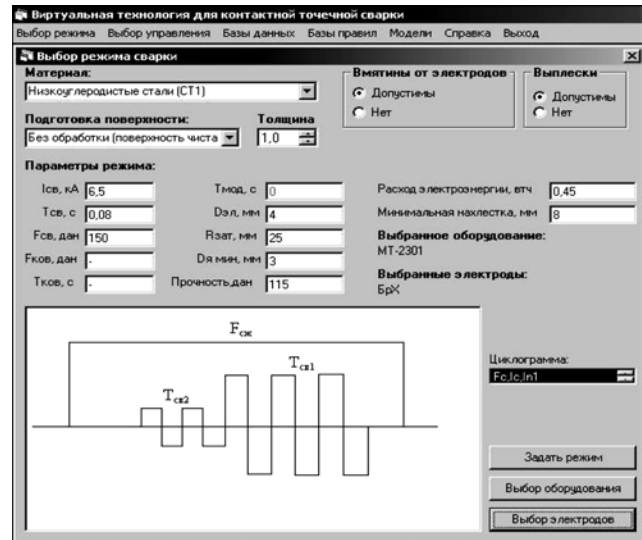


Figure 2. Basic welding mode

evaluation of compensation of disturbances by welding current stabilization it is seen that in this case it is possible to completely eliminate the negative impact on the process of mains voltage disturbances and increase of the secondary circuit resistance. On the other hand, at disturbances related to a change of resistance R (change of clamping force, diameter of electrode working surface, thickness of parts being welded) the error of execution of the spot weld nugget diameter increases compared to feedback control. This effect is related to the known phenomenon of self-adjustment, at which current stabilization is absent.

Ultimately, VT recommendations include the data on welding mode parameters, process control algorithms depending on disturbances characteristic for the considered production, electrode dimensions and material, values of minimum admissible shear strength of the spot weld, cast nugget diameter, size of overlap, as well as the applicable welding equipment and admissible power consumption.

The developed VT program can be used, for instance, in the computer control system KSU KS 02 [3], as it has rather wide capabilities both for control and for monitoring. In order to make a full use of them, a high level of technologist qualification is required for regulator adjustment. The above investigations on selection of the welding mode, stabilization algorithms, and parameters in the algorithm of elec-

Диапазон изменения параметров процесса	Допустимые отклонения			
	Optim	min	%	max
Дя - Диаметр ядра сварной точки, мм	5.00	2.00	60.00	7.00
Исв - Сварочный ток, кА	10.00	8.00	20.00	20.00
Uс - напряжение сети, В	380.0	360.0	5.26	420.0
Тсв - Вреня сварки, с	0.10	0.08	40.00	0.14
Fсж - сварочное усиление скатия, кгс	300.0	249.9	16.67	350.0
Дэ - диаметр рабочей поверхности электрода, мм	5.00	3.00	40.00	7.00
Сд - толщина свариваемых деталей, мм	1.00	0.50	10.00	1.10
Zк - сопротивление вторичного контура, мкОм	120.0	100.0	16.67	140.0
Лш - шаг между сварными точками	20.00	15.00	25.00	25.00
Rн - контактное сопротивление свариваемых деталей, мкОм	200.0	150.0	25.00	250.0

Figure 3. Setting the ranges of disturbance variation for resistance spot welding process

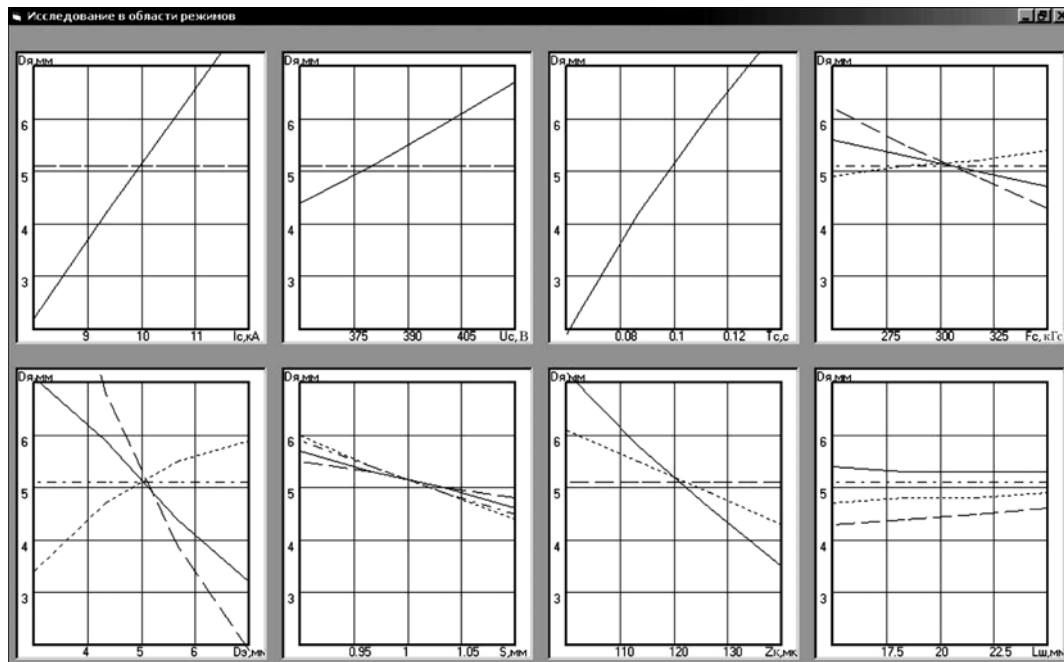


Figure 4. Graphs of the influence of disturbances on welded joint quality: *solid line* — without stabilization of any parameter; *wide dashed line* — welding current stabilization; *fine dashed line* — interelectrode voltages; *dot-dash line* — interelectrode power

trode wear compensation can be formed into a data file and transferred to KSU KS 02 by serial communications channel, built into the KSU KS for communication with a PC or upper level control system. It is obvious that, if required, a feedback from KSU KS 02 can be provided for receipt and acquisition of data for forming and printing out a protocol of structure welding, development of the data base on welding modes and knowledge base on mathematical models of the process or neural networks for welding control or quality control of welded joints.

It is known that over the last years not a single new manual or reference book has been issued or an old one has been re-edited in Ukraine or CIS countries in the field of resistance spot welding technology and

equipment. Organization of VT program, its data and knowledge bases allows not only filling it with the known information from the already published literature, but also simply entering new data into it in the future. On the other hand, the scope and visual nature of the presented information can make VT both useful at initial familiarization with the subject, and as a reference system for a qualified user.

1. Orlov, B.D., Dmitriev, Yu.V., Chakalev, A.A. et al. (1975) *Technology and equipment for resistance welding*. Moscow: Mashinostroenie.
2. (1993) Procedure for spot welding of uncoated and coated low carbon and high strength steels. *IIW Doc. III-1005*.
3. Krivenko, V.G., Rudenko, P.M., Gavrish, V.S. (2004) Computer control system KSU KS 02 for resistance spot machines. *Svarshchik*, 3, 37.



NDT OF WELDED JOINTS

DETERMINATION OF MAIN DIRECTIONS AND VALUES OF RESIDUAL STRESSES IN HIGHLY TEXTURED MATERIALS BY ACOUSTIC METHOD

O.I. GUSHCHA¹, V.A. BRODOVOJ¹ and V.N. SMILENKO²

¹E.O. Paton Electric Welding Institute, NASU, Kiev, Ukraine

²SE SRI «Kvant», Kiev, Ukraine

For the purpose of determining directions of action of main stresses in solid media with high attenuation of ultrasonic oscillations and in anisotropic media, ultrasonic longitudinal oscillations and shear oscillations, polarized in three directions, are introduced into them perpendicular to the plain of action of the stresses. The first direction of polarization is selected along direction of anisotropy with an unknown angle to the main direction. Two other polarization directions are selected inclined to the first one at acute angles, which are equal in value and opposite in signs. The velocity of propagation of ultrasonic oscillations for these directions is investigated. Angle of inclination of main stresses to the selected initial direction and values of these stresses are determined on the basis of these results.

Keywords: main directions, residual stresses, anisotropic media, ultrasonic oscillations, direction of polarization

Practice of application of the acoustic testing method of stresses shows that majority of low-alloy steels and a number of other structural alloys are characterized by a comparatively small dissipation of ultrasound in them. It is possible to observe in such materials up to eight and more packages of so called reflected ultrasonic signals, inhomogeneity of which stipulated by texture of the rolled metal is, as a rule, lower than inhomogeneity caused by the stresses. As a result, maximum signal on the receiver, provided all other conditions are equal, will be observed in case of coincidence of the polarization plain of the oscillations with main directions. Other received signals will be

arranged in a row with regularly diminishing amplitudes (Figure 1, a). In case of non-coincidence of the polarization plain with main directions the row of the received signals will have a form of irregularly diminishing signals (Figure 1, b). It may happen that not the first received signal will have the maximum amplitude; there can be more than one of such maximums. So, in the materials with insignificant attenuation of ultrasonic oscillations and comparatively non-pronounced texture of the rolled metal, main directions may be determined by view of the row of the diminishing signals on the receiver in the process of turning of the sensors.

At the same time for many structural materials appearance of the initial anisotropy, caused for example by rolling, is commensurable with the effect of

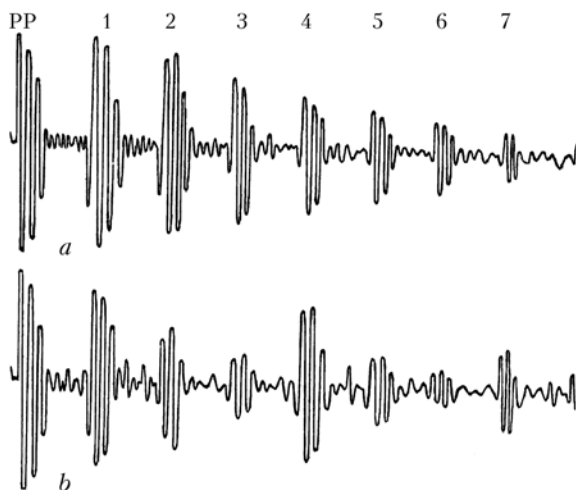


Figure 1. Row of packages of ultrasonic oscillations in case of coincidence (a) and non-coincidence (b) of polarization plain of oscillations with main directions: PP — probing pulse; 1-7 — number of reflected ultrasonic signal

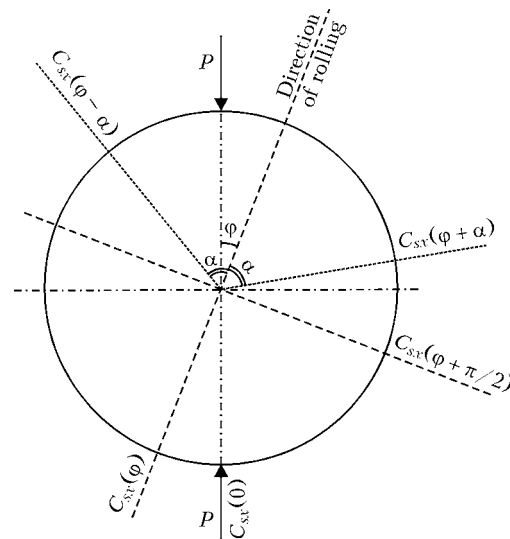


Figure 2. Polarization angles for determining main directions



φ_1 , deg	C_{Ix1}	$C_{sx}(\varphi)$	$C_{sx}(\varphi - 60^\circ)$	$C_{sx}(\varphi + 60^\circ)$	σ_{22} , MPa	σ_{33} , MPa	σ_{calc} , MPa
15	60483	34741	34721	34707	39.9	-90.1	12.1
30	60482	34732	34733	34706	36.1	-94.0	30.9
45	60485	34726	34740	34710	36.3	-93.9	43.9

elastic anisotropy. For a number of materials it significantly prevails over manifestations of elastic anisotropy (titanium alloys, special steels, aluminium alloys and fiberglass). There are also materials with high attenuation of ultrasonic oscillations, when a receiver registers just one-two reflected signals. For such materials the method presented above is unsuitable. That's why in measurement of stresses in such materials by the acoustic method main directions are assumed to be known [1]. In addition, in the measuring devices automatic regulation of the gain is, as a rule, present, whereby all reflected signals are amplified to the same level, which excludes possibility of observation of a natural series of the reflected signals. In this connection for the purpose of determining directions of action of main stresses in media with high attenuation of ultrasonic oscillations and in anisotropic media, shear ultrasonic oscillations, polarized according to the third direction, are additionally introduced into the investigated object perpendicular to the plain of action of the stresses (Figure 2). The first direction of polarization is selected along anisotropy with an unknown angle φ to the main direction, two other --- inclined to the first one at acute angles α , which are equal in value and opposite in signs [2]. For these directions velocities of propagation of the ultrasonic shear oscillations $C_{sx}(\varphi)$, $C_{sx}(\varphi + \alpha)$, $C_{sx}(\varphi - \alpha)$, respectively, are investigated. Then, having introduced the designations

$$\gamma = \frac{C_{sx}(\varphi + \alpha)}{C_{sx}(\varphi - \alpha)}, \quad \gamma_1 = \frac{C_{sx}(\varphi)}{C_{xx}(\varphi + \alpha)}, \quad \gamma_2 = \frac{C_{sx}(\varphi)}{C_{xx}(\varphi - \alpha)}, \quad (1)$$

$$K_1 = \frac{\cos^2 \varphi \sin^2 \alpha + \sin^2 \varphi \cos^2 \alpha}{\sin 2 \varphi \sin 2 \alpha}, \quad (2)$$

$$K_2 = \frac{\cos^2 \varphi \cos^2 \alpha + \sin^2 \varphi \sin^2 \alpha}{\sin 2 \varphi \sin 2 \alpha},$$

and from the dependence

$$\operatorname{tg} 2\varphi = \operatorname{tg} \alpha \frac{\gamma_1(\gamma_1^2 - 1)}{2 - \gamma_1^2 - \gamma_2^2} \quad (3)$$

we obtain velocities of propagation of ultrasonic waves along main directions:

$$C_{sx3} = \frac{C_{sx}(\varphi)}{\sqrt{\gamma_2^2 \left(\frac{1}{2} + K_1 \right) + \gamma_1^2 \left(\frac{1}{2} - K_1 \right)}} \quad (4)$$

$$C_{sx2} = \frac{C_{sx}(\varphi)}{\sqrt{\gamma_2^2 \left(\frac{1}{2} - K_2 \right) + \gamma_1^2 \left(\frac{1}{2} + K_2 \right)}} \quad (5)$$

Values of the residual stress components, directed along main directions, are determined by the expressions

$$\sigma_{33} - \sigma_{22} = \left[\frac{C_{sx3} - C_{s0}}{C_{s0}} - \frac{C_{sx2} - C_{s0}}{C_{s0}} \right] A, \quad (6)$$

$$\sigma_{33} + \sigma_{22} = \left[\frac{C_{sx3} - C_{s0}}{C_{s0}} + \frac{C_{sx2} - C_{s0}}{C_{s0}} \right] B, \quad (7)$$

where $C_{s0} = M(C_{sx3} + C_{sx2} - \Delta C_0) - NC_{Ix1}$ is the initial velocity of the shear acoustic oscillations; C_{Ix1} is the velocity of propagation of longitudinal acoustic oscillations; A , B , M , N are the factors of proportionality, which are determined by Young's modules of second and third orders.

Initial anisotropy, as it is known, affects initial velocity of the acoustic oscillations. That's why velocities of oscillations, polarized along and across direction of rolling, will significantly differ. This initial difference of velocities ΔC_1 may be written in correspondence with the designations, used in Figure 2:

$$\Delta C_1 = C_{sx}(\varphi)_0 - C_{sx}(\varphi + \pi/2)_0. \quad (8)$$

When polarization plain of the oscillations is turned relative the selected initial direction, initial velocity of oscillations will also respectively change. In this case value of initial difference of the velocities ΔC_0 may be written in the form

$$\Delta C_0 = \Delta C_1(\sin \varphi - \cos \varphi). \quad (9)$$

The methodology was tested on the disk from the 10G2S1 steel of 180 mm diameter and 22 mm thickness. The disk was loaded over its diameter with the 20 t force on the PS-50 hydraulic press. Calculated values of stresses were $\sigma_{33} = -96.5$ MPa and $\sigma_{22} = 32.2$ MPa. The specimen was loaded at angles 15, 30 and 45° relative direction of the rolling. Values of the recirculation frequencies were measured in direction of the rolling and at angles +60 and -60° relative this direction. The results were processed on PC according to a specially developed program. Results of the experiment are presented in the Table.

Values of the propagation velocities of ultrasonic oscillations are given in the pulse recirculation frequencies.

So, the acoustic method makes it possible to determine value and main directions of the acting stresses without destruction both in anisotropic materials and in the materials with pronounced anisotropy.

1. Guz, A.N., Makhort, F.G., Gushcha, O.I. (1977) *Introduction into acoustoelasticity*. Kiev: Naukova Dumka.
2. Gushcha, O.I., Makhort, F.G. (1983) Acoustic method of stress determination in solid media. *Byul. Izobreten.*, **36**.



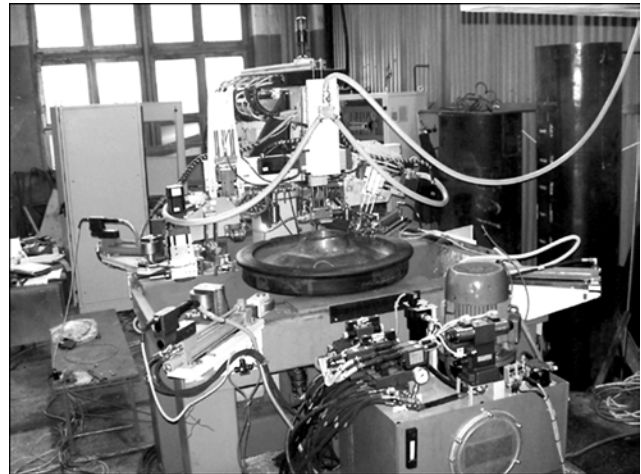
NEWS

AUTOMATED ULTRASONIC TESTING OF RAILWAY WHEELS

SE «Engineering and Design Office of the E.O. Paton Electric Welding Institute» continues its fruitful cooperation with OJSC «Vyksunsky Metallurgical Plant» (Russia), the biggest in Europe producer of pipes for main pipelines and railway wheels. Earlier articles were already published in the journal about developed in the PWI EDO installations of the NK360-362 type for non-destructive testing of welded joints and end portions of the pipes of 508–1420 mm diameter with thickness of the walls from 7 to 50 mm. A lot, consisting of six such installations, was supplied by the PWI EDO to the plant in 2004–2005. They passed foreign inspection according to DNVI, which gave permission to Vyksunsky MP to participate in tender on supply of the pipes for the oil pipeline «Nord stream», including laying of the pipeline over bottom of Baltic sea.

High rating of this equipment allowed the PWI EDO again winning the international tender and getting order on supply to Vyksunsky MP in 2007 of two stations for automatic ultrasonic testing of railway wheels, production of which at the plant constitutes almost one third of the world production.

In this July two stations NK364 for AUST of railway wheels were manufactured and sent to the customer. The installations are designed for detection of



disturbance of continuity of the flak type, laminations, crusts, which turned and sank during casting, gas bubbles, accumulations of non-metal inclusions and other internal defects, and segregations in the wheels of different nomenclature, used on railways of the whole world. An important peculiarity is the fact that the testing is carried out simultaneously over twenty channels on all elements of the wheel: the rim in axial and radial directions, the hub, the disk, and the flange.

NKMZ IMPLEMENTS POLICY OF ACTIVE TECHNICAL REEQUIPMENT

Novokramatorsk Machine Building Plant (NKMZ), Kramatorsk, Donetsk region, adopted the technical reequipment program for the next two years, which ensures further increase of the industrial production volumes. At present an electric melting furnace of own engineering is erected at NKMZ, which will completely replace acting open-hearth furnaces, increase volume of melted steel, and improve quality of the metal, required for manufacturing of the special-purpose equipment. The next year a new press-forging workshop equipped with state-of-the-art equipment, including forging complex with the 5100 t press, will be built at NKMZ. It is assumed that the whole equip-

ment will be designed and manufactured by the plant personnel.

In addition, the program of complete technical reequipment of the profile-casting workshops for 2008–2009 has been developed at the plant. The strategy of reequipment of mechanical workshops by high-productivity equipment will be implemented in parallel. Just in 2008, NKMZ assumes to purchase 26 and modernize 8 big unique machine tools.

It is assumed to invest in 2008 into technical reequipment of NKMZ all together up to 580 mln UAH.

THE 60th IIW ANNUAL ASSEMBLY



The 60th Annual Assembly of the International Institute of Welding (IIW) was held in Dubrovnik (Croatia) from June 30 to July 7, 2007. Croatia Welding Society was the organizer of the Assembly. About 600 delegates from 45 countries participated in the work of the Assembly. Out of

54 IIW member-countries the delegations of Argentina, Greece, Lybia, Pakistan and Chili were absent from the Assembly. The most numerous delegations were sent by Japan (70), Germany (53) and the USA (42 persons) as has been the case for the last 15–20 years. By the number of delegates, they are followed by France (32), Sweden (27), Russia (25), Hungary (19), Great Britain (16), Slovakia (18), Austria (16), Rumania and Ukraine (14), Canada and Finland (13), Holland and Portugal (11) and Australia (10). The delegations from the other countries consisted of 2–3 persons. 82 persons represented the country-organizer of the Assembly.

IIW activity rather completely covers the welding area in all its diversity: research, training, practical application, standards, cooperation and other. That is why for successful and fruitful work of the national delegations they should consist of 8–10 specialists as a minimum, each of which should participate in the working meetings of 2–3 commissions.

The first three days of the work of 60th IIW Assembly were dedicated to the meetings of the commissions, working groups and other subdivision sessions. Ukrainian representatives participated in the work of Commissions I–VI, IX–XV, STAND (standard), Board on International qualification and certification



of welding production personnel (IAB), as well as in the work of Research Group SG-212.

The main point on the agenda of the meeting of the International Accreditation Body (IAB) was studying the organization documents of the international system of certification of welding production, as well as welding production personnel, which is currently being developed at IIW. A similar system has been functioning within the framework of the European Welding Federation (EWF) since 1991. However, the area of its application is naturally limited only to Europe. After this system have been put into action, the creation of a complete integrated system for training and certification of welding production personnel, as well as certification of welding pro-



IIW members countries (by July 2007)			
Europe		America	Africa/Asia/Oceania
Austria	Lithuania	Argentina	Algeria
Belgium	Norway	Brazil	Australia
Bosnia and Herzegovina	Poland	Canada	CPR
Bulgaria	Portugal	Chili	Egypt
Croatia	Romania	Mexico	India
Czech	Russia	USA	Indonesia
Denmark	Serbia		Iran
Finland	Slovakia		Israel
France	Slovenia		Japan
Germany	Spain		KPDR
Great Britain	Sweden		(Korea)
Greece	Switzerland		Lebanon
Hungary	The Netherlands		Libia
Italy	Ukraine		Malaysia
			New Zealand
			Nigeria
			Pakistan
			Singapore
			South Africa
			Thailand



duction proper will be finished. It is anticipated that the system of welding production personnel certification under the auspices of IIW will become active starting from 2008.

ISO 3834 standard specifying the requirements to fusion welding quality will be the base standard of this system that is introduced in the form of harmonized national standard of Ukraine. In particular, the standard emphasizes that the manufacturer should have the corresponding personnel capable of supervising the welding performance, having sufficient authority and at the same time being responsible for welding quality.

Annual EWF Assembly and meeting of its technical committees were also conducted during the work of 60th IIW Assembly. It has been a regular practice of the last years that is caused by two reasons. The first is the desire to reduce financial expenses of the national welding committees. The second and main reason is that after the system of harmonized training of welding industry has been brought under the jurisdiction of IIW, as well as in view of currently performed transferring of the system of welding industry certification to it, the sphere of EWF exclusive activity has been essentially narrowed: practically, just about ten programs of welding production personal training were left in EWF competence, that are

not yet covered by IIW (these are the courses for training the European Specialist on thermal spraying, European Welder of plastics, etc.). The majority of EWF Assembly'2007 delegates characterized such a tendency as negative and spoke in favour of strengthening the EWF positions up to making financial demands of IIW for the harmonized systems of welding industry personal training and certification of welding production transferred to IIW.

Suggestions on solving exactly these matters were the major issues in the programs of candidates to EWF President's position for the following three years (2008–2010), whose election took place during this EWF Assembly. Two obvious favorites were among the four candidates: D. von Hoffe (Germany) and T. Jessop (England), T. Jessop won as a result of secret vote (left in the photo, at the moment of EWF President's responsibilities transfer from H. Fernandez, Spain).

International Conference «Welding and Consumables» (July 5–6, 2007), in which about 90 reports were presented, was held after the activities of 60th IIW Assembly were over.

The next 61th IIW Assembly will be held on July 6–11, 2008 in Gras, Austria.

The honorary mission of IIW Assembly organizer will be delegated to Ukraine in 2010.

V.E. Ponomarev, Cand. of Sci. (Eng.), PWI

COOPERATION OF THE E.O. PATON ELECTRIC WELDING INSTITUTE WITH INDIAN CENTERS ON WELDING INDUSTRY PERSONNEL TRAINING

Acceleration of economic development has been observed in India over the last years. Special attention is paid to the status of welding as the basic industrial process. Indian companies introduce modern welding technologies; buy equipment from leading world manufacturers. And this results in the need for training and retraining the welding production personnel to make the level of their knowledge and skill adequate to the technical level of modern welding fabrication. This cannot always be achieved with the system of welding production personnel training, available in India, and primarily of welders. More flexible approaches are required for such training under the conditions of new welding equipment introduction (both with expanded functional capabilities and with special ones). The duration of specialists training should be minimum possible, while providing a high quality of training. Module technologies of training applied at the E.O. Paton Institute Interindustry Training-Attestation Center (ITAC), meet such demands completely.

Module training technology envisages an individual principle of training. The training process is realized with the help of training elements (Figure 1) that are a brief description in a certain logical order of a concrete scope of knowledge or the procedure of execution of one separately taken practical skill that the student has to master on his own, under the guidance of an instructor or trainer. Training element contains the information necessary for it, in the form of an organic combination of the text and illustrations and is a booklet of 8–10 pages. It also contains a section for checking the material assimilation; a student goes over to studying the next training element only after positive results of the check.

In addition to the training element, video movies and computer animations about physical effects are created, the peculiar features of which can not always

be conveyed in their description in the training element or during an oral explanation. Visualization of such processes allows an essential facilitation of their understanding by students.

The welder is able, first of all, to master those professional skills that are needed by his employer company or those that can bring about his faster employment. This allows an essential reduction of the training time, reacting to the changes of production demands in time and ensuring the achievement of the required level of competence by each welder, guaranteeing his meeting the demands of a specific production.

Technologies for welders' training used in ITAC, also envisage application of a low-ampere trainer DTS-02 (Figure 2) at the initial training stage, with the help of which the welder masters the primary skills of maintaining a preset arc length, electrode (or torch) inclination and welding speed, as well as the technique of electrode tip (or torch) manipulation by the set sample. The latter is promoted by that the arc with 5–7 A current used in DTS-02 trainer does not melt the base metal and only leaves a characteristic trace on its surface. Two years ago the representatives of India Multi-Profile Training Center JSS MAHAVIDYAPEETHA were familiarized with it, and at present two DTS-02 trainers are successfully used in the training process at this Center.

V.E. Ponomarev, Deputy Director of ITAC, Cand. of Sci. (Eng.), visited this educational institution in July 2007 and conducted negotiations with Prof. M.N. Dhananjaya, Director, and leading specialists on further development of cooperation between ITAC and JSS MAHAVIDYAPEETHA in the field of training welding production specialists.

During his trip to India, V.E. Ponomarev also visited Welding Research Institute (WRI) by the invi-

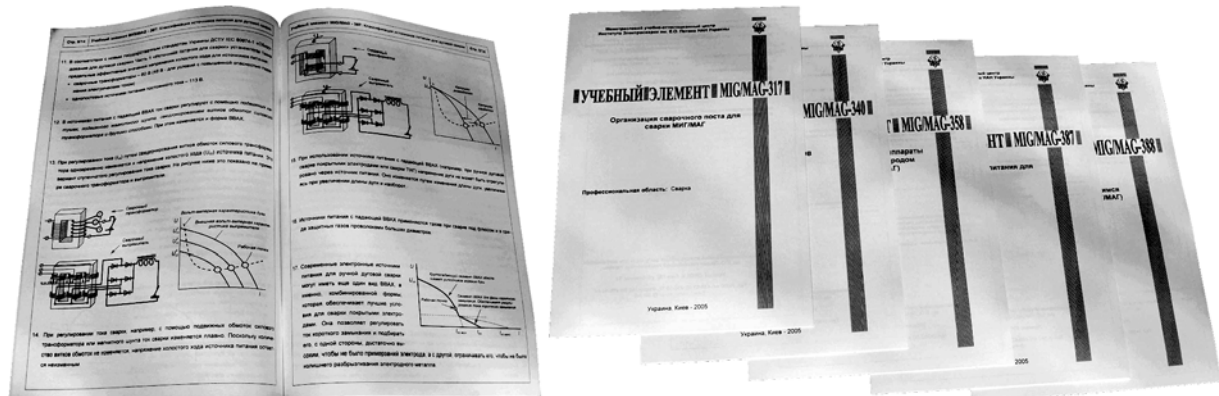


Figure 1. Training elements for mastering the process of MIG/MAG welding



Figure 2. Training with DTS-2 welder's trainer

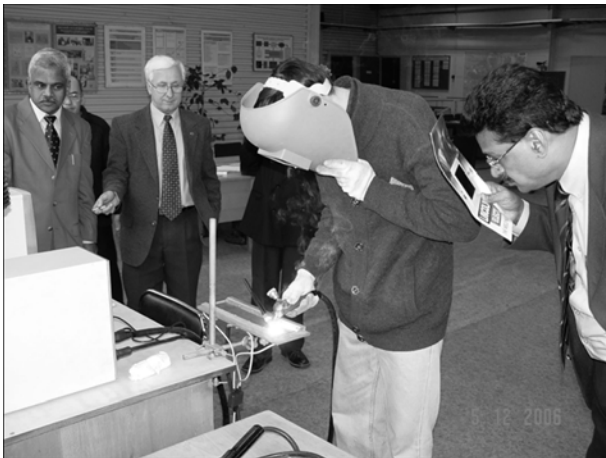


Figure 3. ITAC demonstrates practical training of welders to Indian specialists

tation of its management, which representatives were at ITAC not long ago (Figure 3). WRI is a subdivision of a large Indian concern that produces the equipment for thermal, nuclear and hydroelectric stations.

During the working meetings with Mr. Uma Shanker, Director of WRI (Figure 4), and leading specialists of the Institute the matters of assistance in development of a system for high-speed video filming of the welding arc with simultaneous recording of electric parameters of welding and development of their own program of module training of welders were

discussed, as well as supply of DTS-02 trainer. During the visit to WRI, DTS-02 trainer temporarily provided by JSS MAHAVIDYAPEETHA training center for this purpose, was demonstrated in action. Specialists and welders trained in the Center, highly appreciated its capabilities. Joint participation in conducting research on arc welding and creation of training video movies is also envisaged.



Figure 4. Fragment of a meeting of V.E. Ponomarev with Mr. Uma Shanker

V.E. Ponomarev made a few presentations at WRI, in which he considered the peculiarities of organization of welding production personnel training at the national and international levels, as well the matters of welding production certification, and discussed the latest results of research in the field of arc welding, obtained through video filming with simultaneous recording of the electric parameters of welding. Specialists of WRI expressed interest in the presented reports and a desire to work in these directions together with the E.O. Paton Electric Welding Institute.

V.E. Ponomarev, Cand. of Sci. (Eng.), PWI